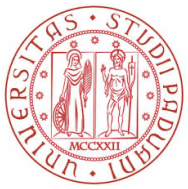

UNIVERSITÀ DEGLI STUDI DI PADOVA
DIPARTIMENTO DI SCIENZE CHIMICHE

CORSO DI LAUREA MAGISTRALE IN CHIMICA INDUSTRIALE

TESI DI LAUREA MAGISTRALE

Making Long Polymers and Breaking Them Apart

Relatore: Prof. Edmondo M. Benetti
Correlatore: Prof. Luca Dell'Amico
Controrelatore: Prof. Antonio Barbon

Laureanda: Agnese Spiazzi

ANNO ACCADEMICO 2025/2026

Indice

Summary of the Thesis

This thesis work is divided into two complementary research projects within the field of polymer chemistry: the fabrication, through surface-initiated controlled radical polymerization (SI-CRP), of ultra-tick polymer brush coatings, and the development of photocatalytic systems for the degradation of these materials and other vinyl polymers.

The first part of this thesis project focused on the synthesis of polymer brush coatings – polymer chains tethered to a surface through one of their ends – with thicknesses exceeding those typically obtained by SI-CRP techniques. Although these "grafting-from" approaches enable the preparation of polymer chains with controlled dispersity *Đ*, irreversible termination reactions between active chain-end functionalities, together with the burial of some of these dormant chain end functionalities below other growing chains, ultimately limit the achievable brush thickness[1–4]. To overcome these limitations and synthesize ultra-high molecular weight (UHMW) polymer brushes, an Atom Transfer Radical Polymerization (ATRP) approach for acrylates was employed using methyl α-bromoacrylate (BrMA) as a comonomer. BrMA belongs to a class of molecules known as "*inibramers*" (initiator branching monomers), which contain a halo substituent in α position relative to the carbonyl group and can act simultaneously as initiators, monomers, and branching units[5]. Originally developed for the controlled synthesis of branched polymers, *inibramers* proved particularly effective for the fabrication of polymer brushes by compensating for the loss of active chain-end functionalities. When present as free monomers, inibramers do not interfere with the ATRP equilibrium because of the high bond dissociation energy (BDE) of the C–X bond. Once incorporated into the growing polymer chain, however, the BDE of the C–X bond is reduced, enabling its activation and the formation of a new branching point from which two polymer chains can subsequently grow. At extremely low BrMA concentrations, ranging from 0.001 to 0.3 mol% relative to the selected comonomer, this dual role of the inibramer—compensation for the progressive loss of accessible chain ends and enhancement of the initial grafting density—enabled the formation of polymer brushes several micrometers thick, far beyond the limits of conventional SI-photoATRP. This behaviour was observed for different acrylates, including tert-butyl acrylate, butyl acrylate, and oligo(ethylene glycol) methyl ether acrylate (Mn ≈ 480 g mol^{-1}). Furthermore, the study highlighted that the effect of the inibramer concentration on the resulting brush thickness depends on the chemical structure of the acrylate monomer employed.

The second part of the thesis investigated photocatalytic approaches for the degradation of these materials and other vinyl polymers. The development of degradable polymers requires the incorporation of cleavable linkages into the polymer backbone, via radical copolymerization, that can be selectively cleaved upon application of an appropriate external stimulus. Among the possible candidates, disulfide bonds were selected because of their facile cleavage through redox processes, photochemical activation, and thermal stimuli[6,7]. To introduce these cleavable functionalities into vinyl polymers, copolymerization of *n*-butyl acrylate (*n*BA) with a disulfide-containing monomer, methyl lipoate (LpOMe), was investigated. The degradation behaviour was studied in solution for both the methyl lipoate homopolymer (PLpOMe) and the corresponding copolymers using different photocatalysts, including eosin Y, thioxanthone, and xanthone. In the case of the homopolymer, the nature of the degradation products was found to depend on the photocatalyst, the utilized light wavelength and the irradiation time, allowing either degradation or depolymerization to be achieved. Eosin Y promoted efficient depolymerization of the homopolymer, with depolymerization yields exceeding 80%. In contrast, when xanthone or thioxanthone was employed, the final product depended on both the reaction time and the irradiation wavelength. At short irradiation times (2 h), the presence of monomer was consistently observed, indicating the occurrence of depolymerization, whereas after prolonged irradiation (16 h) the characteristics monomer signals were no longer detected, suggesting the occurrence of secondary reactions involving the photodegradation products. Further observations of the homopolymer and monomer led to the hypothesis that secondary reactions involving the regenerated monomer may occur under prolonged irradiation and at the wavelengths employed. In the case of the copolymers, the formation of degraded or depolymerized products appears to be related to the number of consecutive methyl lipoate units incorporated into the polymer backbone. In fact, for the disulfide-containing copolymer with a low LpOMe content (70:30 *n*BA:LpOMe), no depolymerized product was appreciated, despite the decrease of the final molecular weight.

Riassunto della Tesi

Questo lavoro di tesi si articola in due progetti di ricerca complementari nell'ambito della chimica dei polimeri: la realizzazione, tramite una tecnica di polimerizzazione radicalica controllata iniziata da superficie (SI-CRP), di rivestimenti (o *coatings*) costituiti da polymer brushes che presentano un elevato spessore e lo sviluppo di sistemi che sfruttano fotocatalizzatori per la degradazione di questi materiali e altri polimeri vinilici.

La prima parte del progetto è dedicata dunque alla sintesi di rivestimenti costituiti da polymer brushes – catene polimeriche attaccate con una delle due estremità ad una interfaccia – con uno spessore maggiore di quello che generalmente si ottiene con tecniche SI-CRP. Queste tecniche di tipo "grafting from" infatti, sebbene permettano di ottenere catene con una dispersità $Đ$ controllata, a causa delle reazioni irreversibili di terminazione tra le funzionalità di fine catena attive e sepoltura di alcune di queste funzionalità al di sotto delle altre catene crescenti dalla superficie, permettono di ottenere polymer brushes di spessore limitato. Per sintetizzare ultra-high molecular weight (UHMW) polymer brushes si è dunque optato per una polimerizzazione di tipo Atom Transfer Radical Polymerization (ATRP) di acrilati usando come comonomero il metil α-bromo acrilato (BrMA). Quest'ultimo fa parte delle classi di molecole chiamate "inibramers" (initiator branching monomers) le quali presentano un alogeno in posizione alfa al carbonile e che svolgono tre funzioni, quella di iniziatore, di monomero e di unità ramificante. Nati per la sintesi di polimeri ramificati in modo controllato, gli inibramers, applicati nella fabbricazione di polymer brushes, si sono rivelati ideali nel compensare la perdita delle funzionalità attive nelle catene crescenti. Questi infatti, quando sottoforma di monomero, non disturbano l'equilibrio di ATRP grazie all'alta "bond dissosiation enegy" (BDE) del legame C-X ma, una volta integrati nella catena crescente, diminuiscono la BDE del legame C-X attivandosi, con la conseguente formazione di una giunzione da cui possono crescere due diverse catene polimeriche. A concentrazioni di BrMA estremamente basse (dallo 0.001 mol% allo 0.3mol% relative al comonomero di struttra) è stato possibile osservare come, con diversi acrilati, tra cui il tert-butil acrilato,butil acrilato e oligo(etilen glicole) metil etere acrilato (Mn ≈ 480 g/mol), il duplice meccanismo degli inibramer - compensazione delle catene terminate e aumento della grafting density iniziale - abbia portato a brushes di spessori superiori a diversi micrometri, senza precedenti. Durante lo studio si è inoltre evidenziato che, dipendentemente

dal monomero acrilato utilizzato, la concentrazione di inibramer nella soluzione di reazione influenza lo spessore dei polymer brushes ottenuti.

Conseguentemente, nella seconda parte del progetto di tesi, si è investigato un metodo di degradazione di questi polimeri e altri polimeri di tipo vinilico sfruttando dei fotocatalizzatori. Per ottenere polimeri degradabili è necessario inserire nel backbone della catena polimerica dei legami che siano scindibili se sottoposti ad opportuni stimoli. Tra le possibili opzioni si sono scelti i disolfuri in quanto legami facilmente scindibili se sottoposti a processi redox, processi fotochimici o stimoli termici. Per ottenere dei polimeri con le caratteristiche appena esplicate si è optato quindi per la copolimerizzazione tra butil acrilato (*n*BA) e un monomero contenente un disolfuro, nel nostro caso l'estere metilico dell'acido lipoico (LpOMe). La degradazione è stata studiata su sistemi in soluzione sia per l'omopolimero del metil lipoato (PLpOMe), sia nel caso dei copolimeri, utilizzando diversi fotocatalizzatori come l'eosina Y, il thioxanthone e lo xanthone. Nel caso dello studio sull'omopolimero si è osservato come, a seconda del catalizzatore, la lunghezza d'onda utilizzata e del tempo di reazione, sia possibile ottenere un prodotto di degradazione o di depolimerizzazione. L'eosina Y promuove la depolimerizzazione dell'omopolimero con rese di depolimerizzazione superiori all'80%. Nel caso dello xantone e thioxantone invece il prodotto finale dipende dal tempo di reazione e dalla lunghezza d'onda con cui si irradia il campione. Si osserva sempre per tempi di reazione brevi, 2 ore, la presenza di monomero ad indicare l'avvenuta depolimerizzazione, ma per tempi di reazione più lunghi, 16 ore, non sono determinabili i caratteristici segnali del monomero, indicando l'avvenimento di reazioni secondarie. Ulteriori osservazioni sul comportamento dell'omopolimero e del monomero hanno conseguentemente fatto ipotizzare l'avvenimento di reazioni secondare sul monomero innescate dalla lunghezza d'onda della luce utilizzata. Per quanto riguarda invece lo studio della degradazione del copolimero, l'ottenimento di prodotto degradato o depolimerizzato sembra essere correlato al numero di unità monomeriche di metil lipoato in successione. Infatti, nel caso di copolimeri con una bassa concentrazione di lipoato (70:30 *n*BA:LpOMe), non è stato possibile determinare la presenza di monomero, nonostante il calo di peso molecolare finale.

Abbreviations

CRP	Controlled radical polymerization
Đ	Dispersity
ATRP	Atom transfer radical polymerization
NMP	Nitroxide-mediated polymerization
PIMP	Photoinferter mediated polymerization
RAFT	Reversible addition-fragmentation chain transfer polymerization
CTA	Chain transfer agent
MAMs	More active monomers
LAMs	Less active monomers
ARGET ATRP	Activator regenerated by electron transfer ATRP
photoATRP	photochemically mediated ATRP
σ	Grafting density
SI-CRP	Surface-initiated controlled radical polymerization
SI-ATRP	Surface-initiated atom transfer radical polymerization
BDE	Bond dissociation energy
HBPs	Hyperbranched polymers
***n*BA**	*n*-butyl acrylate
BBA	*n*-butyl α-bromoacrylate
LA	a-lipoic acid
ROP	Ring-opening polymerization
T_c	Ceiling temperature
LpOEt	Ethyl lipoate
TCEP	Tris(2-carboxyethyl)phosphine hydrochloride
Bu_3P	Tributylphosphine
S_0	Singlet ground state
S_1	Singlet lower excited state
T_1	Triplet lower excited state
ISC	Intersystem crossing
IC	Internal conversion
PC	Photocatalyst
PC*	Excited photocatalyst
HAT	Hydrogen atom transfer

XAT	Halogen atom transfer
EnT	Energy transfer
ET	Electron transfer
PCET	Proton coupled electron transfer
FRET	Förster (Resonance) Energy Transfer
LUMO	Lowest unoccupied molecular orbital
HOMO	Highest occupied molecular orbital
SOMO	Singly occupied molecular orbital
A	Acceptor
D	Donor
UHMW	Ultra-high molecular weight
BrMA	Methyl α-bromoacrylate
***t*BA**	*Tert*-butylacrylate
OEGA	Oligo(ethylene glycol) acrylate
Me_6TREN	Tris[2-(dimethylamino)ethyl]amine
T_{dry}	Dry thickness
P*t*BA	Poly(*tert*-butyl acrylate)
AFM	Atomic force microscopy
RMS	Root mean square
P*n*BA	Poly(*n*-butyl acrylate)
POEGA	Poly oligo(ethylene glycol) acrylate
M_n	Number average molecular weight
θ_s	Static water contact angle
LpOMe	Methyl lipoate
PLpMe	Poly(methyl lipoate)
TXO	Thioxanthone
XO	Xanthone
Φ_{ISC}	Quantum yield of intersystem crossing
TEA	Triethyl amine
THF	Tetrahydrofuran
NMR	Nuclear magnetic resonance
SEC	Size exclusion chromatography
GPC	Gel permeation chromatography

DCM	Dichloromethane
4CzIPN	1,2,3,5-Tetrakis(carbazol-9-yl)-4,6-dicyanobenzene
$\mathbf{E^*_{ox}}$	Excited state oxidation potential
ε	Molar extinction coefficient
L	Ligand
EY	Eosin Y
RB	Rose Bengal
BHT	Butylated hydroxytoluene
MB	Methylene blue
CV	Cyclic voltammetry
SCE	Saturated calomel electrode
$\mathbf{E_{pc}}$	Cathodic peak potential
$\mathbf{E_{pSH}}$	Thiol oxidation peak potential
$\boldsymbol{E_{1/2}^{red}}$	Half-wave reduction potential
$\boldsymbol{E_{1/2}^{ox}}$	Half-wave oxidation potential
$\boldsymbol{E_{red}^{S1}}$	Reduction potential of the singlet excited state
$\boldsymbol{E_{ox}^{S1}}$	Oxidation potential of the singlet excited state
$\boldsymbol{E_{red}^{T1}}$	Reduction potential of the triplet excited state
$\boldsymbol{E_{ox}^{T1}}$	Oxidation potential of the triplet excited state
$\mathbf{E_T}$	Triplet excited state energy
TLC	Thin layer chromatography
CA	Contact angle
MWCO	Molecular weight cut-off
PMMA	Poly(methyl methacrylate)
BiB	α-bromoisobutyryl bromide
APTES	3-Aminopropyl)triethoxysilane
DMSO	Dimethyl sulfoxide
DMAP	4-(N,N-dimethylamino)piridine
EDCI	N-(3-dimethylamino-propyl)-N' ethylearbodimide hydrochloride
AIBN	azobisisobutyronitrile
DMF	N,N-Dimethylformamide
MeCN	Acetonitrile
$\mathbf{TEABF_4}$	tetraethylammonium tetrafluoroborate

Introduction

1. General aspects of controlled radical polymerization

The word "polymer" is derived from the Greek words "poly" (many) and "mer" (part); polymers are macromolecules composed of numerous repeating units called monomers, which are linked together by covalent bonds. Based on their reaction mechanism and kinetics, traditional polymerization processes can be classified in two main categories: *step-growth polymerization* and *chain-growth polymerization*. When polymer chains grow through stepwise reactions between two reactive species (monomer, dimer, oligomer or short polymer chains) this is called step-growth polymerization. In chain-growth polymerizations, on the contrary, polymer chains grow by the addition of one monomer unit at the time to an active chain end. Depending on the nature of the active centre, which might be a radical, a cation or anion, chain-growth polymerizations are classified as anionic, cationic or radical polymerizations. The process also requires an initiator, a molecule capable of generating active species ($R^{\bullet}$, R^{+}, R^{-}) that initiates chain propagation. However, free radical polymerizations generally lack precise control over molecular weight and dispersity, as a result of unavoidable and irreversible chain transfer/termination reactions. Thus, to overcome these limitations, controlled radical polymerizations (CRP) have been developed.

Before discussing controlled radical polymerizations, it is appropriate to first introduce the concept of living polymerization, a system where the contribution of chain breaking reactions (transfer and termination) is minimized. This allows greater control over molecular composition and weight distribution. The main characteristics of CRP are a fast initiation, significantly faster than the rate of propagation, and there are ideally no termination or transfer processes. Termination of propagating chains and side reactions (disproportionation and chain transfers) are minimized by maintaining a low concentration of radicals. If the initiation process and the establishment of active-dormant chain equilibrium are rapid relative to propagation, the breadth of the polymer chain length distributions is minimized and can be described by a Poisson distribution[8]. The development of CRP has enabled the synthesis of polymers with narrow molecular weight distributions, $Đ \leq 1.3$, predetermined degree of polymerization and the control of the chain end functionalities. These features have, in turn, allowed the synthesis of well-defined block and graft copolymers.

In CRP systems there is the establishment of a dynamic equilibrium between active propagating radicals, transient radical $P_n^{\bullet}$ (reactive) and a persistent radical $X^{\bullet}$ (stable), and dormant species P_n-X, with the equilibrium strongly shifted toward the dormant state (Figure 1).

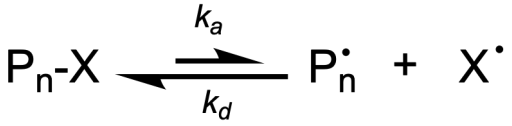

Figure 1*: Equilibrium of a generic controlled radical polymerization (CRP) between dormant and active species. The kinetic constants are k_a for the activation and k_d for the deactivation.*

During the activation-deactivation process propagating radicals $P_n^{\bullet}$ can react with both a monomer unit and continue chain propagation or react with the persistent radical to regenerate the dormant species (Figure 2). Because deactivation occurs rapidly, the concentration of propagating radicals remains low, thereby minimizing side reactions. In contrast to conventional free radical polymerization, in which initiation is relatively slow, and polymer chains are formed over an extended period, CRP is characterized by rapid initiation, allowing nearly all polymer chains to begin growing simultaneously and providing a constant concentration of growing chains[9]. The dormant species can be activated either spontaneously or thermally, in the presence of light or with proper catalysts. Clearly radicals can propagate and terminate but it is essential that persistent radicals terminate with each other but only cross-couple with the growing species[10].

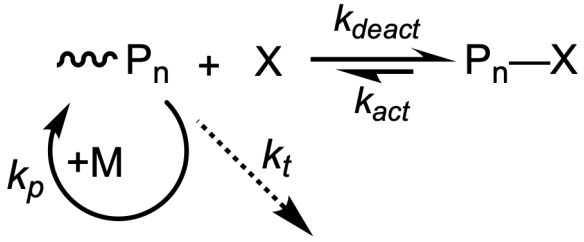

Figure 1*: CRP equilibrium.*

Moreover, the preservation of chain-end functionality throughout the polymerization enables the subsequent extension of the polymer chains by the addition of further monomers. This, in turn, allows the synthesis of macromolecules with complex architectures such as block, star, brush copolymers[8] (Figure 3).

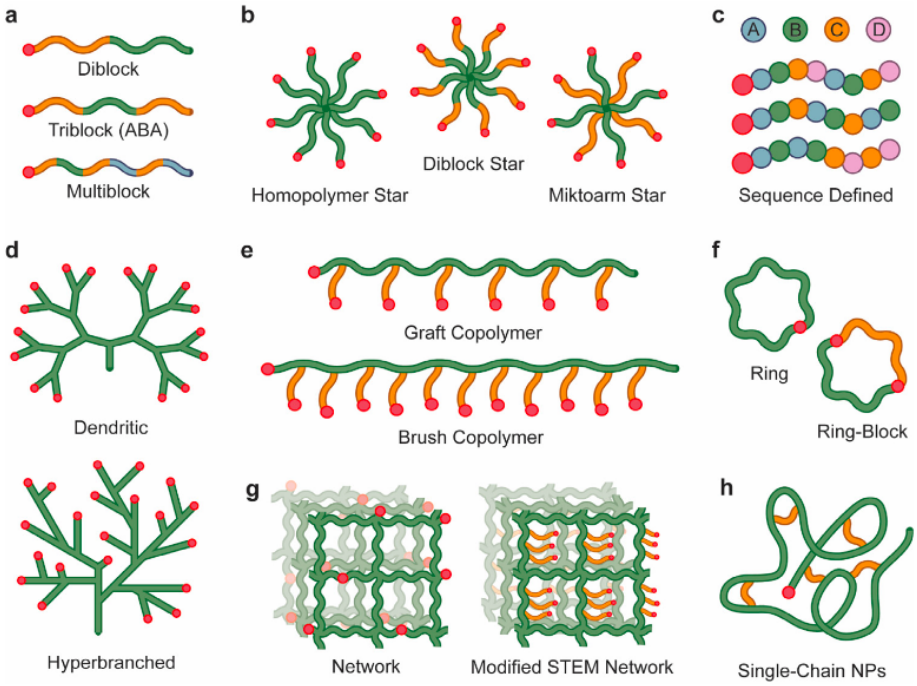

***Figure 3**: Variety of molecular architectures accessible through controlled radical polymerization techniques; (a) block copolymers; (b) star copolymers; (c) sequence defined copolymers; (d) branched copolymers; (e) graft and brush copolymers; (f) ring copolymers; (g) network copolymers; (h) single chain nanoparticles. Reproduced from [8].*

Promoted by their versability, interest in CRP rapidly increased over the years, resulting in the development of effective strategies for imparting living characteristics to radical polymerization. A clear indication of this success is the significant increase in publications over the years (Figure 4).

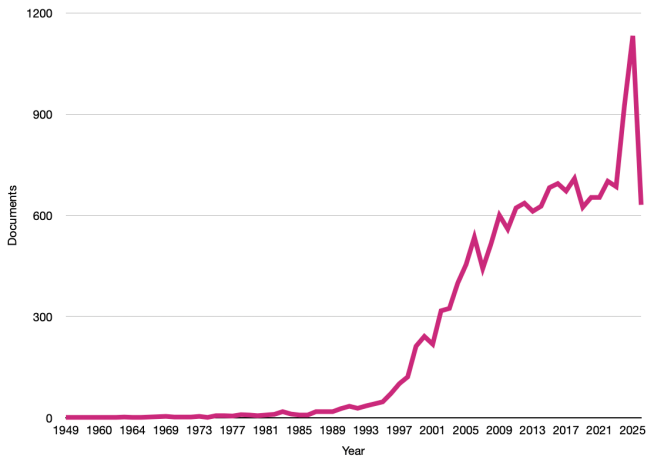

***Figure 2**: Number of publications between 1949 and 2026 (current year). Search term "controlled radical polymerization" on Elsevier Scopus.*

Several effective CRP strategies have been developed over the years, each characterized by distinct reaction mechanisms and differing in the reagents and reaction conditions employed. The most employed CRP techniques include atom transfer radical polymerization (ATRP), nitroxide-mediated polymerization (NMP), photoinferter mediated polymerization (PIMP) and reversible addition-fragmentation chain transfer (RAFT) polymerization.

NMP was the first CRP technique developed and relies on the use of a stable nitroxide as mediator. In this technique, the low concentration of active radicals is maintained through the reversible capping of the growing polymer chain end by the nitroxide. This dynamic equilibrium minimizes termination reactions while regulating the polymerization rate[11] (Figure 5).

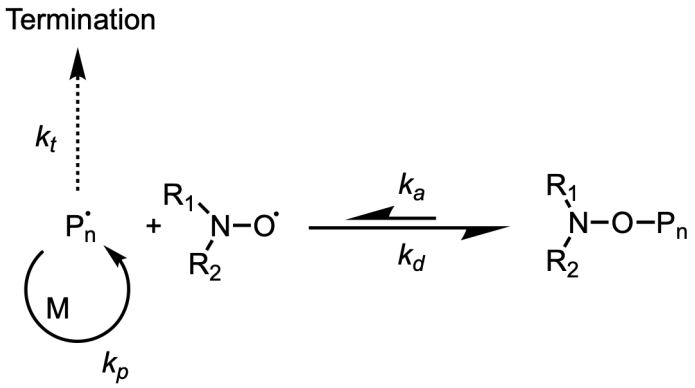

***Figure 3**: General mechanism of NMP polymerization. k_a, k_d, k_p, k_t are respectively the kinetic constants of association, dissociation, propagation, and termination.*

Photoinferter-mediated polymerization (PIMP) exploits an *iniferter* molecule, initiator-transfer-agent-terminator, which is activated upon light irradiation to generate radicals. Radicals initiate the polymerization, while the iniferter reversibly deactivates the growing polymer chains to form dormant species, enabling a controlled polymerization. Since iniferter is activated by light a rather constant concentration of radicals is guaranteed during the reaction, and a re-initiation process can be triggered on demand[12].

Nowadays the most employed CRPs are ATRP and RAFT polymerizations. In this thesis work, polymers are synthetized through those two techniques, described in the following sections.

1.1 RAFT Polymerization

RAFT polymerization, developed in 1998, is a controlled radical polymerization technique that employs thiocarbonylthio compounds, Z-C(=S)S-R, to regulate the degenerative exchange of propagating radicals generated via conventional radical initiators.

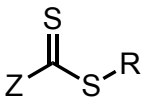

Figure 6*: General structure of a CTA, where the Z group controls the reactivity of the RAFT agent, while the R group serves as the reinitiating species during polymerization.*

These thiocarbonylthio species, commonly referred to as chain transfer agent (CTA) or RAFT agents (Figure 6), reversibly react with propagating radical species to form intermediate radicals. The latter subsequently undergoes fragmentation at the weak C-S bond with the consequent formation of a dormant thiocarbonylthio-capped chain and a new propagating radical (Figure 7, step 5)[8]. The chain transfer step is described as degenerative because it involves an exchange of functionalities between polymer chains without altering their chemical identity[13]. As depicted in Fig. 7, after the activation step (1) where the initiator undergoes homolytic cleavage upon exposure to an external stimulus, the propagating radical $P_n^{\bullet}$ enters in the degenerative chain transfer equilibrium mediated by the CTA (Figure 7, step 3). The RAFT equilibrium is established between active and dormant species through interaction of radicals with CTA (Figure 7, steps 3 and 5). The degree of polymerization (DP) of all chains is expected to be similar at a given time. This uniformity arises because the rate of addition/fragmentation equilibrium is higher than the propagation, resulting in less than one monomer unit added per activation cycle. Important is the use of radical initiator; for RAFT polymerization the number of chains that undergoes bimolecular termination is correlated to the number of radicals initially introduced in the system. Although bimolecular termination does not lead to a loss of living chain ends, the number of chains with the CTA as end group remain the same throughout the polymerization. As a result, the fraction of dead chains can be predicted a priori by controlling the amount of initiator used, providing a unique degree of control over the polymerization process[14]. Following complete monomer conversion, the majority of polymer chains remain in their dormant state, enabling further chain extension through the addition new initiator and monomer. The products obtained through RAFT polymerization are characterised by a narrow polydispersity, $Đ \leq 1.2$, and a linear molecular weight-conversion profile. Furthermore, it is

possible to predict the molecular weight from the ratio of monomer consumed to transfer agent, and block or higher molecular weight polymers are achievable by monomer addition. All these characteristics indicate that the RAFT process has a living character[15]. The depletion of the CTA can be determined by two transfer coefficients (Equation 1):

$$C_{tr} = \frac{k_{tr}}{k_p} \qquad \text{where } k_{tr} = k_{add} * \frac{k_b}{k_{-add} + k_b} \tag{1}$$

Where C_{tr} is describing the reactivity of the propagating radical $P_n^{\bullet}$,

$$C_{-tr} = \frac{k_{-tr}}{k_i} \qquad \text{where } k_{-tr} = k_{-add} * \frac{k_{-b}}{k_{-add} + k_b} \tag{2}$$

Describing the reactivity of the radical $R^{\bullet}$ (Equation 2).

Since each CTA molecule generates one polymer chain, monitoring its depletion is very important.

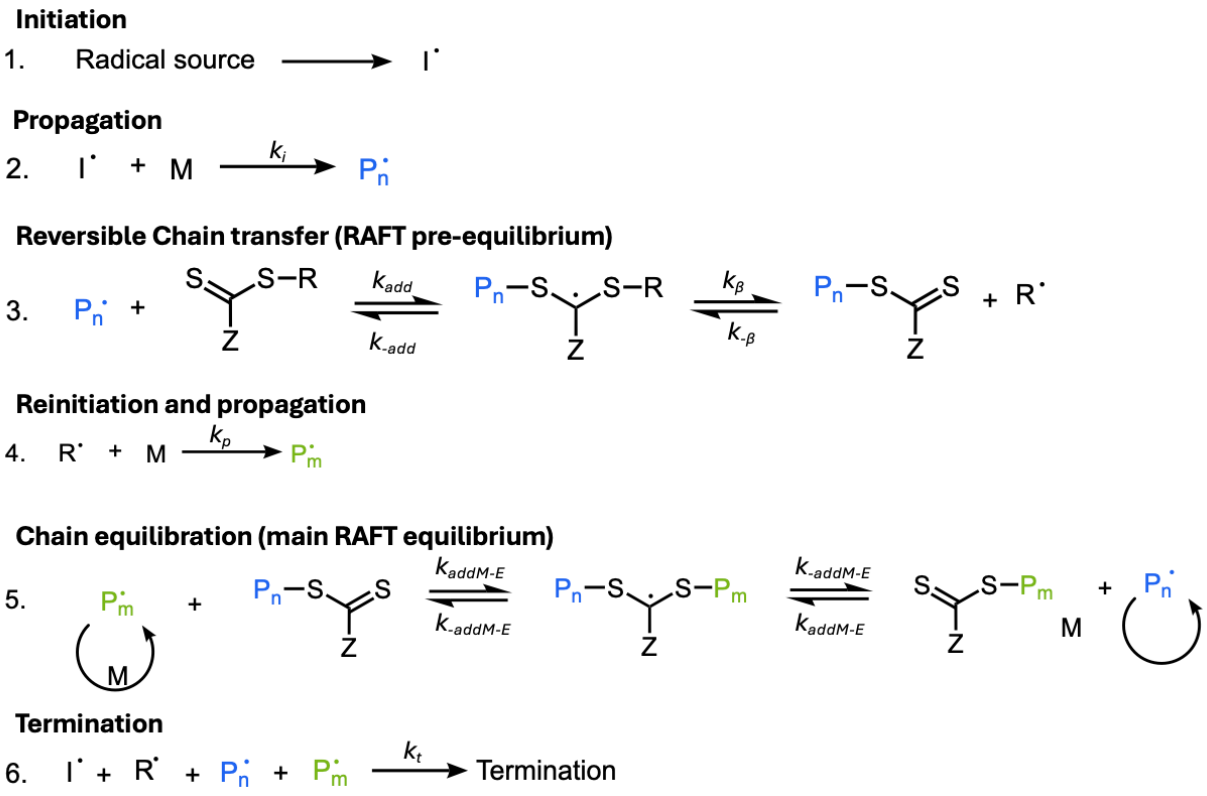

***Figure 7**: General RAFT mechanism; the main stages of the process are illustrated, where k_i, k_p, k_{add}, k_β, k_{-add}, $k_{-\beta}$, k_{addM-E}, $k_{-addM-E}$, k_t, are the rate constants for initiation, propagation, addition for the RAFT pre-equilibrium, fragmentation for the RAFT pre-equilibrium, addition for the RAFT main equilibrium, fragmentation for the RAFT main equilibrium, and termination respectively.*

The RAFT agent's effectiveness in providing living character is due to their high transfer constants which guarantee a rapid rate of exchange between the dormant species and living chains. The choice of Z and R becomes then essential to have a successful RAFT polymerization[15]. RAFT agents can be dithioesters (Z = alkyl or aryl), trithiocarbonates (Z = SR′), xanthates (Z = OR′), and dithiocarbamates (Z = NR′R″), thus, for an optimal control of the polymerization, the CTA must be chosen accordingly to the monomer(s) and the reaction conditions used.

The role of the Z group is essential since it modifies the rate of addition of propagating radicals $P_n^{\bullet}$ to the thiocarbonyl (Figure 7, equilibrium 3) and the rate of fragmentation of the intermediate radicals. CTA with dithioesthers and trithiocarbonates, which have carbon or sulphur near the thiocarbonylthio group, are the most reactive RAFT agents[13]. The choice of the R group is crucial too since it influences the equilibrium between active and dormant species. The R group must include a sufficiently labile bond within the intermediate radical to enable rapid homolytic fragmentation and efficient reinitiation of the polymerization. The $R^{\bullet}$ radical should indeed be more stable than the propagating one, $P_n^{\bullet}$, to guarantee its preferential formation[16].

RAFT polymerization enables controlled polymerization of most monomers that are amenable to conventional free-radical polymerization, making it one of the most versatile controlled radical polymerization techniques. Vinyl monomers are classified in two families, based on their reactivity. The "more active" monomers (MAMs) are the ones with the vinyl group conjugated to a double bond, an aromatic ring, a carbonyl group or a nitrile, the "less active" monomers (LAMs) present a double bond near an oxygen, nitrogen, halogen, sulfur lone pairs or a saturated carbon. Monomers bearing functional groups capable of undergoing side reactions with the RAFT agent can present challenges for this technique. Is it essential then, to achieve efficient control over the polymerization, that the C=S bond is more reactive than the C=C of the monomer, and this is done by selecting appropriately the Z (Figure 9) and the R group (Figure 8)[14].

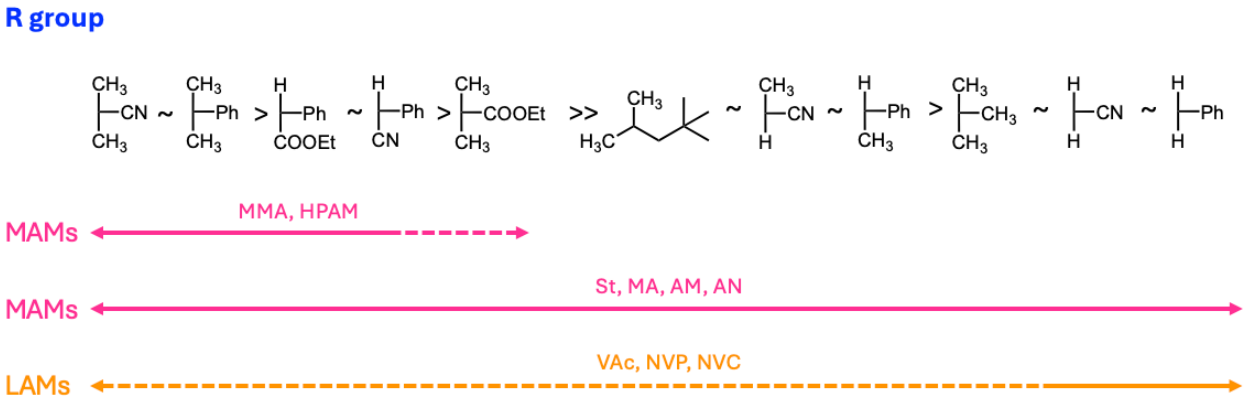

Figure 8: *Guidelines for selection of the R-Group of RAFT Agents for various polymerizations. Transfer coefficients decrease from left to right. Fragmentation rates also decrease from left to right. A dashed line indicates a partial control. Abbreviations: MMA = methyl methacrylate, HPMAM = N-(2- hydroxypropyl)methacrylamide, St = styrene, MA = methyl acrylate, AM = acrylamide, AN = acrylonitrile, VAc = vinyl acetate, NVP =N-vinylpyrrolidone, and NVC = N-vinylcarbazole.*

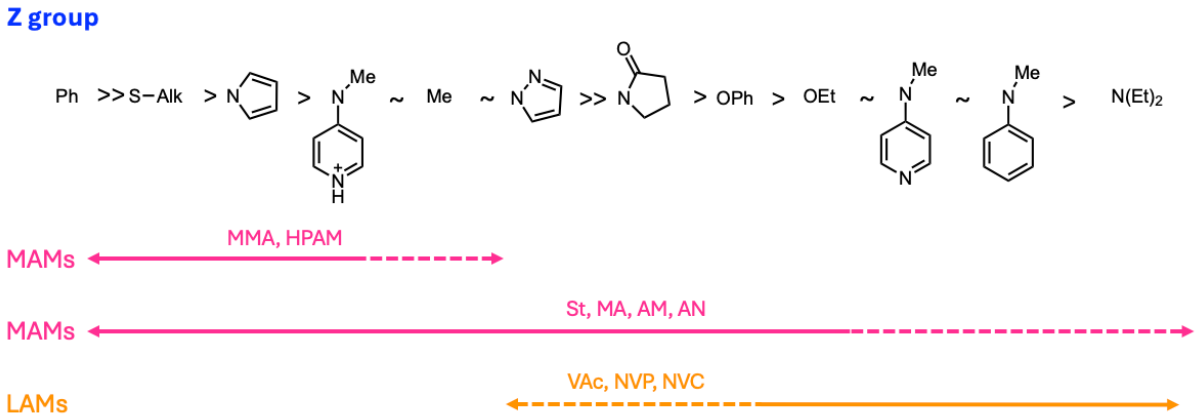

Figure 9*: Guidelines for selection of the Z-Group of CTAs for various polymerizations. Addition rates decrease and fragmentation rates increase from left to right. A dashed line indicates partial control (i.e., control of molar mass but poor control over dispersity or substantial retardation in the case of LAMs such as VAc or NVP). Abbreviations: MMA = methyl methacrylate, HPMAM = N-(2- hydroxypropyl)methacrylamide, St = styrene, MA = methyl acrylate, AM = acrylamide, AN = acrylonitrile, VAc = vinyl acetate, NVP =N- vinylpyrrolidone, and NVC = N-vinylcarbazole.*

1.2 ATRP

Introduced in 1995 by the works of Matyjaszewski[17] and Sawamoto[18], ATRP derives its name from the atom transfer step, which is the key elementary reaction underlying this polymerization technique. ATRP typically employs an alkyl halide as initiator and a transition metal complex, Mt^n/L, as catalyst, where *Mt* is the transition metal in oxidation state *n* and *L* denotes the coordinating ligand. Commonly used transition metals are Fe and Mo, however Cu-centred catalyst are generally the most effective. The dynamic equilibrium between active radicals and dormant alkyl halides ensures precise control over the polymer structure. In ATRP polymerization radicals are generated through a reversible redox process catalyzed by the transition metal complex Mt^n/L. The transition metal complex undergoes a one-electron oxidation while simultaneously abstracting the halogen atom (*X)* from the dormant specie P_m-*X*. This process results in the formation of a metal-halogen bond $X\text{-}Mt^{n+1}/L$ and the carbon centred radical $P_m^{\bullet}$ (Figure 10). The dormant species might be the initiator or the polymer chain. The oxidized metal complex $X\text{-}Mt^{n+1}/L$ acts as a persistent radical and reduces the stationary concentration of growing radicals acting as deactivator, with the consequent minimization of termination reactions. This last point, the fast initiation and rapid reversible deactivation, which promote the uniform growth of all polymer chains, are the key characteristics of a successful ATRP process[19].

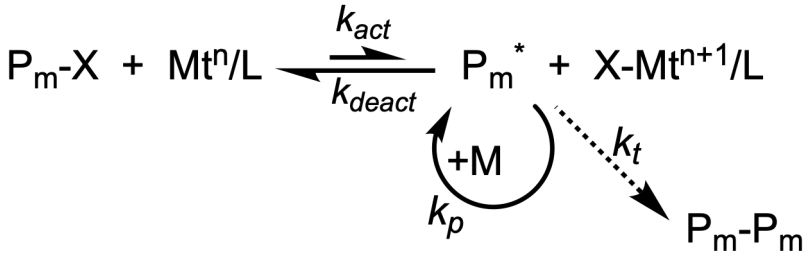

***Figure 10**: General ATRP equilibrium where k_a and k_d are the activation and deactivation kinetic constants, respectively.*

The development of ATRP through the design of highly efficient catalytic systems, the selection of appropriate ligands and initiators and the optimization of the reaction conditions has led to a polymerization technique that provides unprecedented control over both polymer composition (to form block, gradient, alternating or statistical copolymers) and chain topology (stars, branched shaped polymers)[20,21].

Monomers that can typically be used in ATRP processes are styrenes, acrylates and methacrylates, acrylamides and methacrylamides, and acrylonitrile, since those monomers contain substituents that can stabilize the propagating radicals. It is important to consider that, even under the same reaction conditions and catalyst, each monomer has its own intrinsic atom transfer equilibrium constant for its active and dormant species. Each monomer possesses its own radical propagation rate, as consequence, to maintain the polymerization control, the concentration of propagating radicals and the rate of radical deactivation need to be adjusted[20].
In the absence of side reactions, apart from radical termination by coupling or disproportionation, the magnitude of the equilibrium constant K_{eq} (Equation 3) determines the polymerization rate.

$$K_{eq} = \frac{K_a}{K_d} = \frac{[P_n^{\cdot}][Cu^{II}X/L]}{[P_n - X][Cu^{I}/L]} \quad (3)$$

If the equilibrium constant is too small, the ATRP process proceeds very slowly because only a low concentration of active radicals is generated. Conversely, if K_{eq} is too large, the concentration of radicals becomes excessively high, leading to a large amount of termination reactions. As a result, the ATRP equilibrium will be shifted towards dormant species[20,22].
The rate of an ATRP depends on the rate constant of propagation and the concentration of monomer and growing radicals, as well as the equilibrium between active and dormant species. Accordingly, the polymerization rate can be expressed as (Equation 4):

$$v = \frac{d[M]}{dt} = k_p[P_n^{\cdot}][M] = k_p K_{eq} \frac{[P_n X][Cu^{I}/L][M]}{[Cu^{II}X/L]} \quad (4)$$

With the catalyst activity K_{eq}, the rate of ATRP, generally increases but, under certain conditions it can decrease due to radical termination and the resulting low ratio of Cu^{I}/Cu^{II}. As well known reaction conditions, such as the solvent, the temperature and the structure of the ligand affect the rate constant[21].
Ligands, in ATRP reactions, play a crucial role not only by solubilizing the Cu salts but also by tuning the Cu catalyst activity, as they strongly influence the effectiveness of it. The activity of the catalyst increases as the Cu(II) oxidation state is better stabilized by the ligand. Consequently, the catalytic activity of the complex strongly depends on the ligand structure. Favourite ligands are nitrogen-based ones, while S, O or P ligands are less effective for ATRP, due to different electronic effects or unfavourable binding constant (Figure 11)[22].

In a typical ATRP processes Cu(I) complexes are employed to cleave the C-X bond and generate propagating radicals. However, because Cu(I) complexes require a strictly inert atmosphere, ATRP methods based on Cu(II) complexes that are reduced in situ within the polymerization mixture have been developed[23]. Among these, activator regenerated by electron transfer (ARGET) ATRP has been the first to be developed followed by photochemically mediated ATRP (*photo*ATRP).

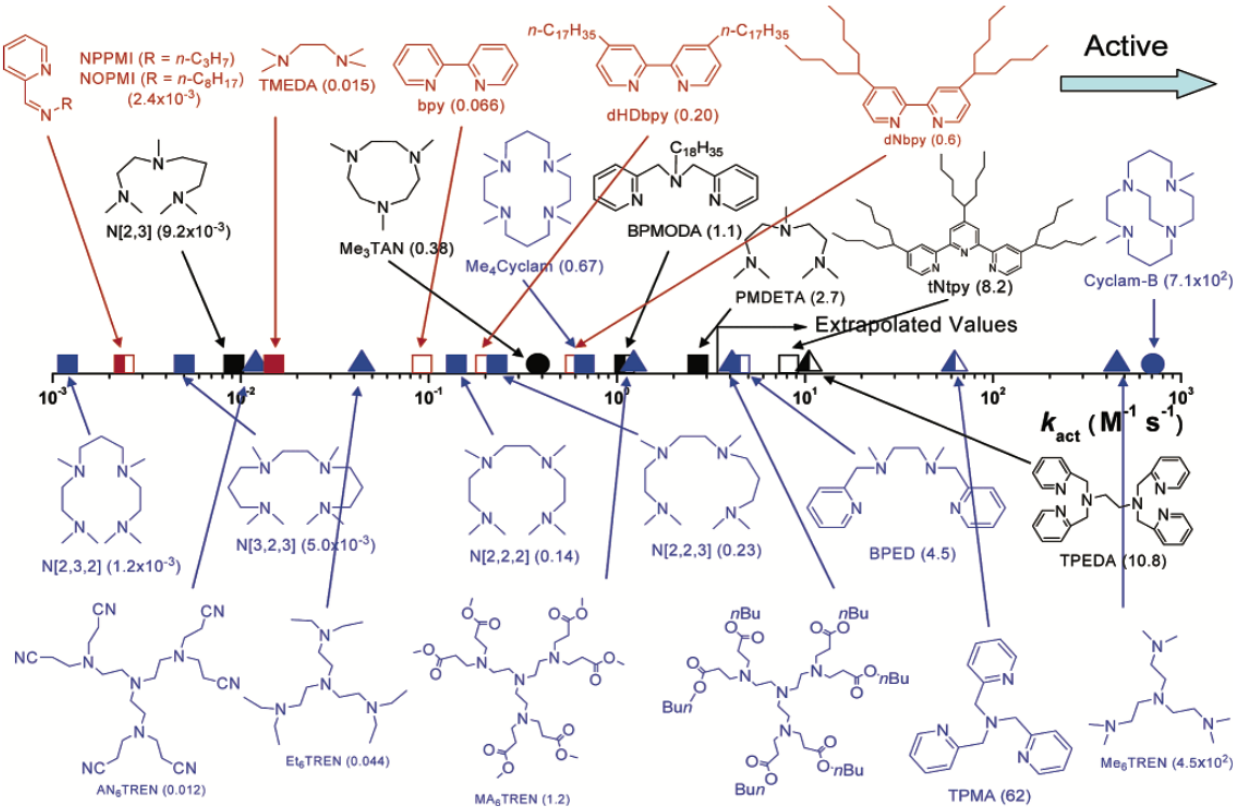

***Figure 11**: ATRP activation rate constants for various ligands with EtBriB in the presence of Cu^{I}Y (Y=Br or Cl) in MeCN at 35°C: N2, red; N3, black; N4, blue; amine/imine, solid; pyridine, open. Mixed, left-half solid; linear, □; branced, ▲; cyclic, ◯. Figure taken from [15]*

1.2.1 Activator regenerated by electron transfer (ARGET) ATRP

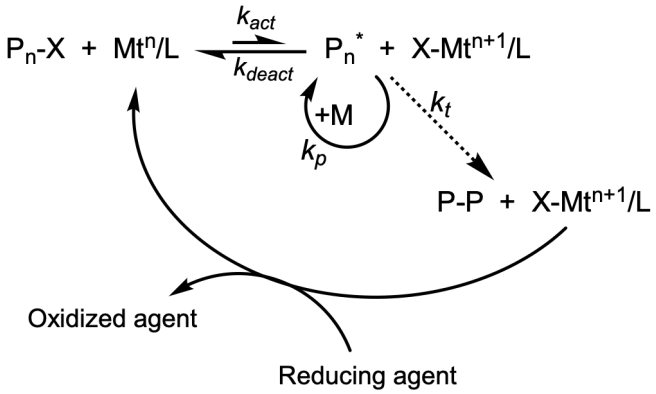

***Figure 12**: ARGET ATRP equilibrium, where k_{act} and k_{deact} are the activation and deactivation kinetic constants, respectively and k_t the termination constant.*

In ARGET ATRP, a reducing agent is added to continuously regenerate activators from deactivators. As represented in Fig. 12, the excess of Cu(II) species formed in termination reactions is continuously reduced back to Cu(I) species by the reducing agent, which is present in excess. This approach enables the polymerization to be conducted with a lower concentration of catalyst (10 ppm or less) without losing control of the polymerization, thanks to the presence of the reducing agent[24,25].

Apart from the advantage of having a more environmentally friendly polymerization process, the use of a smaller quantity of catalyst helps to suppress side reactions between the chain ends and the catalyst. As consequence this leads to high molecular weight polymers with low polydispersity. Further advantages of using Cu(II) species, in addition to their lower costs and easier handling, include the enhanced tolerance to a limited amount of air, which is provided by the continuous action of the reducing agent[23,24].

1.2.2 Photoinduced ATRP

In photoinduced atom transfer radical polymerization (photoATRP) the (re)generation of Cu(I) activator species occurs under light irradiation through the photochemical reduction of the excited Cu(II) species by a free aliphatic amine. The reductive quenching pathway is enabled by a free ligand (L), which acts as the sacrificial electron donor and is typically present in the reaction mixture in excess. In other words, the mechanism starts with the photoreduction of the Cu(II) deactivator complex to generate Cu(I) species and a halogen radical. The halogen radical

can then react with monomer and initiate the growth of the polymer chain subjected to the ATRP equilibrium. Therefore, the electron donors act as reducing agents that regenerate Cu(I) like in ARGET ATRP (Figure 13)[26].

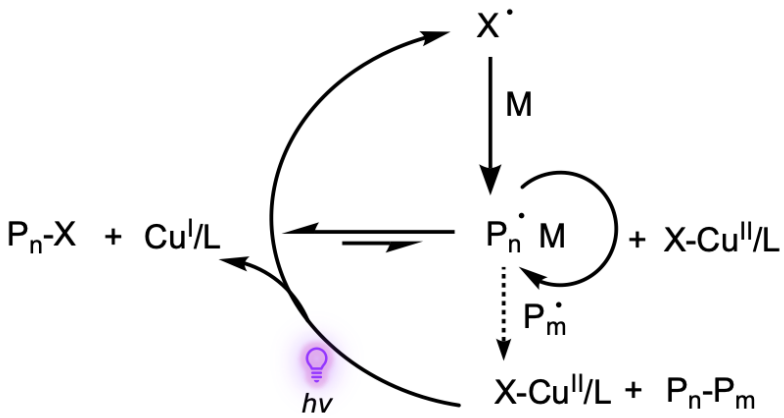

Figure 13: *General photoATRP equilibrium.*

In the absence of light, the polymerization ceases, demonstrating the excellent temporal control through on-off light switching. This allows the synthesis of polymer chains with a narrow dispersity, a molecular weight close to the theoretical one and a controlled architecture[27].

Mechanistic studies have highlighted the unique tolerance of photoATRP toward oxygen, which distinguishes it from conventional ATRP methodologies. In the presence of oxygen $Cu^{I}X/L$ generates $Cu^{II}X(O_2)/L$ species which recombine with an electron donor or L in the excited state regenerating $Cu^{I}X/L$ activators and producing oxidized species L_{ox}. Because of that, working with excess of ligand (or other electron donors) makes photoATRP tolerant toward environmental conditions avoiding the need of tedious deoxygenation processes prior to polymerization. This approach translates, for example, into the possibility of synthetizing polymer brushes in a controlled manner even in the presence of oxygen, broaden its applicability (Figure 14)[26,28].

The role of the light source is important since it influences the photoATRP reactions. It has been reported that generally in photoATRP the higher is the light intensity the faster is the chain activation, resulting in a faster polymerization. On the other hand, the use of high-intensity light rises the probability of having side reactions, leading to a loss of control over the polymerization.

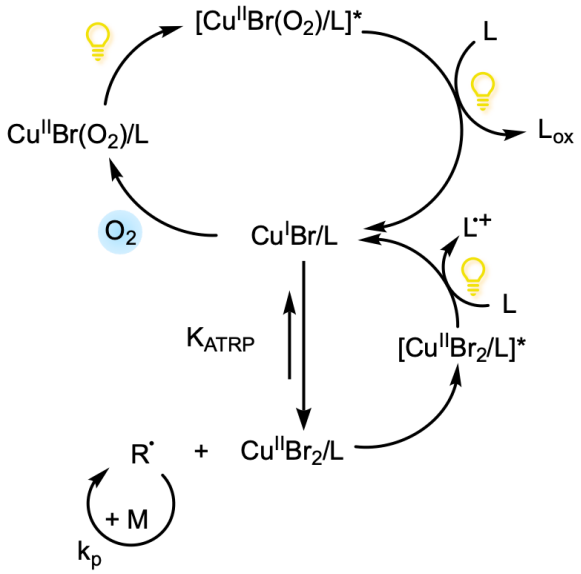

***Figure 14**: Proposed mechanism for an oxygen-tolerance photoATRP.*

2. Polymer Brushes

Polymer brushes are defined as long-chain polymer molecules attached by one end to an interface at relatively high coverage stretch away from the interface to avoid overlapping, forming a polymer *"brush"* [29]. Owing to their remarkable versatility, polymer brushes are widely employed as coatings in numerous industrial applications. These include their use as lubricants, as coatings for biomaterials, to stabilize colloidal solution or can be exploited to fabricate anti(bio)fouling films[30,31]. There are two different approaches for the synthesis of polymer brushes: the *grafting to* and the *grafting from* (Figure 15). In the *grafting to* approach pre-synthetized polymer chains with end-group functionality are grafted to a surface through a physical or chemical interaction (physisorption and chemisorption), thanks to the functionalization of one of the two ends of the polymer chain[32]. This approach involves many limitations, such as the formation of polymer layers with a low grafting density (σ) and a low average of layer thickness caused by steric repulsions. The *grafting from* approach requires a substrate modified with functional groups able to initiate a polymerization process in order to grow polymer chains via a surface-initiated polymerization[33]. This strategy, known as surface-initiated controlled radical polymerization (SI-CRP), is preferred over the first one since allows for precise control over polymer architecture, grafting density, composition, molecular weight and brushes thickness.

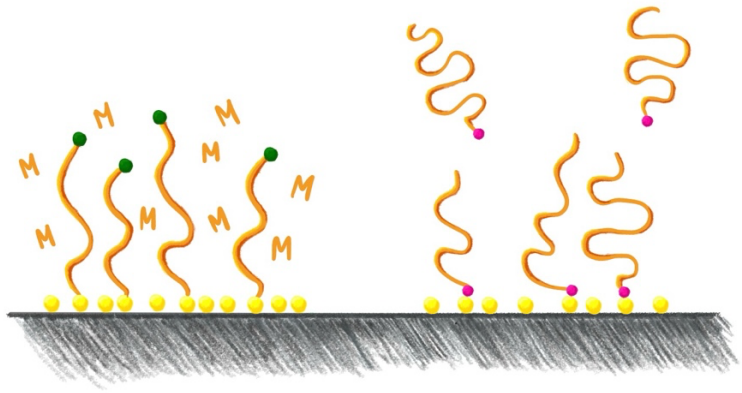

***Figure 15**: Schematic representation of grafting from approach (left) and grafting to approach (right).*

The molar mass, in *grafting from* approach, is governed by the mechanism of polymerization chosen to grow polymer brushes and is correlated to the thickness of the obtained polymer film. Different thicknesses lead to different employments of the functionalized surface: low thickness films can be employed for their bio inertness, lubrication[34] and wettability characteristics, on the other hand, high thickness is required for catalytic support.

Brush conformation, osmotic pressure at the interface and the surface density of functional groups are all influenced by the grafting density σ (amount of polymer chains per certain surface area).

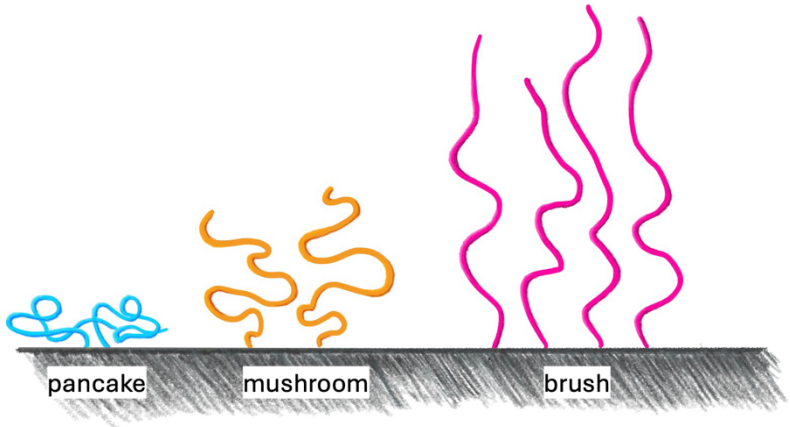

***Figure 16**: Brush conformations, from left to right: pancake, mushroom and brush.*

About the brush conformation, in relation to the grafting density, polymer chains can adopt the "mushroom", the "pancake" or the "brush" regime[33], (Figure 16) and the conformation of polymer brush can even be more pronounced depending on the solvent interaction, since a good solvent leads to a swollen state while a poor solvent causes the collapse of brushes. Furthermore, the thickness of the polymer film is proportional to the grafting density[35].

Đ has also been recognised as an additional parameter to alter the interfacial properties of polymer brushes. Steric stabilization, lubrication and biopassivity of polymer brushes have indeed shown dependence on dispersity. Obtaining polymer brushes with a controlled structure and a narrow dispersity has hence been represented a prerequisite to provide polymer films with well-defined properties. Surface-initiated controlled radical polymerizations (SI-CRPs) methods are the most effective techniques to modulate *Đ,* and recent advancement on this approach have demonstrated that dispersity can be tuned over a relatively broad range without compromising control over polymer chain growth or chain-end fidelity[36–38].

SI-CRP techniques also provide precise control over brush thickness (*i.e.*, polymer molar mass), σ, and polymer architecture. Despite these advantages, SI-CRP techniques tend to be strongly sensitive towards the reaction conditions, particularly to the presence of oxygen. This represents a limitation to large-scale synthesis of brushes and has consequently driven the development of processes compatible with non-deoxygenated reaction mixtures or exposure to the environment. To prevent the radical recombination with molecular oxygen, whit the consequent quench of the reaction, several oxygen-tolerant SI-RDRP techniques have been developed, employing sacrificial catalysts/cocatalysts, zerovalent metals and enzymes as oxygen scavengers[39].

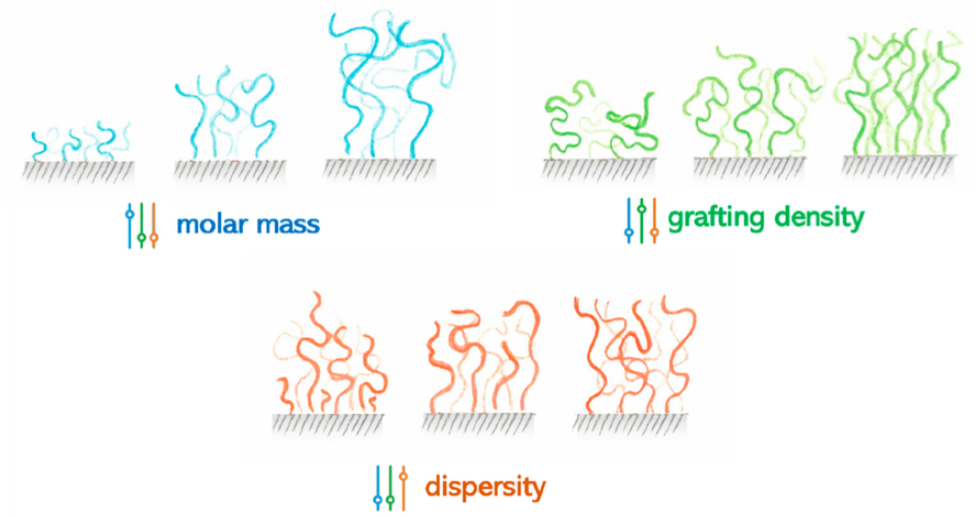

Figure 17*: The main structural parameters of polymer brushes: molar mass, grafting density and dispersity. By tuning these parameters the properties of polymer brushes can be modulated. Image taken from [36].*

2.2 SI-ATRP

Surface-initiated atom transfer radical polymerization (SI-ATRP) is a *grafting from* method that enables control over brush thickness, chain density and composition, by doing so ATRP can be used for surface modification. The most frequently used modified surfaces are flat surfaces and spherical particles, although SI-ATRP has largely been applied to a broad variety of substrates, including nanostructured and porous materials (Figure 18). Using a controlled radical polymerization provides the synthesis of polymers brushes with well-defined properties such as length, composition, dispersity and end groups on various substrate surfaces. Thanks to its controlled nature, SI-ATRP polymerization results convenient for the synthesis of multiblock copolymer brushes, providing a wide range of surface modifications[1].

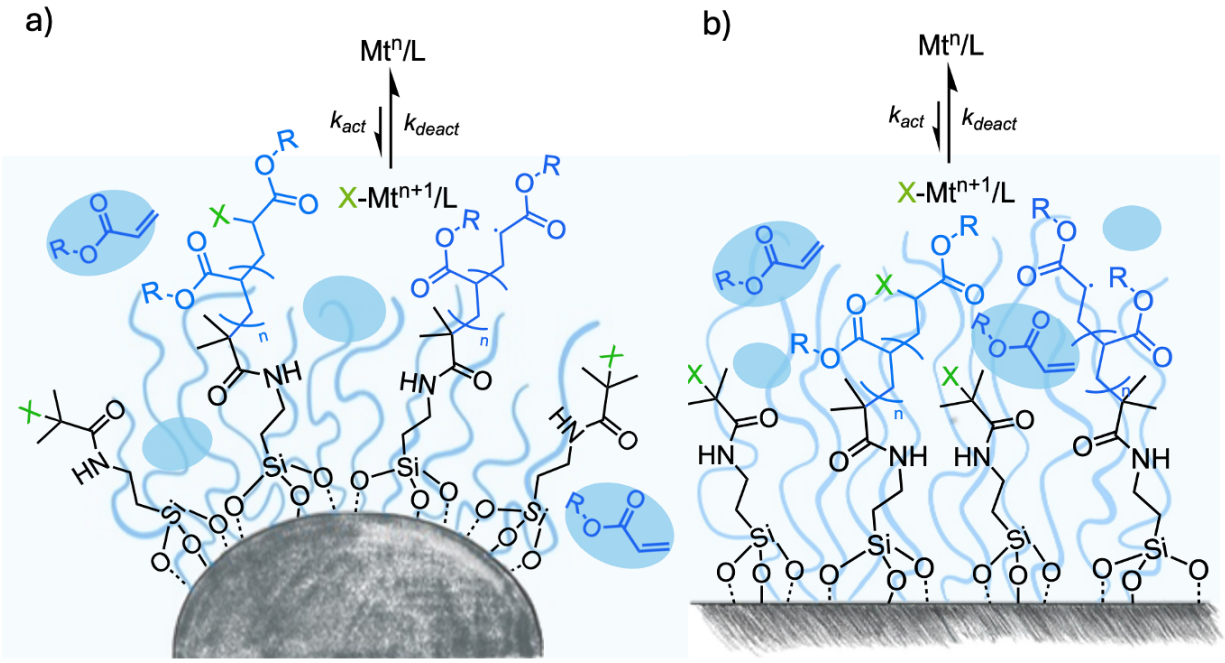

***Figure 18**: Graphic representation of brush growth through SI-ATRP from initiator functionalized surfaces: (a) spherical surface, (b) flat surface.*

The initial step of this method involves the functionalization of the substrate surface with a suitable ATRP initiator, which enables the subsequent surface-initiated polymerization. The initiator can be immobilized on the surface through either chemical bonds or noncovalent interaction. The functionalized substrate is then immersed in a solution containing the monomer and the other ATRP reagents. Upon activation, the initiator generates radicals that can initiate the polymerization, resulting in the growth of polymer brushes from the surface. As all ATRP reactions, to ensure the controlled polymerization, a transition metal catalyst, usually a Cu

catalyst, is used in order to achieve the equilibrium between dormant and active species[40]. As in classical ATRP, several SI-ATRP techniques have also been developed to circumvent the use of Cu(I) species. These methods employ copper complexes in different oxidation states, which are activated by an external stimulus (*e.g.*, a reducing agent or light). SI-ARGET ATRP exploit a large excess of reducing agent (typically ascorbic acid) to prevent inhibition of polymerization by oxygen.

In the presence of free ligand, Cu(I) species are oxidized to Cu(II) species, establishing the activation/deactivation equilibrium. In those types of systems, oxygen affects only the edges of the substrate. SI-photoATRP is another possibility to grow polymer brushes in a controlled manner, where the polymerization proceeds under irradiation of light and in the presence of electron donors capable of converting Cu(II) photoexcited species into Cu(I) activator[41]. As already mentioned, through mechanistic studies of photoATRP, in the presence of excess ligand and in a confined system, the polymerization results tolerant towards oxygen. This, translated in surface-initiated polymerization (SI-photoATRP), broaden the applicability of this method and facilitate the scaling-up of the system. Furthermore, classical surface-initiated ATRP requires the use of large quantities of catalyst, while applying this technique, lower concentrations of catalyst are required[26].

Differently from classicals CRP, in particular ATRP polymerization, in SI-ATRP the confinement of surface-tethered polymer chains affects the growth of polymer brushes, resulting in a shorter and more heterogeneous system. Notably chains tethered to a substrate compete for monomer and catalyst within an environment that becomes increasingly crowded as polymer brushes grow, progressively reducing the accessibility of the growing chain ends[3,4]. From a kinetic point of view, the behaviour of surface-initiated systems appears to differ from that observed in homogeneous media. The most prominent difference is the limited growth of polymer brushes through SI-ATRP polymerization, to be precise, brushes generated through SI-ATRP are generally restricted to a few tens to a few hundreds of nanometres. In surface-initiated ATRP, in fact, termination reactions are generally enhanced due to the proximity of radicals to the surface, resulting in changes in termination reactions compared to solution ATRP. Indeed, many kinetic studies have demonstrated that polymer brush growth progressively slows with increasing polymerization time, indicating an increasing contribution of termination reactions as the reaction proceeds. Cooperating to termination, loss of active catalyst and the hindered mass transport of monomers to propagating radicals limit the resulting thickness. Furthermore, as active chain ends are progressively lost, the continued growth of

polymer brushes progressively buries dormant chain ends under the outer brush layer, rendering them increasingly inaccessible to the catalyst activation and subsequent reaction with monomers[1,2,4]. Strategies to enhance polymer brush growth relies on the modification of polymerization environment to reduce termination reactions. To do so, systems with lower concentration of catalyst are largely studied, since lower concentrations of catalyst decrease the frequency of activation-deactivation cycles suppressing termination reactions[1,42].

This limitation has driven the development of strategies for the synthesis of ultra-thick polymer brushes. The high-pressure SI-ATRP method by Hsu et al. uses an expensive high-pressure equipment that works at 500 MPa and a Cu(I)/Cu(II) catalyst system to produce PMMA brushes up to 2 μm thick[43]. Other alternative approaches include the use of a tridimensional (3D) polymer initiator layer, such as poly(vinyl chloride), spin-coated on a silicon surface, obtaining 15.1 μm thick brushes. However, this strategy is constrained by the weak noncovalent binding of the initiator layer that provides physically entangled polymer grafts rather than covalently bound brush architectures. Additional methodologies rely on conductive surfaces, including glassy carbon and stainless steel, thereby significantly restricting the range of substrates that can be functionalized and limiting their broader applicability[44,45].

3. Inibramers

With the term *inibramer* we are defining a molecule that, in a polymerization process, can act as an *ini*tiator, a *bra*nching junction creator and a mono*mer* (Figure 19)[5].

These monomers trigger the branching process only after their incorporation into the growing polymer chain since they form a junction and from this junction can grow two distinct polymer chains. Containing a vinyl halide bond (C(sp^2)-X, X=Cl, Br) in the alpha position, inibramers are unreactive under normal ATRP conditions due to the high bond dissociation energy (BDE) of the C(sp^2)-X bond. Despite this, once the propagating radical is added to the inibramer, the resulting C(sp^3)-X bond, which has a lower BDE energy, can be activated, prompting the initiation of a new branch[46,47]. More explicitly, the branching junction is provided by the reactivation of the two C-X bonds at the alpha position, resulting from the radical addition of the inibramer and the subsequent deactivation (Figure 20)[48].

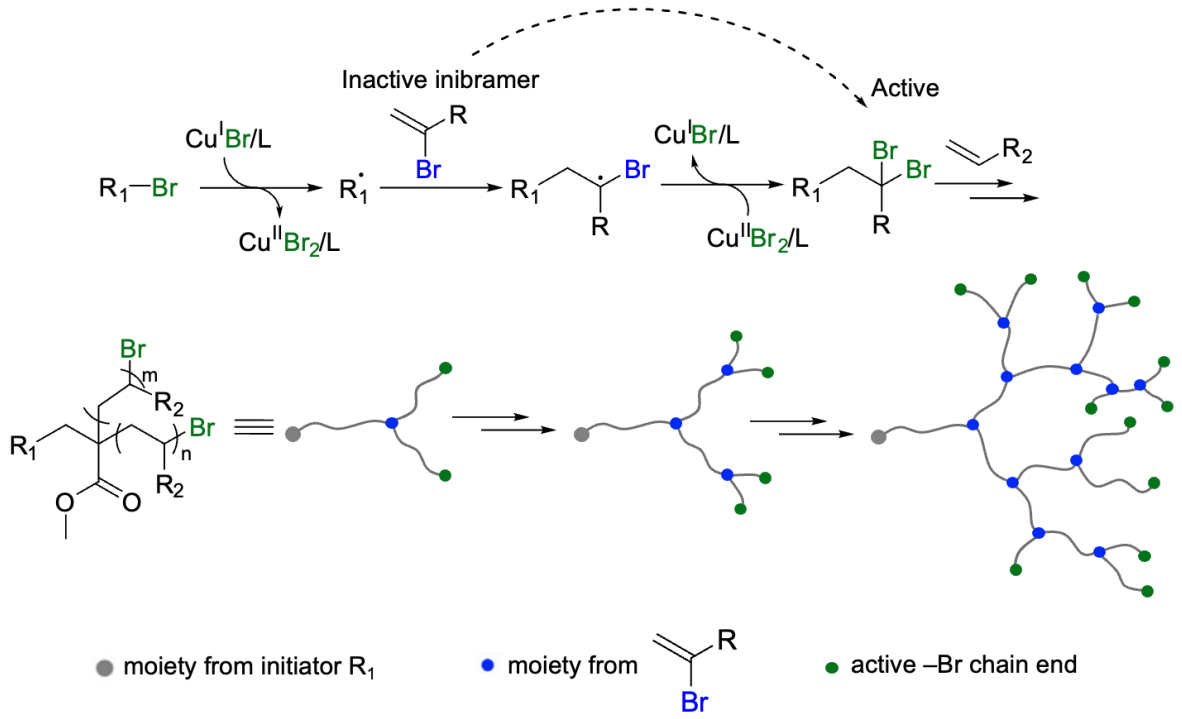

***Figure 20**: Proposed mechanism of an inibramer-enabled branching radical polymerization via ATRP.*

Those molecules have been synthetized to overcome some of the limitations associated with the synthesis of hyperbranched polymers (HBPs). Emerging as the most promising alternative to dendrimers, HBPs have attracted considerable interest thanks to their distinctive physical properties – weaker entanglements, lower intrinsic viscosity, multiple modifiable end-groups and the presence of cavities –. These characteristics have enabled their widespread use in the development of advanced functional materials. Despite this, achieving structural control over molecular weight and dispersity in the synthesis of HBPs remains a persistent challenge[5,46]. Zhong et al. developed a controlled radical polymerization technique using inibramers to achieve the synthesis of HBPs with a precise structural control, investigating the copolymerization under ATRP conditions of *n*-butyl acrylate (*n*BA) with *n*-butyl α-bromoacrylate (BBA) as inibramer. As a result of the distinct reactivity of the two monomers, explained by the reactivity ratios r_{BBA}=9.77 and r_{nBA}=0.24, the incorporation of inibramers in the growing polymer chains results higher compared to the acrylate. This results in an exponential increase in the concentration of propagating radicals with the consequent polymer gelation[48]. The resulting gradient copolymerization give rise to branched copolymers enriched in inibramer units in the early stages of the polymerization resulting in a heterogeneous distribution of branching junction along the polymer chains[49]. The higher reactivity of

inibramers originates from the presence of the branch-initiating functionalities at the α-position, which stabilizes the propagating radical, resulting in a faster incorporation. Consequently, regulating copolymerization kinetics remain challenging. Furthermore, for a given reactivity, the final architecture of the HBPs is influenced by the relative portion of inibramers compared to the monomers. Since each inibramer acts as a branching point, increasing its concentration leads to the formation of a greater number of branches and, consequently, to a higher degree of branching[50].

To achieve a more homogeneous incorporation of inibramers into the growing polymer brushes, a slow feed of this monomer in the polymerization solution proved to be the optimal strategy. Copolymers with a lower dispersity ($Đ$ < 1.3) and a more uniform distribution of the two monomers are indeed reported to be obtained[48].

4. Disulfide-Containing Vinyl Copolymers: Synthesis and Degradation

Commodity vinyl polymers, such as polyacrylates and polystyrenes, are largely used on a global scale in numerous applications, such as packaging materials, adhesives, coatings, electronics, constructions and for biomedical products. Due to the chemical inertness of the C-C bond along the backbone though, their degradation is limited, raising substantial concerns regarding environmental pollution. A smart solution to the degradability limitation is introducing in the polymer backbone a cleavable bond through a copolymerization, to obtain a polymer degradable under desired conditions[6],[7]. A promising moiety thanks to its facile degradability is the disulfide bond, which together with its low toxicity and biocompatibility is attractive for responsive biomedical applications but also for the generation of degradable polymeric materials. Those dynamic bonds can indeed be easily cleaved in the presence of reducing agents, nucleophiles, electrophiles or photochemically. The reductive scission of the sulfur-sulfur bridge can be regulated by the given environment since the redox potential of the R-S-S-R^I disulfide depends on the nature of the substituents R and R^I and the reaction environment[51]. Their facile degradation has generated a great deal of interest in polymers containing multiple disulfide groups in the backbone, owing to the broad range of applications of the resulting materials, including biomedical applications, dynamic and self-healing materials, adhesives and many others.

Disulfide moieties can be integrated into polymer structures via appropriately designed initiators or monomers. A promising monomers family is the one derived from α-lipoic acid (LA) as LA is commercially available at large scale and a natural occurring edible molecule.

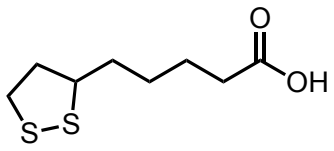

***Figure 21**: Structure of a-lipoic acid (LA).*

Further αLA and its derivatives copolymerize with various vinyl monomers, including acrylates[6,52]. Acrylates monomers have indeed been reported to undergo both traditional and controlled radical polymerization with lipoates. ATRP seems to be not a good pathway to polymerize these copolymers, in fact the coordination of sulfur atoms to the Cu catalyst can alter the ATRP equilibrium and reduce catalyst activity, resulting in poor control over the polymerization. RAFT polymerization appears to be the most suitable CRP technique to proceed with[6,7]. Acrylates are reported to be good comonomers to copolymerize with LA compared to other vinyl monomers (methacrylates or styrenics) due to their ability to cross-propagate[53].

Albanese et al. demonstrated, through a kinetic study of the copolymerization between LA and n-butyl acrylate (nBA), that the incorporation of the disulfide-containing monomer is faster compared to the acrylate monomer. This aspect is crucial for achieving more effective degradation, as this kinetic behaviour promotes the formation of disulfide bonds within diads along the polymer backbone. Furthermore, the higher is the mol% of LA the higher is the number of disulfides along the backbone, a feature that can be exploited to tailor polymer properties for specific applications[6].

A variety of methods have been developed for the synthesis of disulfide-containing polymers. Among all those, to typically obtain high molecular weight polymers, chain-growth reactions are the most suitable ones. Notably ring-opening polymerization (ROP) of cyclic disulfides, following both a radical or anionic mechanism, are appealing for the introduction of heteroatoms in the polymer backbone. As already mentioned before, among cyclic disulfides, lipoic acid and its derivatives are interesting as readily available and essentially non-toxic, but also for their kinetic and thermodynamic behaviour. First, LA easily polymerize when heated and presents a ceiling temperature, the specific temperature at which the rates of polymerization and depolymerization are exactly equal, of 139 °C. This latter point together with the

reversibility of the radical ROP explain why the polymerization is always incomplete (highest conversions achieved with the polymerization of ethyl lipoate around 75%)[54].

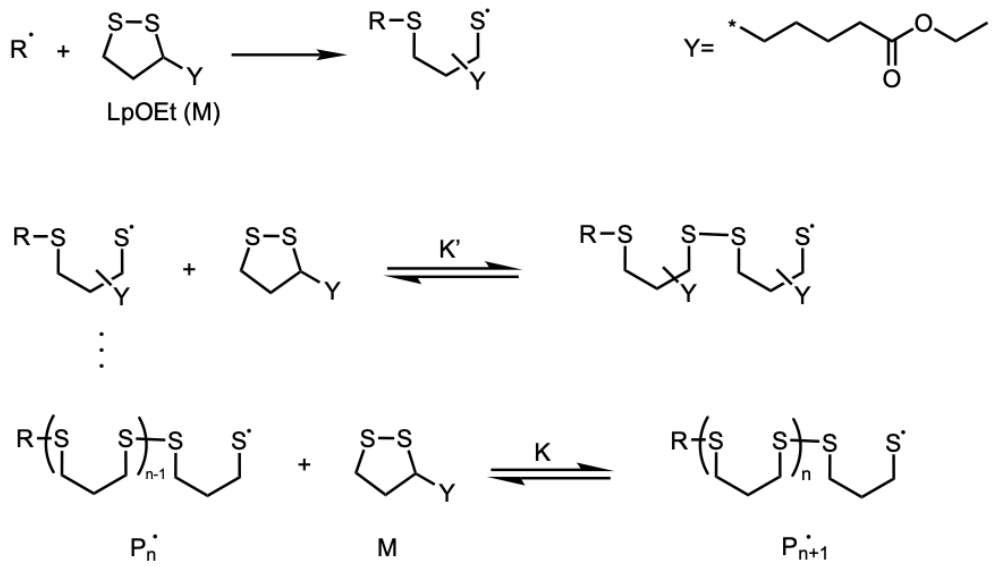

***Figure 22**: Mechanism of the reversible polymerization of LpOEt.*

4.1 Degradation of Disulfides Containing Polymers

Disulfide links can be cleaved reversibly, through reduction to thiol that can be reoxidized to disulfide, or irreversibly. The thiol-disulfide exchange has largely been explored in biochemistry, to cleave disulfide bonds in cysteine containing proteins. The degradation of the S-S bond is affected by both the polarity and composition of the reaction medium, as well as the nature and polarity of the polymer backbone. In the work by Tsarevsky and Matyjaszewski, it was shown how phosphines, more precisely Bu_3P, are good reducing agents for disulfide-containing polymethacrylates[51]. Further studies on the degradation of vinyl copolymers based on LA where conducted, highlighting the importance of tris(2-carboxyethyl)phosphine hydrochloride (TCEP) for its selectivity towards S-S bonds. The degree of depolymerization for copolymers containing those reducible bonds, derived from the reduction of the molecular weight observed, depends on both the loading of disulfide-containing monomers and the number of disulfide-containing diads formed. This is because of the selectivity of the reducing agents. To further enhance the molecular weight loss it is either possible to increase the incorporation of cleavable bonds, by arising the percentage of the monomer, or to employ reactants that target the C-S bonds in the backbone[7]. Thanks to the higher reactivity of lipoic

acid (LA) compared with acrylate monomers, the formation of degradable LA–LA diads is favoured, resulting in a greater reduction in molecular weight[6].

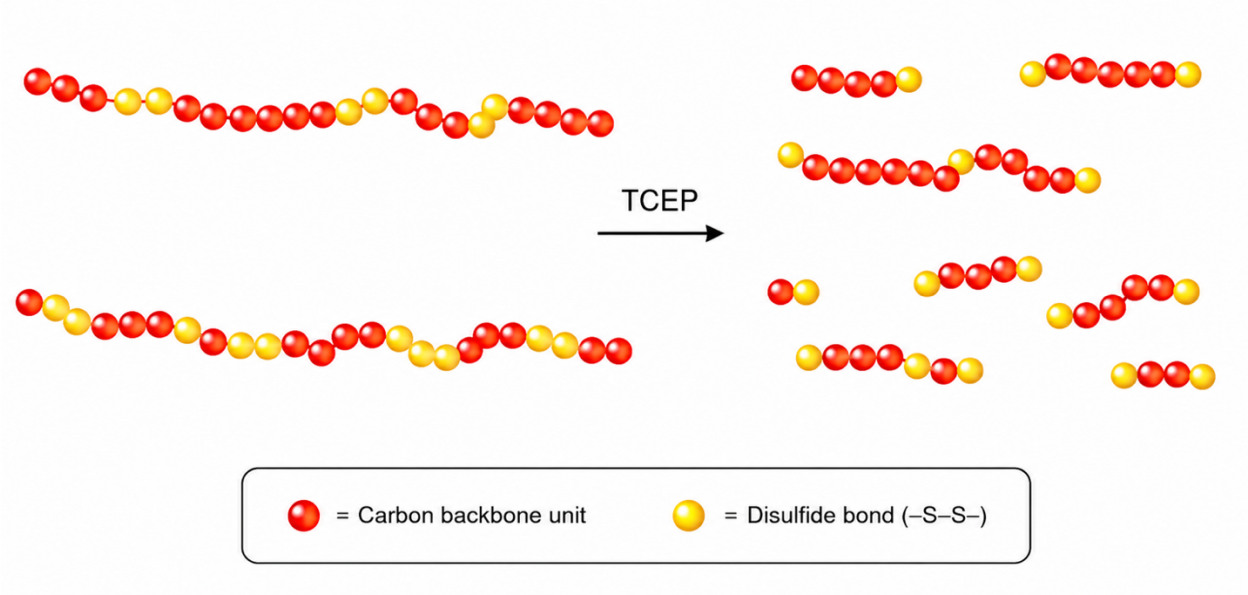

***Figure 23**: Graphic representation of disulfide-containing polymers degradation induced by TCEP. Increasing the incorporation of the disulfide-containing monomer results in a higher degree of degradation.*

.

5. Photochemistry and Photocatalysis

In photocatalysis visible light is used to promote organic transformation under mild reaction conditions, through the formation of reactive intermediates. Developed at the beginning of the twentieth century, particularly thanks to the work of Giacomo Ciamician, the interest in photocatalysis exponentially growth in the last decades[55].

The growing interest in photocatalysis arises from the possibility of obtaining products under milder conditions compared to thermal processes along with the opportunity of accessing compounds that are difficult to obtain with conventional methods.

A photochemical process starts when a compound in its singlet ground state S_0 absorbs a photon with its consequent promotion to one of the excited singlet states S_n, as reported in the Jablonski Diagram (Figure 24). From this excited state, which compared to the ground state possesses higher energy and a different reactivity, the molecule can undergo different relaxation pathways. It can be subjected to radiative decay through a florescence emission, in which the

decay occurs only form the first excited state S_1 as stated by Kasha's rule, or through a phosphorescence emission from the triplet state T_1. The latter scenario occurs when the molecule undergoes intersystem crossing (ISC), a non-radiative transition between electronic states with a different spin multiplicity. This allows phosphorescence, which according to the Kasha's rule should be forbidden. Other decays the molecule can undergo illustrated in the Jablonski Diagram (Figure 24) is the internal conversion (IC), the fastest non-radiative transition that brings the molecule to the ground state of a given electronic state.

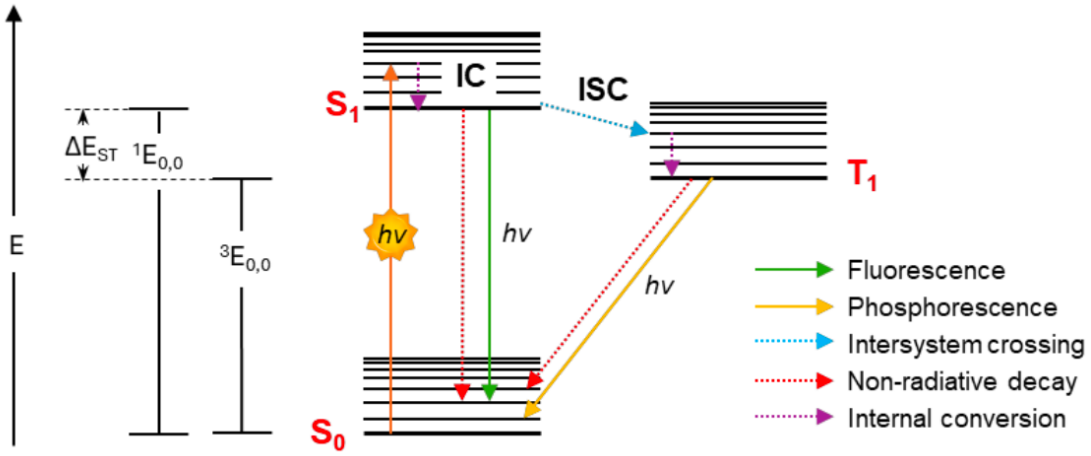

Figure 24: *Jablonski diagram.*

Exist two different ways to photochemically activate a molecule which differ in light-absorbing component: direct photochemistry and photocatalysis. In direct photochemistry one of the reactants directly absorbs light reaching an excited state, from which subsequently undergoes a chemical transformation. Ciamician and Silber largely contributed to the development of this strategy, explaining processes like the syn-anti isomerization of oximes, in which thanks to the photoexcitation of the substrate are accessible products not accessible under thermal conditions[56]. On the other hand, in photocatalysis is not directly absorbing light the reactant molecule, but it is a photocatalyst, working as an intermediary. The photocatalyst absorbs light, reaching an excited state that enables it to transfer energy, electrons or atoms to the reactants (the substrates), hence initiating a series of chemical transformation. It is subsequently regenerated at the end of the process, allowing it to participate in further catalytic cycles. Photocatalysts are indeed defined by IUPAC as *Catalysts able to produce, upon absorption of light, chemical transformations of the reaction partners. The excited state of the photocatalyst repeatedly interacts with the reaction partners forming reaction intermediates and regenerates*

itself after each cycle of such interactions. In the beginning photocatalyst were based on metal-based complexes, predominantly of iridium and ruthenium, such as tris(2,2′-bipyridine) ruthenium(II), or $Ru(bpy)_3^{2+}$ [57]. Their use though presents some issues, firstly because they are made from expensive rare-earth metals. They are commonly toxic and their synthesis usually request non environmentally friendly steps[58]. As consequence an increasing interest in visible light organo-photoredox catalysts has been developed, proving the synthetic potential and the versatility of metal-photocatalysts[59]. Moreover, organic photocatalysts present the advantage of an easy modification of their chemical structure to adjust properties like solubility, redox potential and light absorption with the consequent enhancement of the catalytic activity. Significant examples of organic photocatalysts are dyes such as Eosin Y, Rose Bengal, Fluorescein and many others.

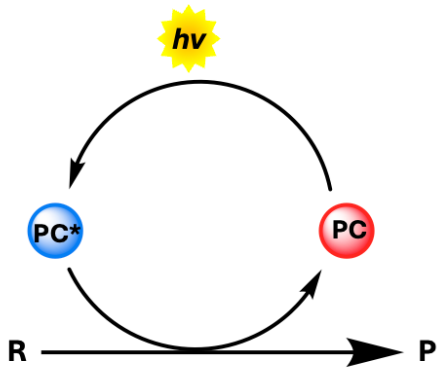

***Figure 25**: General scheme of a photocatalyzed reaction.*

In photocatalysis is possible to distinguish different mechanisms: hydrogen atom transfer (HAT), halogen atom transfer (XAT), energy transfer (EnT), electron transfer (ET) and proton coupled electron transfer (PCET).

In hydrogen atom transfer (HAT) the photocatalyst in its excited state (PC*) is capable of abstract an hydrogen atom from a substrate, activating it. Subsequently the protonated photocatalyst (PC-H) can donate the hydrogen atom to another substrate closing the photocatalytic cycle (Figure 26). Thus far, only a few photocatalysts have been reported to perform this chemistry, most of which belong to the families of aromatic ketones, polyoxometalates and a few others[60].

When the starting substrate is an organic halide (R-X), interaction with the excited photocatalyst PC* leads to the formation of the carbon-centred radical, through C-X bond cleavage, and a halogen-bound photocatalyst (PC-X). This process is commonly referred to as halogen atom

transfer (XAT) (Figure 27). As in the previous process, the PC-X can donate the halogen atom (X*) to another substrate whit the consequent regeneration of the catalyst[61].

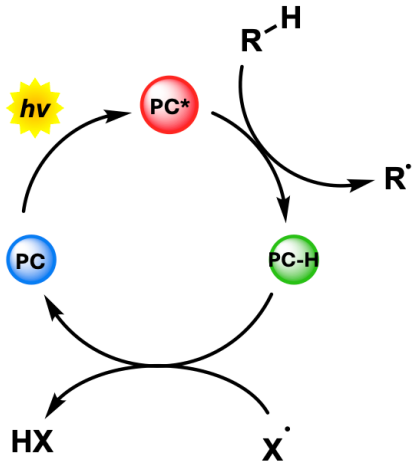

***Figure 26**: HAT mechanism pathway.*

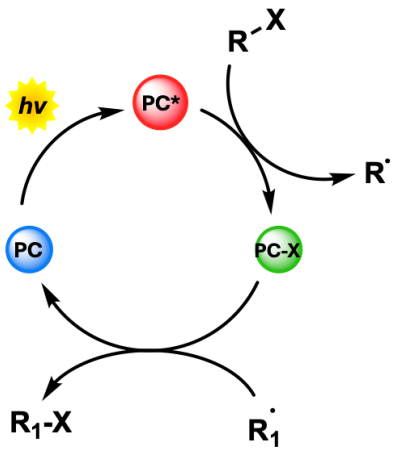

***Figure 27**: XAT mechanism pathway.*

Energy transfer (EnT) catalysis operates through the triplet excited state of the photocatalyst (Figure 28). From its excited S_1 state the PC can undergo inter system crossing (ISC) accessing its triplet state T_1. The excited catalyst can thereafter transfer its excited state energy to a substrate (or acceptor), thereby indirectly promoting the acceptor to an excited state. Since the acceptor generally does not exhibit significant visible light absorption, this indirect, non-radiative energy transfer pathway is required to achieve its excitation. For this non-radiative EnT have been proposed two different mechanisms. The first one proceeds through dipole-

dipole interactions between molecules where energy can be transferred via a *transmitter-antenna mechanism* (donor-acceptor mechanism). This process is known as Förster (Resonance) Energy Transfer (FRET). The second mechanism, proposed by Dexter, involves the simultaneous intermolecular exchange of ground-state and excited-state electrons. In this process, the excited PC* donates an electron to the LUMO of the substrate which simultaneously donate an electron to the HOMO of the photocatalyst. As a consequence of this concerted electron exchange, the substrate is promoted to its excited state, whereas the photocatalyst returns in its ground state[62].

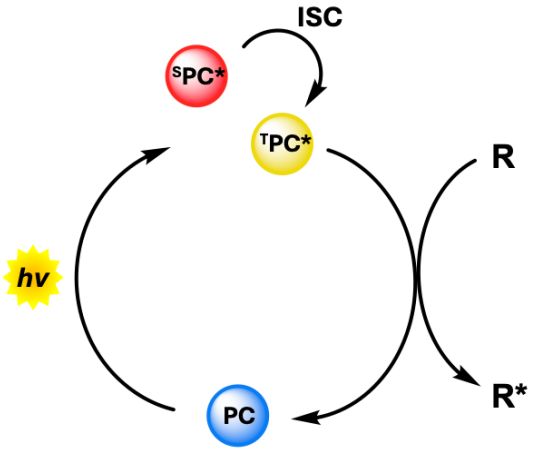

***Figure 28**: EnT mechanism pathway.*

In electron transfer (ET) processes the photocatalyst reaches its excited state, generally the singlet excited state, becoming both more reductive and oxidative due to changes in its molecular orbitals.

This is a consequence of the promotion of an electron from the highest occupied molecular orbital (HOMO) to the lowest unoccupied molecular orbital (LUMO), which results in the formation of two singly occupied molecular orbitals (SOMOs) (Figure 29). The lowest SOMO in energy is more stable than the corresponding HOMO of the ground state, resulting in a better oxidant PC*. On the contrary higher SOMO is destabilized with respect to the LUMO of the ground state giving rise to a PC* with enhanced reductant properties[63].

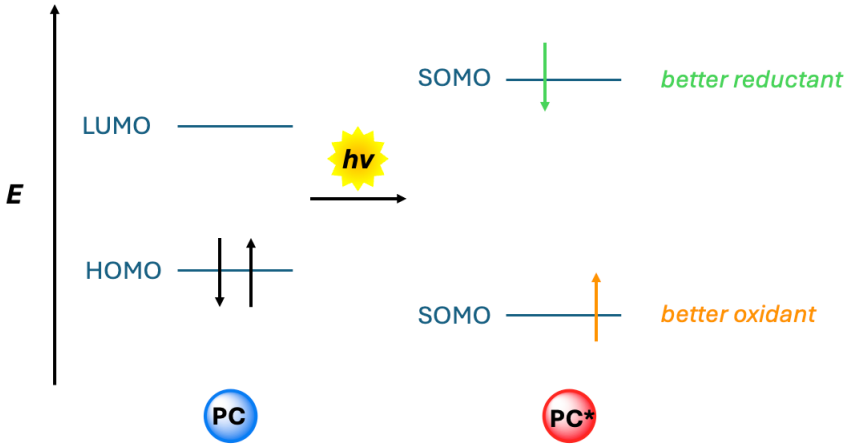

***Figure 29**: Energy level comparison between ground state and excited state of a photocatalyst.*

Hence the excited photocatalyst can donate or accept an electron, giving access to two different pathways: a reductive quenching and an oxidative quenching (Figure 30).

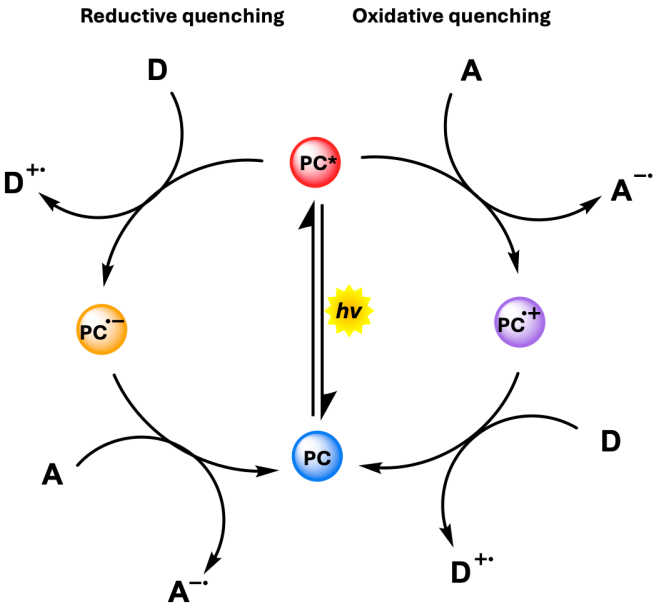

***Figure 30**: Electron transfer mechanism.*

In the oxidative quenching pathway, the excited photocatalyst (PC*) donates an electron to an acceptor (A), forming a radical cation (PC^{*+}) and the reduced acceptor species (A^{*-}). Then, a donor molecule (D) donates an electron to PC^{*+}, regenerating the ground state photocatalyst, with the consequent reduction of the substrate.

Whereas, in the reductive quenching pathway, the excited photocatalyst (PC*) accepts an electron from an electron donor (D), generating the radical anion (PC^{*-}). Subsequently the

photocatalyst transfers an electron to an acceptor molecule (A), thereby regenerating the ground state photocatalyst (PC).

Proton coupled electron transfer (PCET) is used for the activation of C-H or X-H (X=N, S, O) bonds with the generation of C* or X* radicals (Figure 31). This is because this strategy combines aspects of both electron and hydrogen atom transfers. The excited photocatalyst in fact transfers simultaneously both an electron and an hydrogen atom generating the radical species of the substate. As in the electron transfer process, also in this process are distinguished a reductive and an oxidative quenching[64,65].

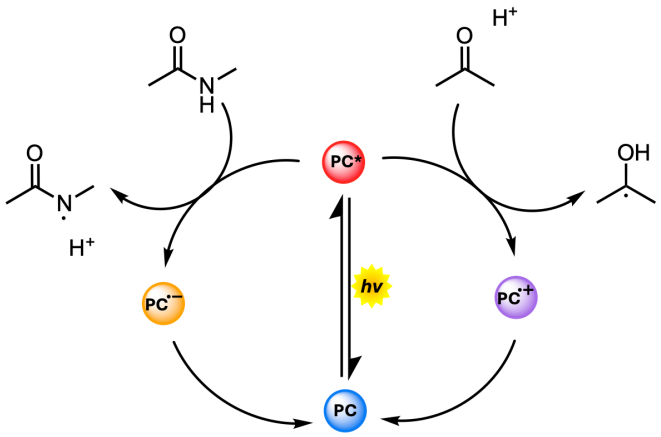

***Figure 31**: PCET mechanism.*

Multiple factors determine whether the excited PC is reacting from its triplet state (primarily an energy transfer process) or its singlet state (predominantly an electron transfer mechanism). Typically, the energy transfer process necessitates the substrate to exhibit a lower triplet energy compared to the excited photocatalyst's one. Conversely, when both pathways are possible, the formation of the complex between the substrate and the excited photocatalyst is determined by the relative rates of intersystem crossing (k_{ISC}) and diffusion (k_{diff}). When k_{ISC} is lower than k_{diff} the formation of the complex in its singlet state, $^{1}PC^*$, is enhanced, making the electron transfer favourable. If k_{ISC} is higher than k_{diff} though, the energy transfer is favoured, since the complex in the triplet state ($^{3}PC^*$) is formed. Consequently, by selecting an appropriate photocatalyst, it is possible to control the dominant reaction pathway and, ultimately, achieve the desired reaction outcome.

6. Aim of this project

The first part of this thesis was motivated by the evident limitations in the brush thickness attainable by conventional SI-ATRP, which arise from the progressive depletion of accessible propagating chain ends during polymerization. Kinetic studies of ATRP polymerization have indeed revealed a different behaviour of surface-initiated systems compared with that observed in homogeneous media. In the former, enhanced termination reactions progressively reduce the rate of polymer brush growth. This effect, combined with loss of active catalyst, hindered mass transport of monomers to propagating radicals, and the progressive burial of active chain ends within the growing polymer brushes, ultimately restrict the achievable brush thickness to only a few hundreds of nanometres[1,2,4]. Furthermore, the alternative methods reported in literature, although highly effective, require complex systems that limit their accessibility[1,42,42]. The idea was then to find an alternative strategy to continuously regenerate propagating sites, mitigating the progressive depletion of accessible chain ends.

The recent studies on *inibramers* inspired this work. Those initiator-branching-monomer agents combine a polymerizable vinyl group with a latent ATRP initiating functionality possessing markedly different reactivities. During solution ATRP, preferential incorporation of the vinyl group followed by delayed activation of the initiating functionality generates hyperbranched macromolecules with programmable branching density[5]. The assumption is that, under SI-ATRP conditions, inibramers, rather than solely controlling the polymer architecture, could, once incorporated into the growing brush, continuously generate new propagating grafts, thereby compensating for the progressive loss of accessible chain ends caused by radical termination and chain-end burial. The study of this system, with particular emphasis on the inibramer concentration and its behaviour with different monomers, aims to enable the synthesis of ultrahigh-molecular weight (UHMW) polymer brushes under otherwise conventional polymerization conditions.

After achieving the controlled growth of UHMW polymer brushes, the second part of this thesis focused on the development of photocatalytic methods for the controlled degradation of vinyl polymers. This objective was motivated by the desire to develop degradable materials that retain the properties of the most widely utilized non-degradable polymers, vinyl polymers. This goal can be pursued by copolymerizing vinyl monomers, in this case acrylates, with cyclic disulfide monomers, thereby introducing cleavable bonds into the polymer backbone. Inspired by the work of Zhou *et al.*[66], who demonstrated the light-induced reduction of disulfide bonds in peptides and proteins using thioxanthone, a photocatalyst, our work focused on finding suitable

photocatalysts able to promote the degradation of polymers containing disulfide bonds in their backbone. Importantly, this photocatalytic strategy enables degradation under mild conditions using visible or near-UV light, thereby avoiding the need for deep-UV irradiation typically required for direct disulfide photolysis.

Results and discussion

7.1 Programming Propagating Radicals Through Inibramers for Sustained Polymer Brush Growth

The first part of this thesis focuses on developing an alternative strategy to overcome the limited thickness of polymer brushes obtained through SI-ATRP polymerization. Since the primary limitations arise from the progressive depletion of accessible propagating chain ends during polymerization, caused by irreversible bimolecular radical termination[1,2], and the progressive burial of dormant chain ends beneath the brush layer[3,4], our strategy relies on the continuous regeneration of propagating sites throughout brush growth, replenishing the progressive loss of active chains. Although initially developed for different purposes, *inibramers* (initiator-branching-monomer agents) appear to be well suited to enable this concept. The hypothesis is that those molecules, under the unique conditions of SI-ATRP, may assume a fundamentally different role compared to their function in solution ATRP, and the presence of the halogen in the alpha position to the carbonyl group can have a different effect instead of controlling the polymer architecture. Trace amounts of inibramers can generate new propagating grafts upon incorporation into the growing polymer chains, thereby replenishing the active functionalities lost through radical termination and chain-end burial.

To support this hypothesis, the growth of polymer brushes incorporating methyl α-bromoacrylate (BrMA) as a model *inibramer* was investigated employing SI-photoATRP. The choice of SI-photoATRP as polymerization techniques derives from its operational simplicity and mild reaction condition, together with the lower concentration of copper catalyst required[26]. In combination with BrMA, synthetized following a modified literature procedure (Supporting Information), acrylates have been selected as comonomers. The exclusion of methacrylates from this study is motivated by the reported β-carbon fragmentation of the backbone via formation of mid-chain radicals upon activation of the C-Br bond[46].

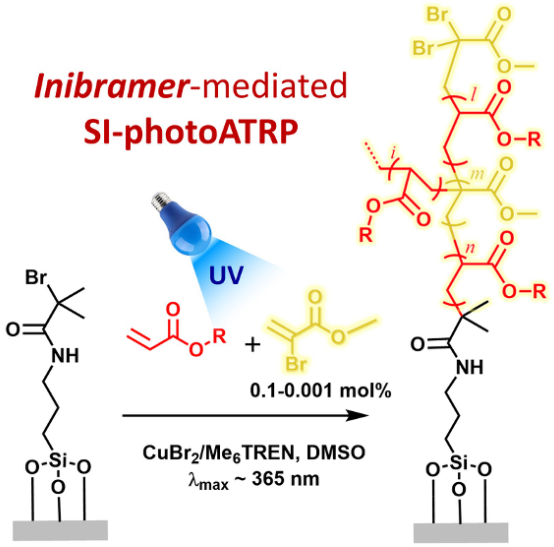

***Figure 32**: Inibramer-mediated SI-photoATRP for the synthesis of polymer brushes from silicon surfaces.*

The selected acrylates tested in this thesis are *tert*-butylacrylate (*t*BA), *n*-butyl acrylate (*n*BA) and oligo(ethylene glycol) acrylate (OEGA, M_n ~ 480 g mol^{-1}) (Figure 32).

7.1.1 SI-photoATRP of tert-butylacrylate (tBA) Brushes

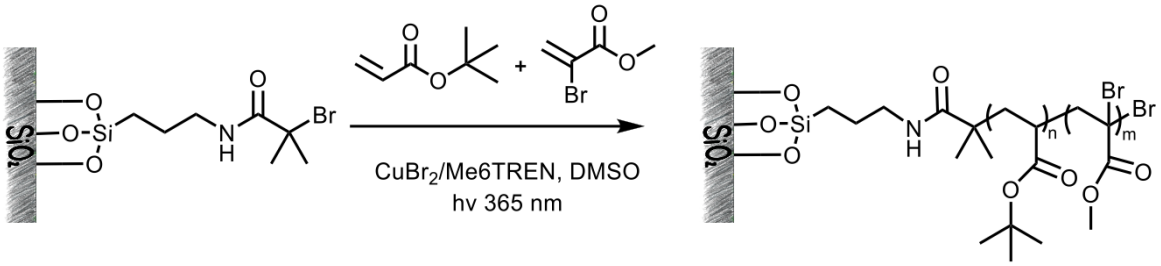

***Figure 33**: Schematic representation of the BrMA-mediated SI-photoATRP of tert-butyl acrylate (tBA) from silicon surfaces under UV irradiation.*

SI-photoATRP mixtures comprised $CuBr_2$, tris[2-(dimethylamino)ethyl]amine (Me_6TREN) as ligand (L) (with [$CuBr_2$]:[L] of 1:6), *tert*-butylacrylate (*t*BA) and variable amounts of BrMA (Figure 33). Under UV light irradiation (λ_{max} =365 nm, 7.0 mW cm^{-2}) and in the absence of *inibramer*, polymerization of *t*BA yielded polymer brushes with a dry thickness (T_{dry}) of 389 ± 21 nm after 1 h. Extending the UV light irradiation time to 3 h led to a slight increase in brush thickness, with T_{dry} reaching 508 ± 3 nm (Figure 34). This observation is consistent with

previous studies on polymer brush growth through SI-ATRP techniques, which have demonstrated how, beyond a certain polymerization time, termination reactions and the progressive burial of active chain ends significantly impede further brush growth[1,2,4].

With the addition of BrMA at concentrations of 1-5 mol% the growth of poly(*tert*-butyl acrylate) (P*t*BA) brushes was significantly inhibited, with T_{dry} not exceeding 2 nm after 3h of irradiation time (Figure 34). Considering the highly unbalanced reactivity ratios for closely related acrylates and *inibramer* reported in literature (for the *inibramer* r_{BBA}=9.77 and for the acylate r_{nBA}=0.24)[48], the observed behaviour can be rationalized. This suggests that BrMA is incorporated into the growing polymer chains preferentially over the acrylate during the early stages of polymerization. Consequently, the local enrichment of latent initiating sites is expected to generate a high local radical density once these sites are activated. As a result, the probability of bimolecular termination increases, overweighting the expected benefit of the *inibramers* in replenishing the lost chain-ends. Furthermore, the excess number of latent initiating sites generates highly branched layers at the early stages of brush growth, thus increasing steric congestion and limiting the propagation of neighbouring grafted chains.

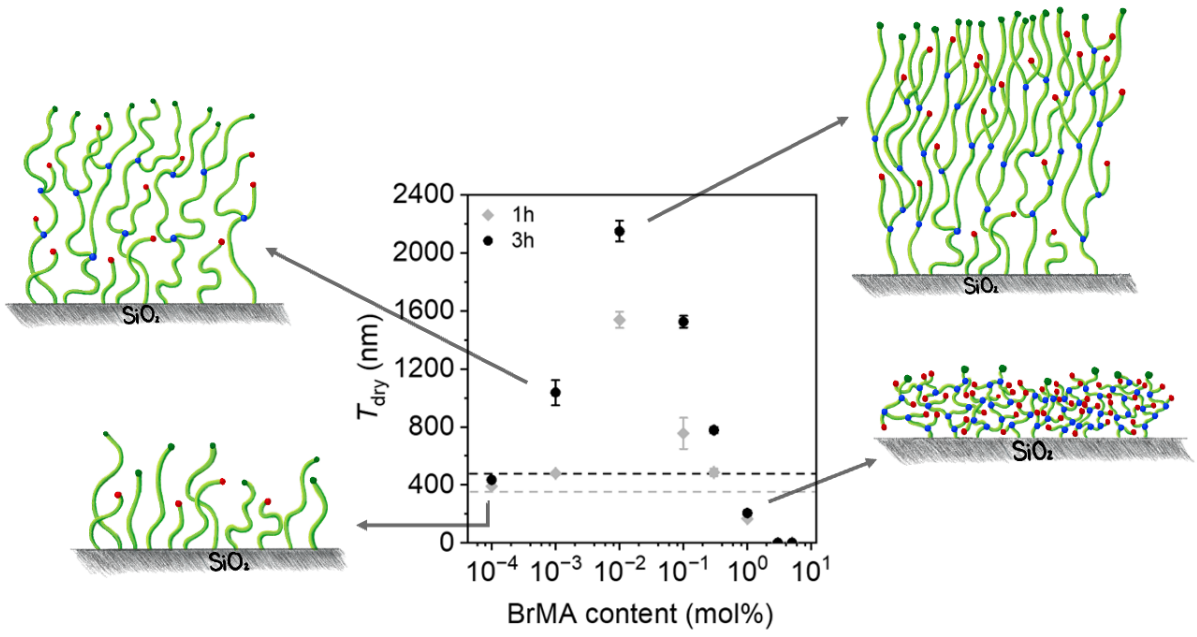

***Figure 34**: SI-photoATRP of tBA (1.35 M) with $CuBr_2$/Me_6TREN under UV irradiation (λ_{max} = 365 nm, 7.0 mW cm^{-2}). Dry PtBA brush thickness measured by ellipsometry and AFM as a function of BrMA content (mol% relative to tBA). The dotted lines indicate the control without BrMA.*

On the other hand, the addition of lower concentrations of BrMA, in the range of 0.5-0.001 mol%, significantly enhanced polymer brush growth. In particular, the dry thickness of P*t*BA brushes depends on the *inibramer* concentration. The maximum brush thickness was achieved

with the addition of only 0.01 mol% of BrMA, yielding T_{dry} values exceeding 1.5 μm after 1 h of irradiation, and reaching more than 2 μm after 3 h (Figure 34). Here, although BrMA is still incorporated preferentially relative to *t*BA, under these reaction conditions its trace concentration limits the rate at which new initiating sites are introduced during brush growth.

Differently from conventional solution ATRP, in which increasing monomer conversion continuously alters the instantaneous feed composition and, consequently, the incorporation profile of highly reactive comonomers, in surface-initiated ATRP, due to the absence of sacrificial initiator, the overall monomer conversion results negligible, causing minimal changes in bulk feed composition. This latter effect, together with the low concentration of *inibramer*, effectively distributes the formation of new propagating grafts throughout the course of brush growth. This mechanism of generation of new growing points replenishes the population of accessible propagating chain ends compensating for their progressive depletion through radical termination and chain-end burial.

As mentioned before has been found an optimum concentration or BrMA, at which, despite the unfavourable reactivity of BrMA, the generation of new growth points and the chain-end depletion counterbalance each other. As revealed in Figure 34, at higher *inibramer* concentration, the excessive incorporation promotes radical termination and steric congestion. On the other hand, decreasing the BrMA concentration gradually reduces the generation of new propagating sites, resulting in brush growth that progressively resembles that observed in the absence of *inibramer*. At a BrMA concentration of 0.0001 mol%, the effect of the inibramer becomes almost negligible. The observation of this trend elucidates the role of inibramer, which is not only to maximize the numbers of initiating sites but also to balance their generation with the progressive depletion during SI-ATRP.

This is also confirmed in the kinetic studies for the growth of P*t*BA brushes in the absence of BrMA and for polymerization mixtures containing different inibramer concentrations (Figure 35).

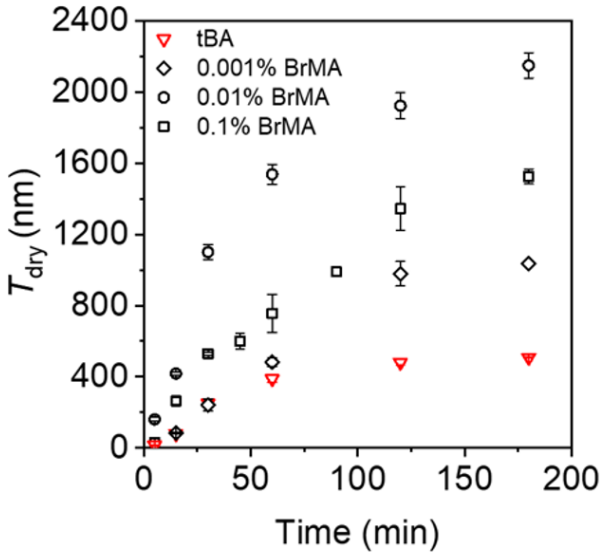

***Figure 35**: Brush growth kinetics of PtBA brushes at BrMA contents of 0, 0.001, 0.01, and 0.1 mol% relative to tBA.*

As can be observed in Figure 35, the growth of P*t*BA in the absence of inibramer increases during the first 60 minutes of polymerizations, as evidenced by the progressive thickening of the film. Thereafter the growth reaches a plateau due to the depletion of accessible chain ends through radical termination and chain-end burial. The addition of only 0.001 mol% BrMA delayed the onset of the growth plateau, enhancing brush thickening over longer polymerization times and yielding a T_{dry} approaching 1 µm after 2 h of irradiation. This behavior aligns with the continuous generation of new propagating growth points, which counterbalances the progressive loss of accessible chains due to radical termination reactions and chain-end burial, allowing the polymerization of polymer brushes with thicknesses beyond the limits typically achieved by conventional SI-ATRP. During the early stages of polymerizations (≤60 minutes), at this BrMA concentration, is evident how the polymer brush growth remains essentially unaffected by the presence of the inibramer, as the brush thickening kinetics closely overlap with those observed for BrMA-free polymerization mixtures. Thus, as the inibramer concentration increases (0.01-0.1 mol%), a second effect becomes apparent. In addition to delaying the onset of the late-stage growth plateau, the inibramer progressively influences the kinetics of the initial stages of brush growth. This significantly faster brush growth observed during the first 20-30 minutes of polymerization is in line with the mechanism described above: the different reactivity ratios, of the *inibramer* and the monomer, favour the BrMA early incorporation, which generates a higher effective density of propagating growth points within

the developing brush. This increased population of growing points complements to the accelerated initial thickening while continuously replenishing the loss of propagating chain-ends. The continuous replenishment of chain ends combined with the initial increase in the density of propagating growth points give rise to polymer brushes with a remarkably enhanced thickness. Indeed, after only 3 h of polymerizations, P*t*BA brushes synthetized with the inibramer incorporated achieve dry thicknesses exceeding 2 µm, corresponding to an approximately twenty-fold increase over conventional SI-photoATRP.

Through atomic force microscopy (AFM) measurements, the morphology of the ultra-thick brushes obtained by inibramer-mediated SI-photoATRP was also investigated. This revealed that the morphology of these ultra-thick brushes was very similar to that of thinner brushes generated using conventional ATRP mixtures. Topography micrographs recorded on ~ 2 µm thick P*t*BA brushes were characterized by a root mean square (RMS) roughness of only 3.4 nm (recorded over 5×5 µm²), which agreed well with the corresponding RMS roughness for 508 nm-thick P*t*BA brushes fabricated through standard SI-photoATRP (Figure 36). This demonstrated that incorporation of inibramer units did not significantly altered the micro/nanostructure, preventing the cross-linking between grafts or the formation of aggregates[30,31].

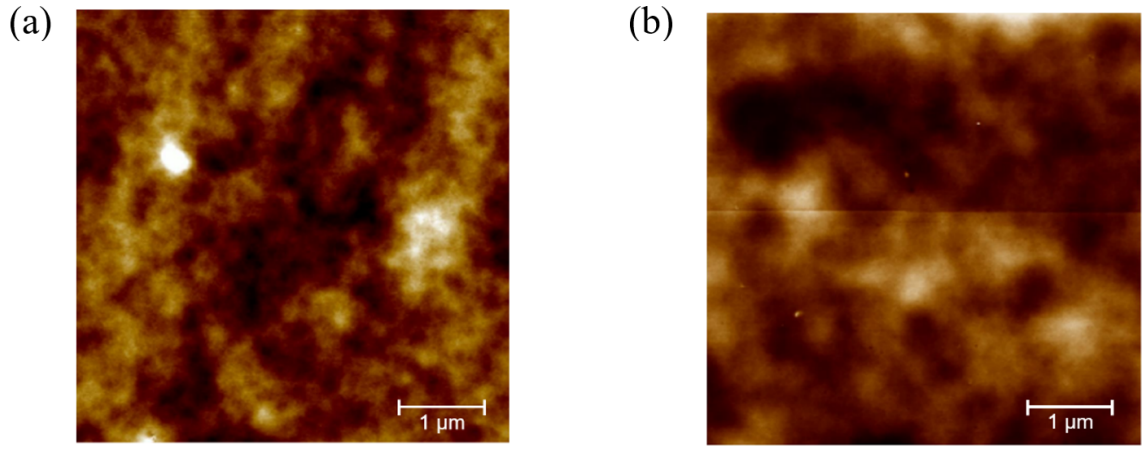

***Figure 36**: AFM topography images (5 × 5 µm²) of PtBA brushes prepared with (a) 0 and (b) 0.01 mol% BrMA. The corresponding dry thicknesses were approximately 500 and 2150 nm, with RMS roughness values of 1.9 and 3.4 nm, respectively.*

Once understood the mechanism underlying *inibramer*-mediated brush growth in P*t*BA, different acrylate monomers have been investigated to determine whether the combination of the two proposed kinetic contributions is generally applicable.

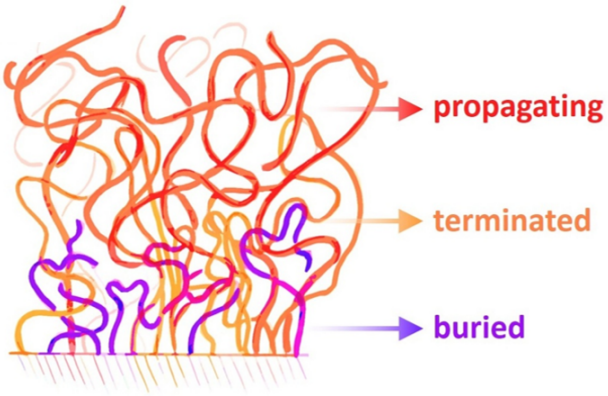

***Figure 37**: Schematic depicting polymer brush growth in the absence of inibramer, where propagating, terminated, and buried chains are highlighted.*

7.1.2 SI-photoATRP of *n*-Butyl Acylate Brushes

Under reaction conditions closely matching those optimized for P*t*BA, polymer brushes using *n*-butyl acrylate (*n*BA) and BrMA were synthetized using SI-photoATRP (Figure 38).

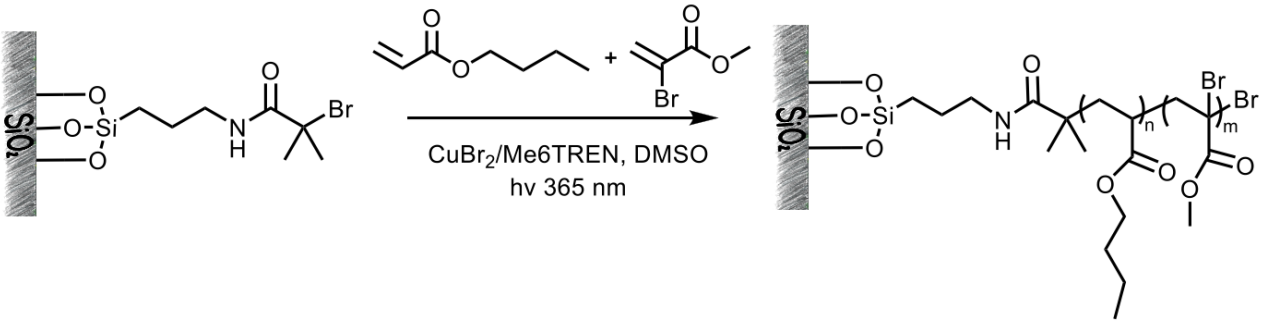

***Figure 38**: Schematic representation of the BrMA-mediated SI-photoATRP of n-butyl acrylate (nBA) from silicon surfaces under UV irradiation.*

Also in this case, as shown in Figure 39a, the addition of trace amounts of inibramer dramatically enhanced the growth of poly(*n*-butyl acrylate) (P*n*BA) brushes, demonstrating an optimal BrMA concentration window (0.01-0.1 mol%) analogous to that identified for P*t*BA. Within this concentration range, P*n*BA brushes exceeding 1.3 µm in dry thickness were readily obtained after 3 h of SI-photoATRP. Notably, as illustrated in Figure 39b, P*n*BA reproduced the two kinetic signatures previously identified for P*t*BA. The addition of 0.1 mol% BrMA enhanced both a faster brush growth rate during the early stages of polymerization (first 60 minutes) and a significant delay in the onset of the growth plateau associated with radical termination reactions and chain-end burial. Conventional SI-photoATRP of *n*BA, after

approximately 2 hours of light irradiation achieved a limiting thickness of T_{dry} close to 600 nm. Polymer brushes grown in the presence of inibramer continued to thicken at an almost constant rate, reaching a dry thickness of approximately 1.5 µm after 4 h. The preservation of these two kinetic contributions reveals that the dual contribution of the inibramer, the early generation of additional propagating growth points and the persistent replenishment of accessible chain ends, represents a general feature of acrylate SI-photoATRP (Figure 40).

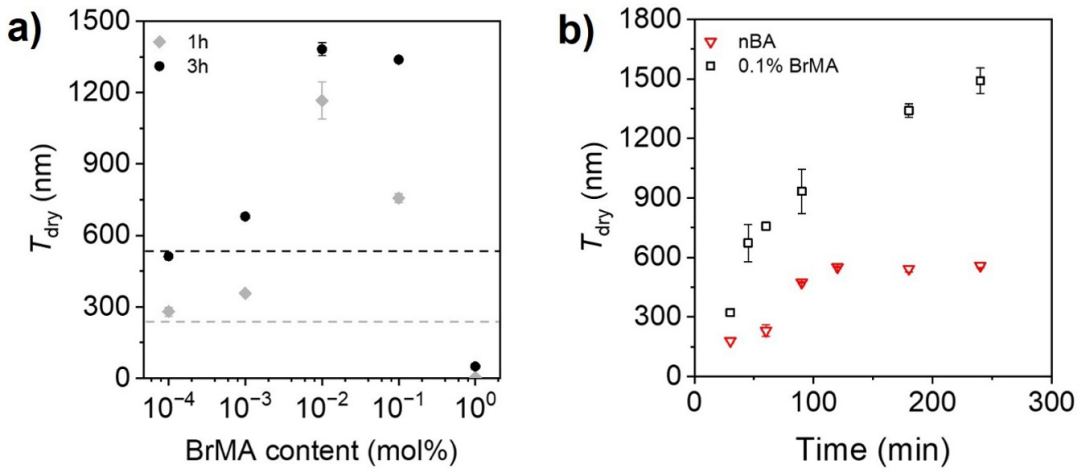

***Figure 39**: SI-photoATRP of nBA (1.35M) with $CuBr_2$/Me_6TREN with UV light irradiation (λ_{max} =365 nm, 7.0 mW cm^{-2}). (a) Dry thickness of PnBA brushes measured by VASE and AFM as a function of BrMA content (mol%) relative to nBA. The dotted line corresponds to the control experiment performed in the absence of the inibramer. (b) Growth kinetics for PnBA brushes at 0 and 0.1 mol% of BrMA content relative to nBA.*

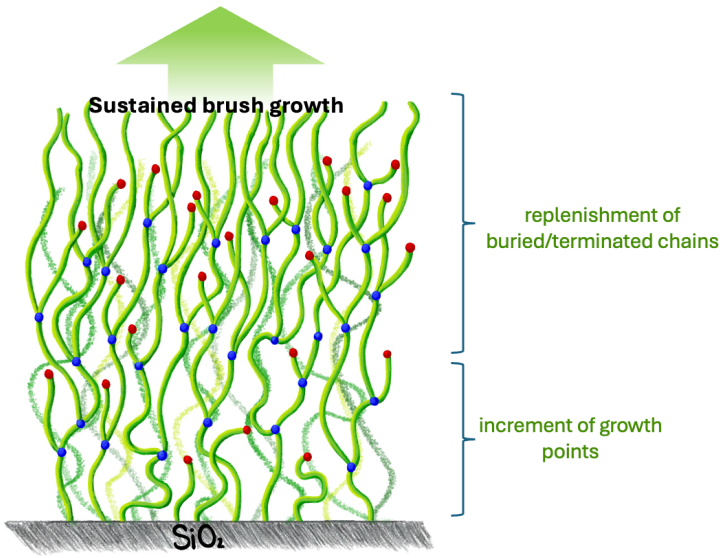

***Figure 40**: Schematic depicting the sustained brush growth mechanism via inibramer incorporation. This includes the increase of growth points at the early stages of polymerization followed by the replenishment of accessible propagating chains.*

7.1.3 SI-photoATRP of OEGA Brushes

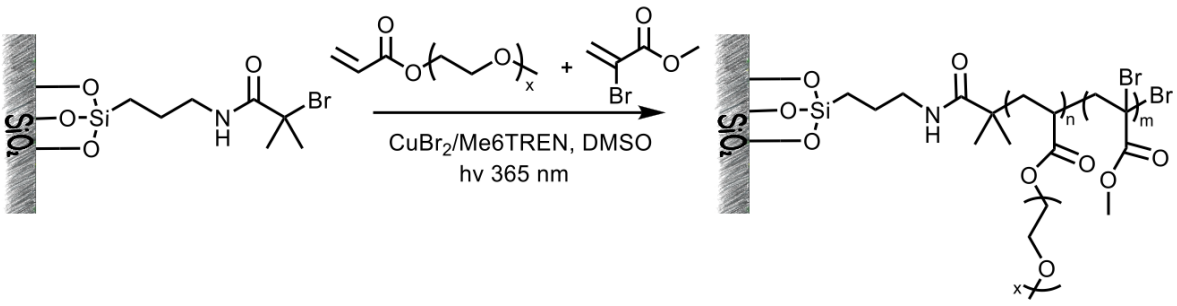

***Figure 41**: Schematic representation of the BrMA-mediated SI-photoATRP of oligo(ethylene glycol) acrylate (OEGA, M_n ~ 480 g mol^{-1}) from silicon surfaces under UV irradiation.*

SI-photoATRP of oligo(ethylene glycol) acrylate (OEGA, M_n ~ 480 g mol^{-1}) revealed a kinetic behavior in contrast with those previously observed, allowing the decoupling of the two proposed contributions of the inibramer. Despite the fact that POEGA brushes exhibited an optimal BrMA concentration range similar to those observed for P*t*BA and P*n*BA (Figure 42a), during the early-stage of polymerization was not appreciated acceleration in brush-growth (Figure 42b).

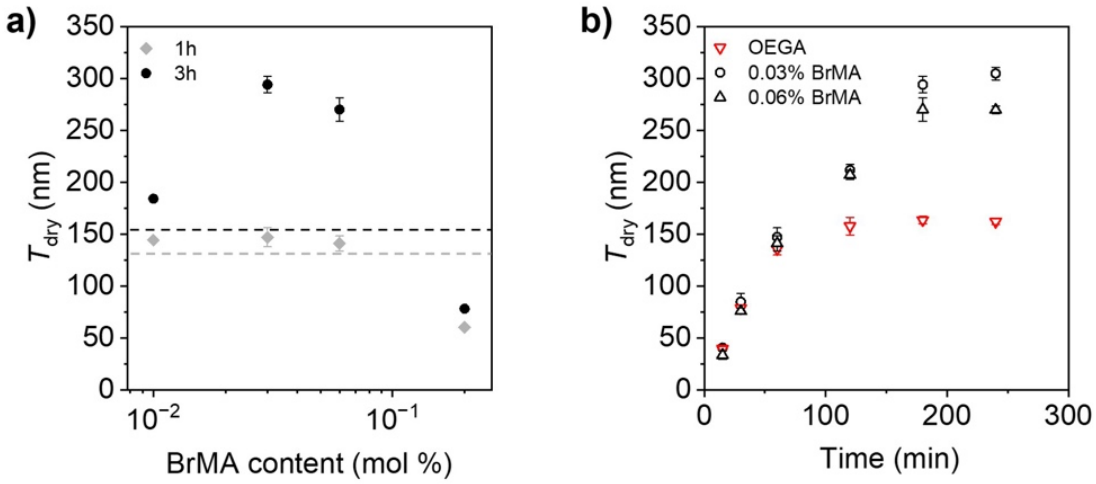

***Figure 42**: SI-photoATRP of OEGA (0.71 M) with $CuBr_2$/Me_6TREN with UV light irradiation (λ_{max} =365 nm, 7.0 mW cm^{-2}). (a) Dry thickness of POEGA brushes measured by ellipsometry and AFM as a function of BrMA content (mol%) relative to OEGA. The dotted line corresponds to the control experiment performed in the absence of the inibramer. (b) Growth kinetics for POEGA brushes including 0 and 0.03 mol% of BrMA relative to OEGA.*

During the first 60 min of polymerization, no appreciable difference was observed between the growth kinetics of OEGA brushes prepared with 0.03 mol% BrMA and those obtained in the

absence of the inibramer. This suggests that the additional propagating growth generated through early BrMA incorporation does not necessarily result in faster brush thickening. This behavior can be rationalized thinking the bulky side chains of OEGA, which sterically constrain the maximum attainable chain density within the brush. As a result, the effective density of propagating chains is limited predominantly by brush packing rather than by the availability of initiating sites. Although the absence of this early acceleration on brush growth, at longer polymerization times the beneficial effects of inibramer are still evident. In conventional SI-photoATRP of OEGA brush thickening rate is gradually reduced and eventually approached a plateau, whereas POEGA brushes prepared in the presence of inibramer sustained brush growth over extended reaction times, yielding POEGA brushes with T_{dry} exceeding 300 nm after 4 h of irradiation, more than twice those obtained under BrMA-free conditions.

Taken together, all the obtained results provide independent support for the proposed mechanism.

The inibramer contribution of the early generation of additional propagating growth points depends on the evolving architecture and steric constraints of the growing brush. On the other hand, the continuous replenishment of chain ends is independent on the acrylate system and emerges as the more general mechanism through which inibramers extend polymer brush growth under surface-confined ATRP conditions.

7.1.4 Chain-extension experiments

To further investigate the influence of inibramer in the polymer brush growth in surface-confined ATRP conditions chain-extension experiments were performed. P*t*BA brushes were first synthesized by SI-photoATRP for 20 min from polymerization mixtures containing 0, 0.001, 0.01, or 0.1 mol% BrMA. Following complete removal of the reaction solution, brush extension was performed using a fresh SI-photoATRP formulation containing pure *t*BA for an additional 60 min (Figure 43a).

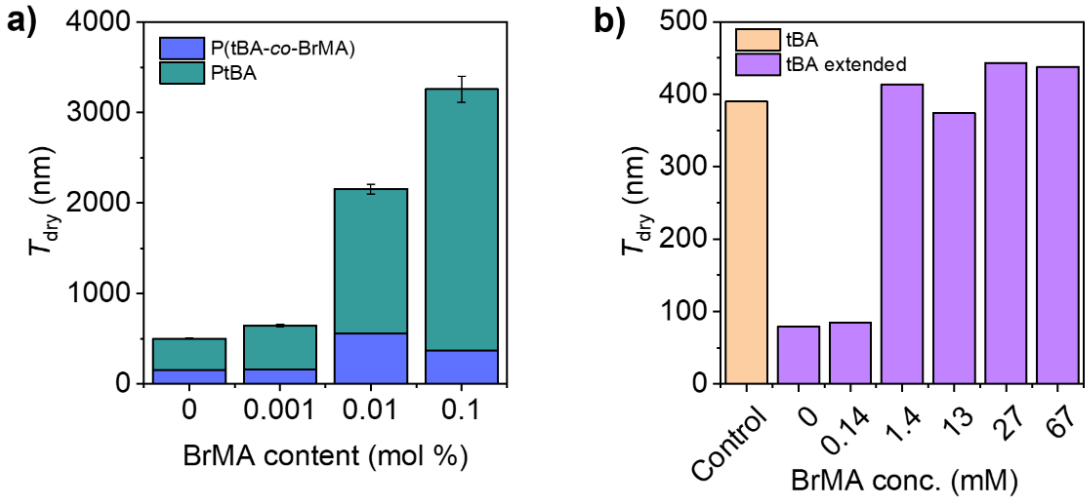

***Figure 43**: (a) Dry thickness of PtBA brushes grown for 20 min (blue bars) with varying contents of BrMA (0, 0.001, 0.01, and 0.1 mol% relative to tBA), followed by chain extension with pure tBA for 1 h (green bars). (b) PtBA brushes synthesized by SI-photoATRP (60 min) from ultrathin layers generated exclusively from BrMA prior to chain extension (20 min).*

The extension of P*t*BA brushes grown initially in the absence of inibramer gave rise to polymer chains with a final dry thickness of approximately 500 nm, in line with the values obtained from the growth kinetics of pure *t*BA in conventional SI-photoATRP (Figure 35). In contrast, brushes prepared in the presence of BrMA exhibited a concentration-dependent enhancement of the extension process. A modest increase in final thickness was measured for brushes prepared with 0.001 mol% BrMA; however, in the case of initial brush blocks synthetized using 0.01 and 0.1 mol% BrMA the second growth step yielded brushes with final dry thicknesses exceeding 2 µm and approximately 3.3 µm, respectively (Figure 43a). Importantly, the magnitude of the second growth step was not proportional to the thickness of the first brush block, indicating that the enhanced extension cannot simply be attributed to a larger amount of polymer formed during the initial polymerization. These observations provide direct evidence supporting the proposed mechanism of inibramer-mediated brush growth. Due to the unbalanced reactivity ratios and

the consequent preferential incorporation of BrMA during the initial copolymerization stage, a three-dimensional population of dormant ATRP initiating sites becomes embedded throughout the first polymer layer. During the subsequent UV irradiation in the presence of pure *t*BA, these latent initiating sites are progressively activated, generating new propagating grafts throughout the brush volume. Thus, despite the complete absence of BrMA during the extension step, the second polymerization proceeds from a substantially higher effective density of propagating growth points than conventional SI-photoATRP.

To further investigate this hypothesis, the possibility of achieving a similar enhancement by replacing the PtBA/BrMA first block with an ultrathin layer generated exclusively from BrMA prior to chain extension was studied (Figure 43b). In order to do so, silicon substrates were subjected to SI-photoATRP of BrMA alone for 20 minutes using different inibramer concentrations, followed by chain extension with pure *t*BA for additional 60 minutes. In all cases, the initial BrMA-derived layer remained extremely thin (T_{dry} < 2 nm), and the final P*t*BA brush thickness after chain extension never exceeded 400-450 nm, irrespective of the BrMA concentration employed. These results demonstrate that simply increasing the density of initiating groups at the substrate interface is insufficient to sustain ultra-thick brush growth. Alternatively, the inibramer must be incorporated throughout an actively growing polymer brush, thereby establishing a three-dimensional distribution of dormant initiating sites capable of generating new propagating grafts across the brush thickness.

Overall, these experiments provide direct mechanistic evidence that the exceptional brush growth achieved by inibramer-mediated-SI-photoATRP originates from the spatial distribution of latent initiating sites within the growing polymer layer rather than from an increased density of surface-bound initiators.

Finally, the *inibramer* strategy also enables the preparation of ultra-thick block-copolymer brushes comprising chemically distinct segments. To demonstrate this capability, a P*t*BA brush was first synthesized by SI-photoATRP from a *t*BA formulation containing 0.001 mol% BrMA, followed by a second SI-photoATRP step using OEGA containing 0.03 mol% BrMA. This sequential polymerization resulted in an additional increase in brush thickness of 120 ± 7 nm. Successful formation of the block-copolymer brush was confirmed by static water contact angle (θ_s) measurements (Figure 44), which showed a decrease in θ_s from 77° for the initial P*t*BA brush to 49° after growth of the interfacial POEGA block, demonstrating complete coverage of the brush surface by the hydrophilic second block.

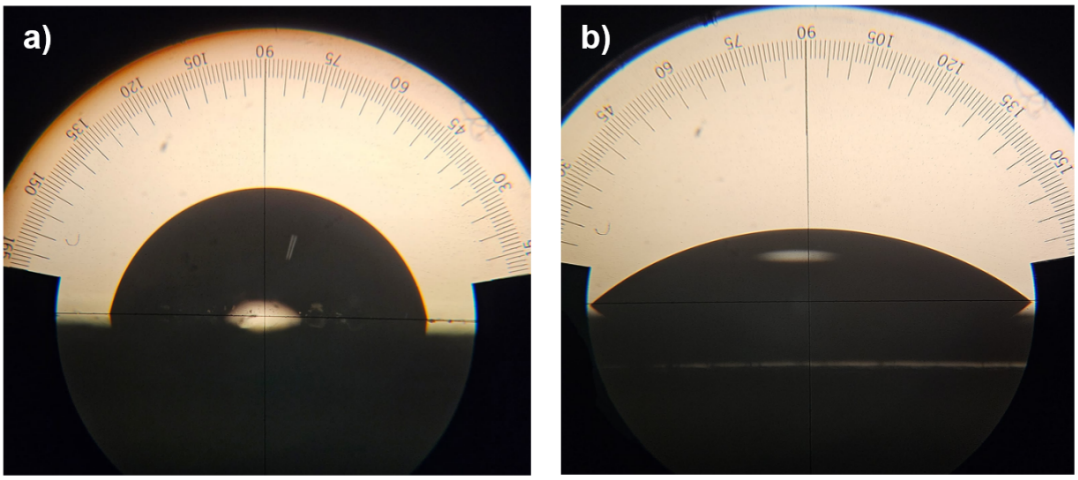

***Figure 44**: a) Picture of a droplet deposited on P(tBA-co-BrMA) brushes, b) picture of the droplet deposited on the P(OEGA-co-BrMA) block grown on top of P(tBA-co-BrMA).*

7.1.5 Conclusions

In summary, these results demonstrate that trace amounts of an *inibramer* incorporated during conventional SI-photoATRP fundamentally reshape the evolution of polymer brush growth, enabling dry brush thicknesses well into the micrometer regime under otherwise conventional polymerization conditions. Unlike solution ATRP, where *inibramers* primarily control the formation of branched macromolecular architectures, their incorporation into surface-grown polymers establishes a three-dimensional distribution of dormant ATRP initiating sites throughout the growing brush. Upon activation, these sites continuously generate new propagating growth points that compensate for the progressive depletion of accessible chain ends caused by radical termination and chain-end burial, thereby sustaining polymerization far beyond the thickness limits typically achieved by conventional SI-ATRP. This simple strategy provides straightforward access to polymer films that retain the defining characteristics of surface-tethered polymer brushes while reaching thicknesses typically associated with conventional polymer coatings, thereby bridging the long-standing gap between molecularly defined polymer brushes and robust functional coatings.

More broadly, the obtained results demonstrate that monomer reactivity ratios in surface-initiated controlled radical polymerizations should not be viewed solely as descriptors of copolymer composition. Under the unique kinetic conditions imposed by surface confinement

and negligible overall monomer conversion, preferential monomer incorporation can instead be exploited to control the spatial and temporal generation of propagating sites, thereby engineering the evolution of polymer brush growth. This work therefore demonstrates that, under surface-confined controlled radical polymerization, monomer reactivity governs not only polymer composition but also the evolution of the propagating-site population within the growing brush. This concept is expected to extend beyond *inibramer*-mediated SI-photoATRP, providing a general strategy for engineering growth processes in surface-confined polymerizations and enabling the rational design of polymer interfaces with properties inaccessible through conventional solution polymerization.

Regardless of the promising results obtained in this work, several aspects still require further investigation. One of the main limitations affecting the scalability of SI-ATRP polymerization is the oxygen sensitivity of the reaction. Oxygen indeed can quench the radical propagation by reaction with the carbon centered radicals with the consequent formation of peroxyl radicals. Through careful optimization of both the reaction conditions and the experimental setup, the objective is to establish an oxygen-tolerant polymerization methodology with improved robustness and enhanced suitability for industrial-scale applications. One strategy can rely on the use of Cu/L complexes as oxygen scavengers while confining the reaction medium between the substrate and a confining surface, such as a glass slide. A second, more attractive approach is based on a catalytic system employing methylene blue under red-light irradiation, allowing the polymerization to proceed under ambient atmospheric conditions[39].

Further studies should also aim to expand the monomer and inibramer library to enable the synthesis of ultra thick polymer brushes with tailored functionalities and broader application potential. The already developed polymer brushes are predominantly hydrophobic, as are based on *tert*-butyl acrylate and *n*-butyl acrylate, or slightly hydrophilic, as in the case of OEGA. Consequently, the monomer scope must be extended to include highly hydrophilic monomers, such as zwitterionic monomers, as well as inert monomers, such as fluorinated acrylates. This broader monomer scope would expand the applicability of polymer brush coatings to, for example, superlubricating brushes for aqueous environments and anti-fouling coatings.

7.2 Programming Vinyl Polymer Degradation through Disulfide Chemistry and Light

The second part of this thesis focuses on the degradation of *n*-butyl acrylate (*n*BA)-based copolymers containing the disulfide-functional monomer methyl lipoate (LpOMe), which introduces cleavable disulfide linkages into the polymer backbone. Incorporating cleavable bonds into the polymer chain is one of the most widely employed strategies for the design of degradable polymers. Among the various dynamic covalent linkages investigated, disulfide bonds (S-S) are particularly attractive because of their facile cleavage under different types of stimuli, enabling efficient polymer degradation.

Our strategy relies on the use of photocatalysts to promote the degradation. It has been reported how visible or near-UV light photocatalysis enables degradation of disulfides in proteins under mild conditions, thereby eliminating the need for deep-UV irradiation typically required for direct disulfide photolysis. Using light, the excited photocatalyst enables controlled activation of chemical pathways via electron transfer (ET), energy transfer (EnT) or hydrogen atom transfer (HAT)[60,62,63]. However, it is important to consider that the efficiency of those reactions depends on the matching between the photocatalyst's excited state energy and the bond dissociation energy (BDE) of the disulfide bond[66]. Considering this, different photocatalysts have been investigated, exploring different light wavelengths on both the homopolymer of polymethyl lipoate (PLpOMe) and the copolymer poly(*n*BA-co-LpOMe).

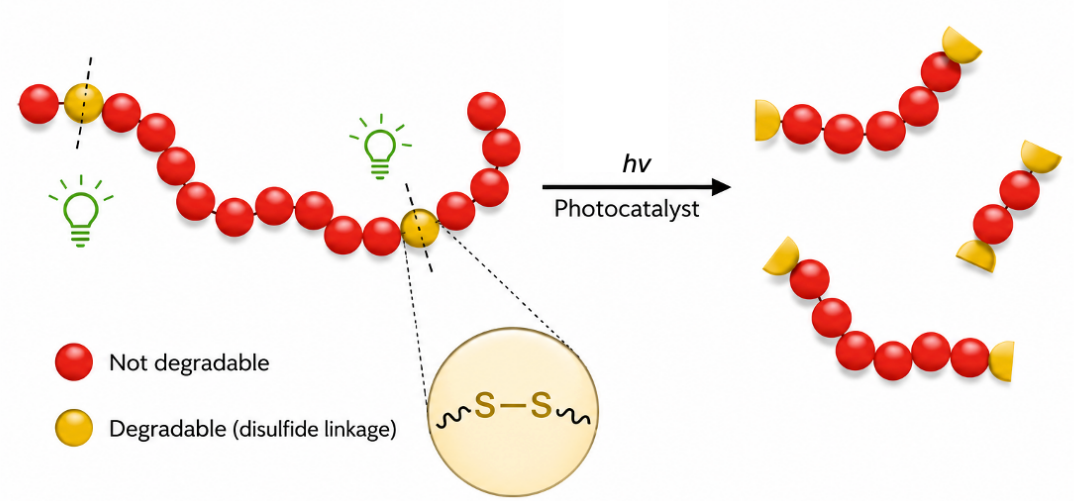

***Figure 45**: Schematic representation of the objective of the study: synthesis of polymers containing a cleavable unit, namely a disulfide bond, which promotes polymer degradation upon light irradiation in the presence of a photocatalyst.*

7.2.1 Homopolymer Degradation with Thioxanthone and Xanthone

To investigate whether the strategy originally developed for the cleavage of disulfide bonds in proteins can be translated to polymeric systems, the first photocatalysts employed were thioxanthone and xanthone (Figure 46).

***Figure 46**: Molecular structures of thioxanthone (TXO) on the left and xanthone (XO) on the right.*

Thioxanthone (TXO) exists in two discrete conformations, each characterized with a different absorption band in the UV-Vis region; one corresponds to a planar conformation with its absorption band at 376 nm, while the second to a non-planar conformation, with its absorption band at 361 nm. Upon irradiation, thioxanthone is excited to the singlet state and subsequently undergoes intersystem crossing (ISC) to populate its triplet state. Furthermore, it has been reported that the configuration of the triplet state depends on the polarity of the solvent[67].

The combination of a high Φ_{ISC} and a long triplet lifetime makes this photocatalyst highly suitable for energy transfer processes[68]. Xanthone (XO), whose absorption maximum is shifted toward lower wavelengths, exhibits characteristics similar to those of thioxanthone, with a slightly higher triplet energy compared to TXO, making it suitable for energy transfer processes[69].

Of particular interest for the cleavage of disulfide bonds is the work of Zhou *et al.*[66] where it has been reported how thioxanthone, together with an electron donor, enables an efficient disulfide cleavage of peptides and proteins under 420 nm light irradiation, following a reductive quenching (Figure 47).

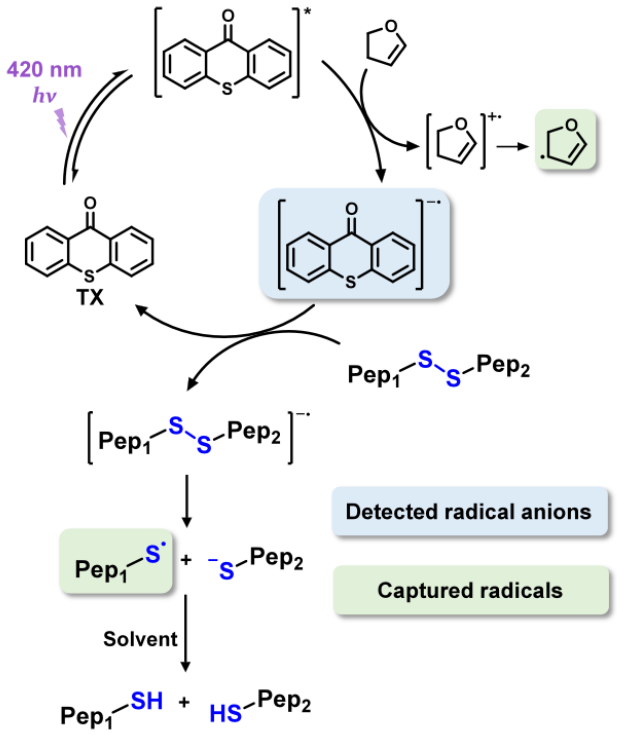

***Figure 47**: Proposed reaction pathway by Zhou et al [66] for the visible light-induced disulfide reduction, utilizing TXO as catalyst and 2,3-dihydrofuran as electron donor. The reaction proceeds via photoredox process involving a cascade of SET steps.*

As disulfide-containing monomer, the methyl ester of lipoic acid (LpOMe) was selected and synthesized from lipoic acid according to the modified literature procedure (Supporting Information), and the acrylate *n*-butyl acrylate (*n*BA) was selected as comonomer.

To optimize the reaction conditions for copolymer degradation, poly(*n*BA-co-LpOMe), preliminary studies were conducted on the corresponding homopolymer PLpOMe.

Prior to the addition of the photocatalysts, a control experiment was performed to verify the stability of PLpOMe under 365 nm light irradiation, confirming that shorter-wavelength irradiation is required to induce direct disulfide bond cleavage, as previously reported in literature[70].

The degradation reaction mixture comprised 0.09 M of homopolymer (PLpOMe), 5 mol% of photocatalyst and 10 mM of triethyl amine (TEA) as electron donor in 1 mL of tetrahydrofuran (THF). Xanthone (XO) and thioxanthone (TXO) were initially investigated as photocatalysts (Table 1).

5 mol% catalyst	TEA (mM)	Solvent	Reaction time	Light wavelength (nm)	O_2	Depolymerization yield	Initial M_n (kDa)	Final M_n (kDa)
TXO	10	THF	24 h	356	no	/	127	1.1
TXO	10	THF	16 h	365	yes	degradation	693	0.4
TXO	10	THF	16 h	427	yes	/	693	1.1
TXO	10	THF	2 h	427	yes	57%	693	1.1
XO	10	THF	24 h	365	no	/	127	1.9
XO	10	THF	2 h	365	yes	29%	693	1.8
XO	10	DCM	16 h	365	yes	/	/	/

***Table 1**: Reaction conditions and obtained results for the degradation experiments of PLpOMe with TXO and XO as photocatalysts.*

Following 24 hours of UV light irradiation (λ_{max} =365 nm) under oxygen-free conditions and in the presence of the photocatalyst, both thioxanthone and xanthone promoted the degradation of PLpOMe. This was evidenced through ^{1}H NMR spectroscopy, as the characteristics signals of the homopolymer, in particular the signal at 2.8 ppm assigned to the protons of the carbons adjacent to the sulfur atoms in the polymer backbone, where no longer detectable in the spectra of the resulting products (Figure 48).

Thiols are though not detectable by NMR spectroscopy. To further investigate the extent of polymer degradation, the products were analysed through size exclusion chromatography (SEC). Starting from a molecular weight (M_n) of 127 kDa, the M_n values decreased to 1.1 and 1.9 kDa for TXO and XO respectively (Figure 49). Both the GPC traces show that many populations with different molecular weights were formed, suggesting that the degradation is either incomplete or accompanied by secondary processes.

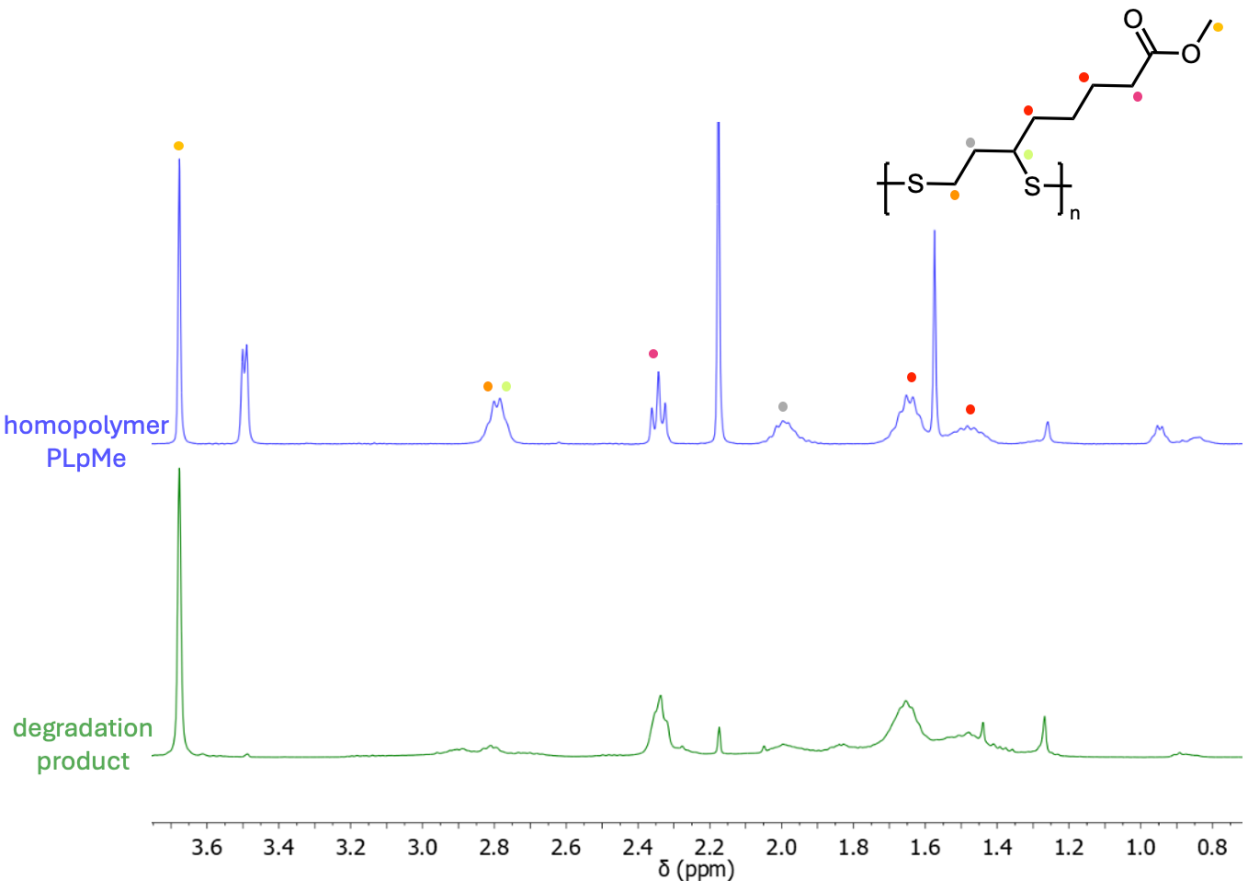

Figure 48: *^{1}H NMR spectra of the homopolymer (blue) and the degradation product (green) obtained with TXO after 24 h of light irradiation (λmax=365 nm).*

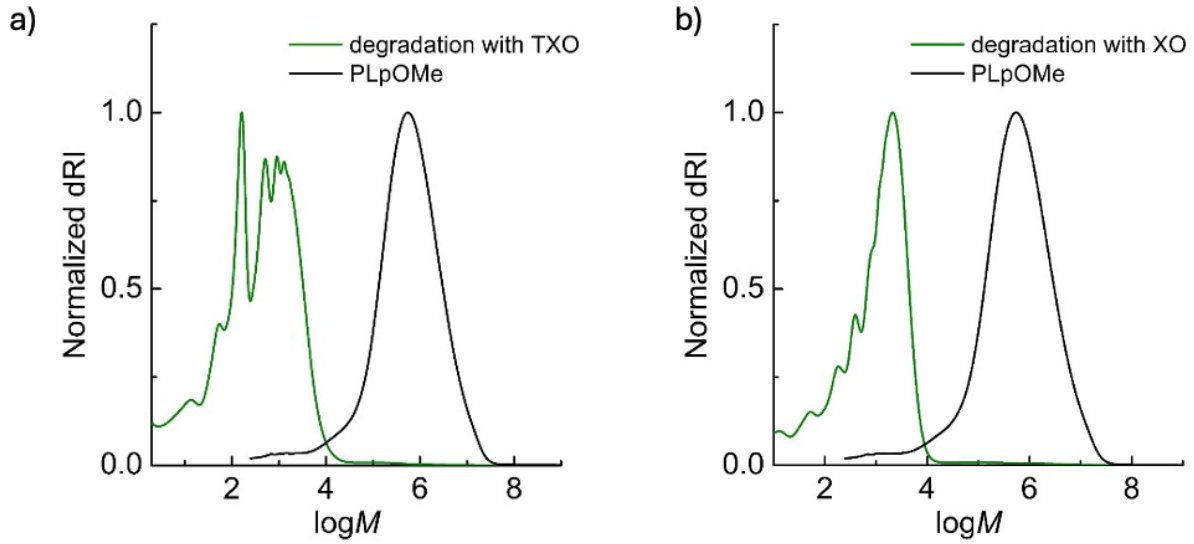

Figure 49: *SEC traces of the degraded homopolymer in the presence of thioxanthone (a) and xanthone (b) after 24 h irradiation at 365 nm.*

When the degradation reaction with TXO was performed with a shorter irradiation time (16 h) and without prior deoxygenation, the resulting product exhibited a final M_n value of 0.4 kDa, starting from an initial M_n of 693 kDa, indicating the negligible effect of oxygen concentration on the degradation process (Figure 55). Based on these results, all subsequent reactions were performed without prior deoxygenation.

To investigate the role of the solvent, degradation with xanthone was performed for 16 hours dissolving PLpOMe in dichloromethane (DCM). The resulting product, analysed through ^{1}H NMR spectroscopy revealed a complete degradation, since no monomer signals were detected (S11). This result points out that the reaction pathway is not influenced by the type of solvent used.

To determine whether the depolymerization process could be completed in less than 16 h, the reaction mixture was irradiated at 365 nm for 2 hours in the presence of xanthone. Unexpectedly the ^{1}H NMR spectrum (Figure 50) revealed the presence of the characteristic signals corresponding to the monomer, indicating that depolymerization - the process of converting a *polymer* into a *monomer* or a mixture of monomers[71]– rather than degradation, has occurred. According to this, ^{1}H NMR analysis revealed that 29% of the initial PLpOMe had been depolymerized to the corresponding monomer, LpOMe. A decrease in molecular weight was still observed by size exclusion chromatography (Figure 51b) technique, although the resulting product exhibited a broad molecular weight distribution at low M_n values. The final M_n is indeed 1.8 kDa, starting from a 693 kDa homopolymer.

The same experiment was conducted in the presence of thioxanthone, except that the reaction mixture was irradiated with 427 nm light. This wavelength was selected based on the absorption spectrum of TXO, reported in the Figure 53. Also under these conditions, depolymerization was observed, affording a monomer yield of 52% and a decrease in M_n of 692 kDa, also in this case with a broad molecular weight distribution, indicating the formation of different oligomeric species (Figure 51a).

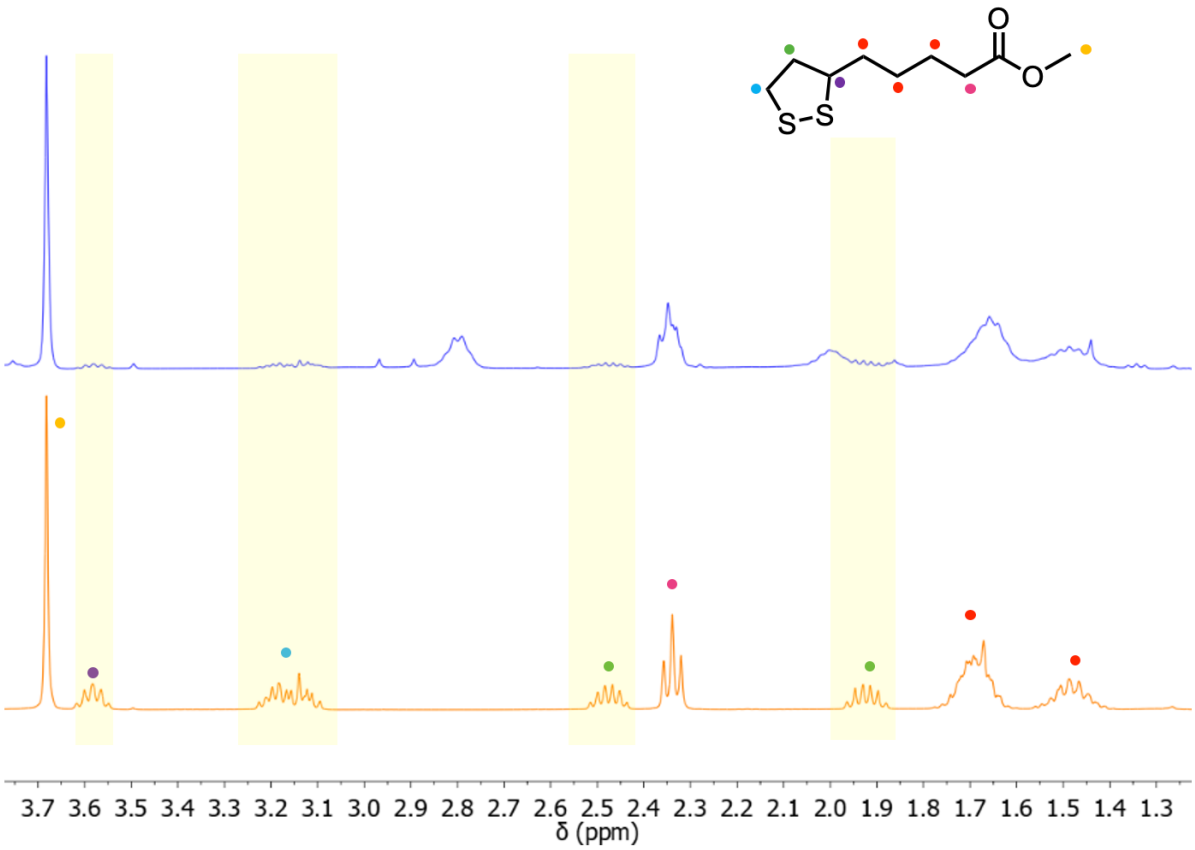

Figure 50: *^{1}H NMR spectra of the degradation product obtained after 2 h irradiation with XO at 365 nm (blue) and of the monomer (orange). The characteristic signals of the monomer signals are highlighted in yellow, confirming the presence of LpOMe in the product.*

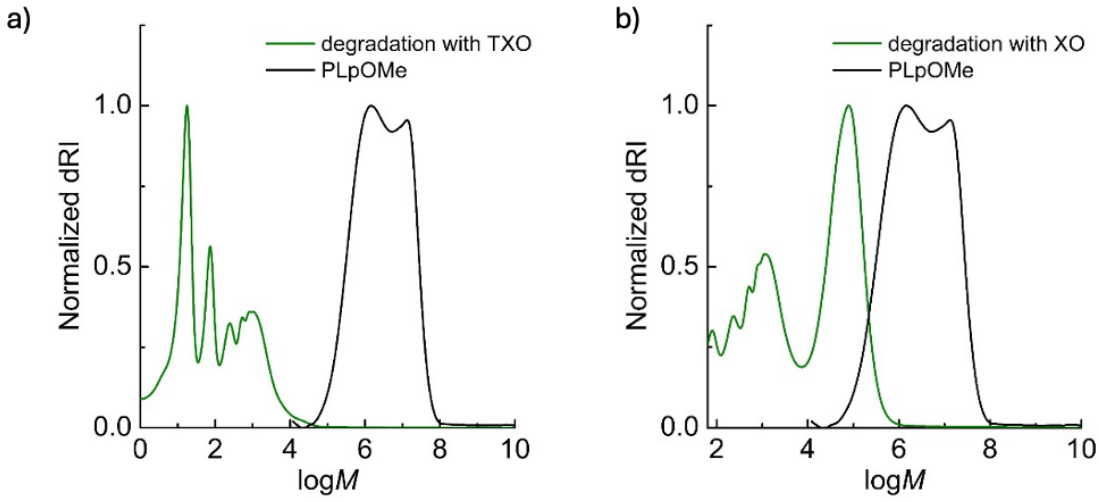

Figure 51: *SEC analysis results of the 2 h degradation of PLpOMe in the presence of xanthone at 365 nm (b) and thioxanthone at 427 nm (a).*

The difference between the obtained results after 2 hours and 16 hours irradiation suggests that irradiation time plays a key role in the degradation process. For short reaction time the presence of monomer was detected, whereas for longer reaction times no monomer signals were identified, instead signals including peaks around 1.2-1.4 ppm, that are consistent with thiol formation[72], were identified (Figure 52). A plausible explanation is that the photocatalyst promotes the depolymerization, generating the corresponding monomer, and this one interacts with UV-visible light. The latter interaction causes direct photolysis, leading to the homolytic cleavage of disulfide bonds with the consequent formation of sulfur-centred radical that can subsequently propagate resulting in the reformation of oligomers. Notably, the polymerization of lipoic acid and its derivatives upon exposure of the monomer to UV light is extensively reported in literature. This behaviour is attributed to the ability of the five-membered disulfide-containing ring in lipoate monomers to undergo ring opening polymerization (ROP) in response to heat or UV irradiation[73]. These findings suggest that the PLpOMe initially undergoes photocatalyst-mediated depolymerization, generating the corresponding monomer, then the monomer formed may subsequently interacts with light, promoting the formation of oligomeric species and thereby resulting in a product with a lower and broader molecular weight distribution. The re-formed homopolymer might then undergo backbiting-induced degradation obtaining oligomers with lower and broader molecular weight distributions.

The higher depolymerization yield of 57% obtained when thioxanthone is employed and the system is irradiated for 2 h at 427 nm, compared with the 29% depolymerization yield obtained after 2 h irradiation at 365 nm with XO, is in line with the absorption spectrum of methyl lipoate. The monomer exhibits lower absorbance at 427 nm than at 365 nm, indicating that at higher wavelengths less light is directly absorbed by the disulfide bonds of the chromophore, potentially promoting less direct cleavage of disulfide bonds.

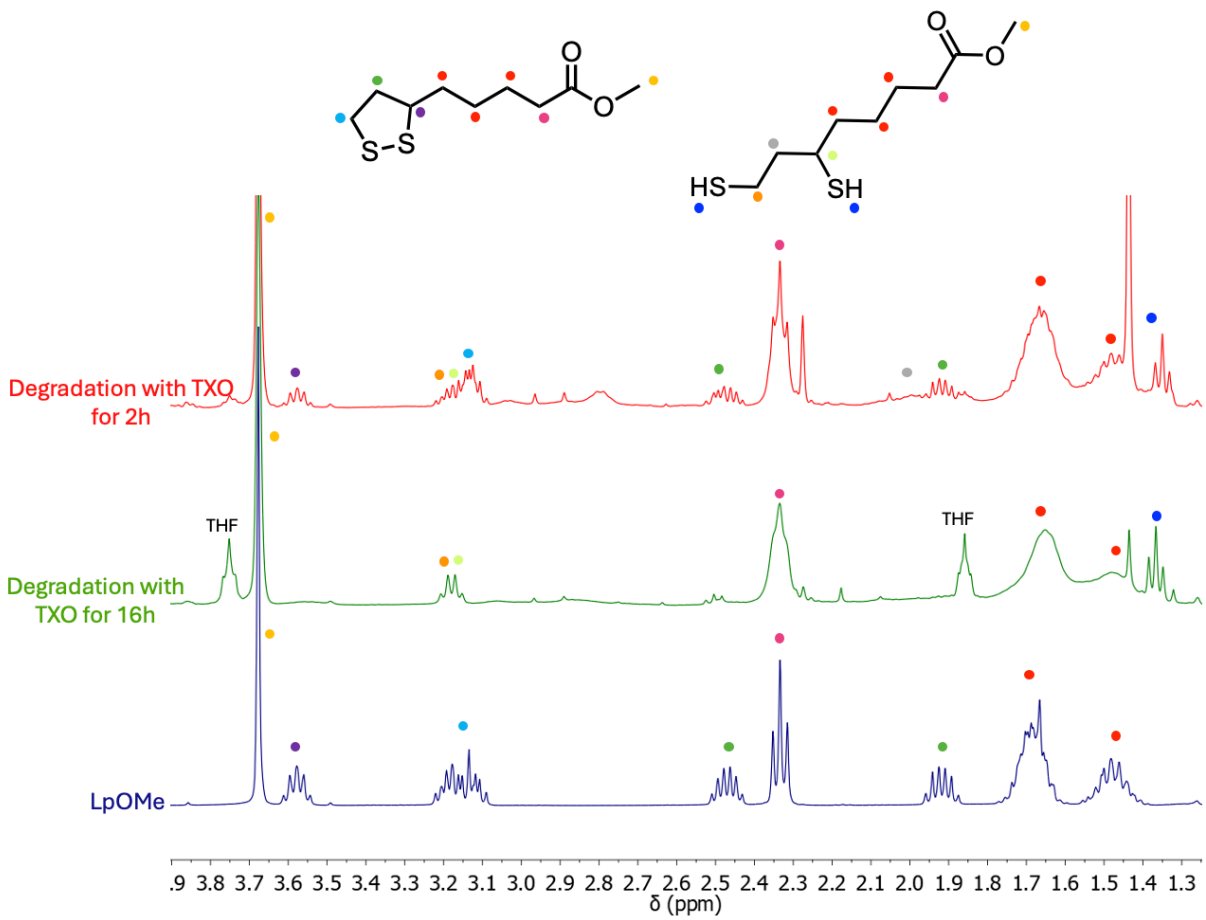

***Figure 52**: [1]H NMR spectra of the degradation/depolymerization products obtained with TXO after 2 h irradiation (red) and 16 h irradiation (green) at 427 nm. The products spectra are confronted with the one of the monomer LpOMe (blue).*

To support this hypothesis, the UV–Vis absorption spectrum of LpOMe in THF was recorded. The resulting spectrum (Figure 53) confirmed that LpOMe exhibits significant absorption in the UV region, supporting the hypothesis that the regenerated monomer undergoes direct photoexcitation upon prolonged irradiation.

Moreover, as control experiment, the monomer LpOMe was irradiated in a solution of THF at 365 nm and 427 nm for 16 hours. In both cases, the resulting products evidenced the disappearance of the monomer signals and the ^{1}H NMR spectra revealed broaden peaks at low ppm, from 1.8 to 1.4 ppm, suggesting the formation of oligomers (Figure 54).

To conclude, the homopolymer degradation with 5 mol% of thioxanthone both at 365 nm and 427 nm for 16 hours were confronted. Both the degradation products were made of many populations, supporting that in this wavelengths range (365-427 nm) side reactions such as the formation of oligomers, are enhanced by light irradiation (Figure 55).

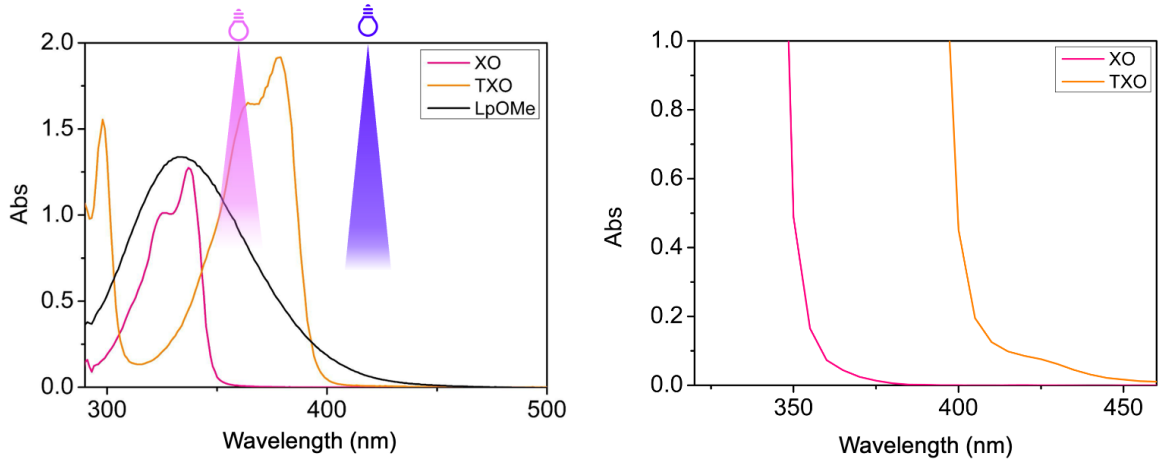

***Figure 53**: UV–Vis absorption spectra of TXO and LpOMe in THF. The 300–450 nm region is highlighted to emphasize the absorption of the photocatalysts at the irradiation wavelengths.*

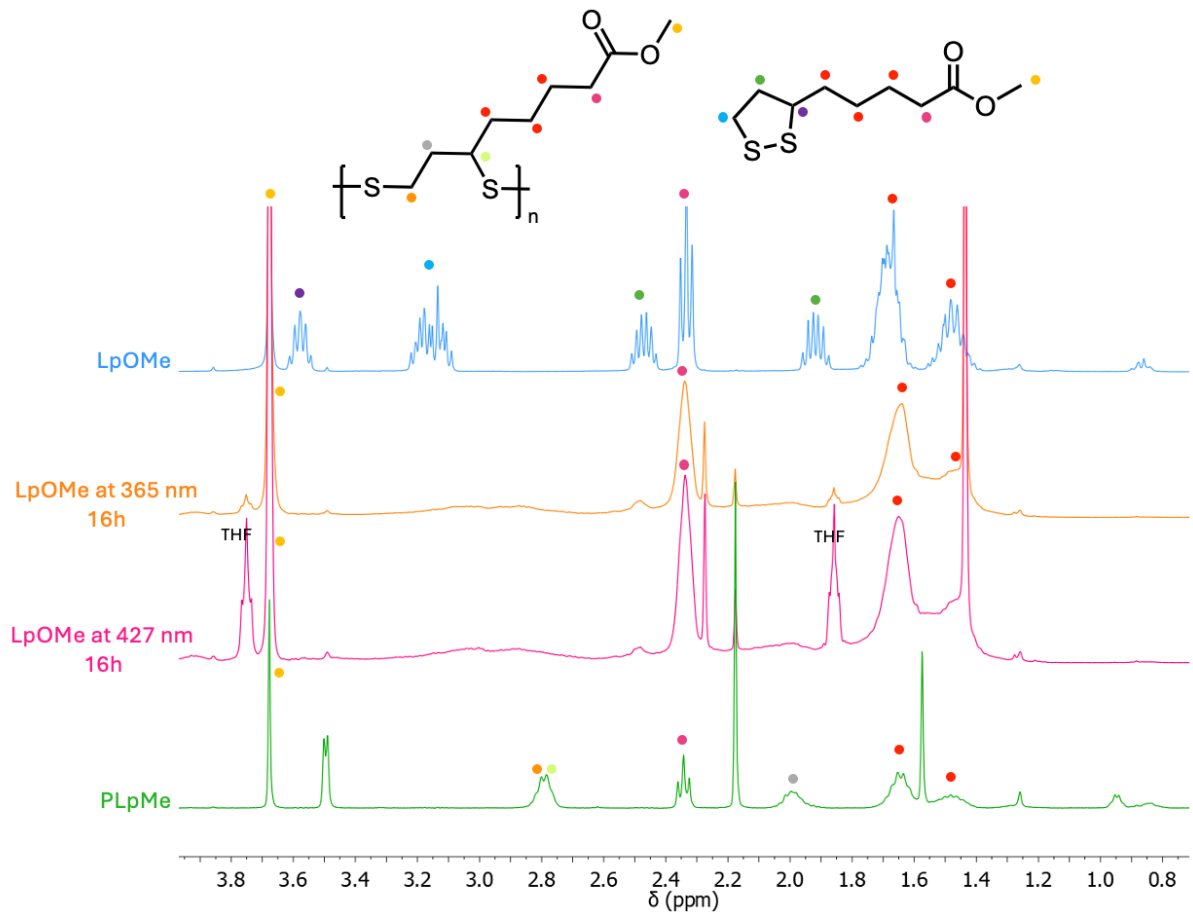

***Figure 54**: ^{1}H NMR spectra of the monomer irradiated for 16 h under 365 nm light (orange) and 427 nm light (fuchsia). The products spectra are confronted with the one of the monomer LpOMe (light blue) and the homopolymer PLpOMe (green).*

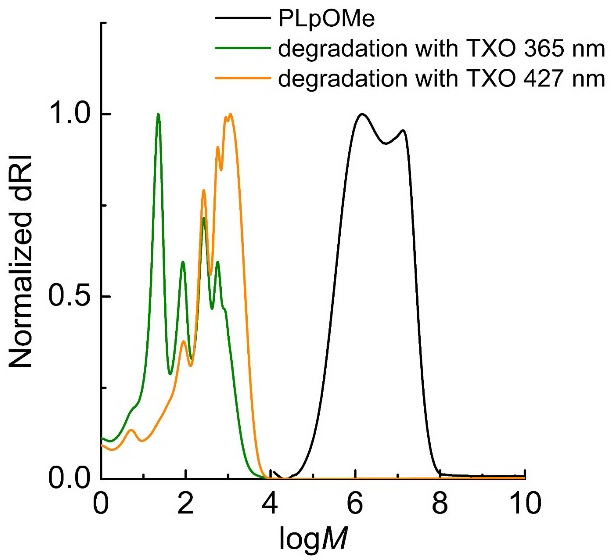

***Figure 55**: GPC traces of the homopolymer before and after degradation with xanthone and thioxanthone for 16 h irradiation time. For TXO a 427 nm light was employed, for XO a 365 nm light.*

Collectively, these observations provide independent confirmation of the proposed mechanism. Upon irradiation at either 365 or 427 nm, the excited photocatalyst initially promotes the depolymerization of PLpOMe, leading to the formation of the monomer LpOMe. The regenerated monomer, in the presence of those light wavelengths, subsequently absorbs light and undergoes homolytic cleavage that causes the disulfide bond cleavage, generating sulfur centred radicals. The highly reactive radical species then propagate, promoting the reformation of oligomeric species.

7.2.2 Homopolymer Degradation using Alternative Photocatalysts Excited in the 365-427 nm Range

To further investigate the role of light wavelength in the photodegradation process, additional photocatalysts that are photoexcited in the 365-427 nm spectral range were evaluated (Table 2). A common trend was observed: short irradiation times (2 h) resulted in the formation of depolymerization products, containing the regenerated monomer, whereas longer irradiation times (16 h) led to the disappearance of the monomer, as evidenced by the ^{1}H NMR spectra (Supporting Information Figure S13-S16). The only photocatalyst showing a different behaviour was 1,2,3,5-Tetrakis(carbazol-9-yl)-4,6-Dicyanobenzene (4CzIPN). Indeed, in this case, a relatively low degree of depolymerization was observed even after 16 hours reaction,

with a depolymerization yield of 39% (Figure 56). To rationalize this behaviour, several hypotheses were considered.

This behaviour may be attributed to its less negative excited-state reduction potential ($E^*_{ox} \approx -1.04$ V vs. SCE[74]) relative to the reduction potential of the disulfide bonds in the homopolymer ($E_{pc} \approx -2.4$ V vs SCE), which might prevent efficient reduction of the disulfide bonds if a SET pathway is considered. Consequently, the depolymerization process is likely to proceed more slowly, allowing the formation of the monomer even at higher reaction times. As a result, the homolytic cleavage of disulfides induced by light is expected to occur to a lesser extent, thereby limiting the subsequent formation of oligomeric species.

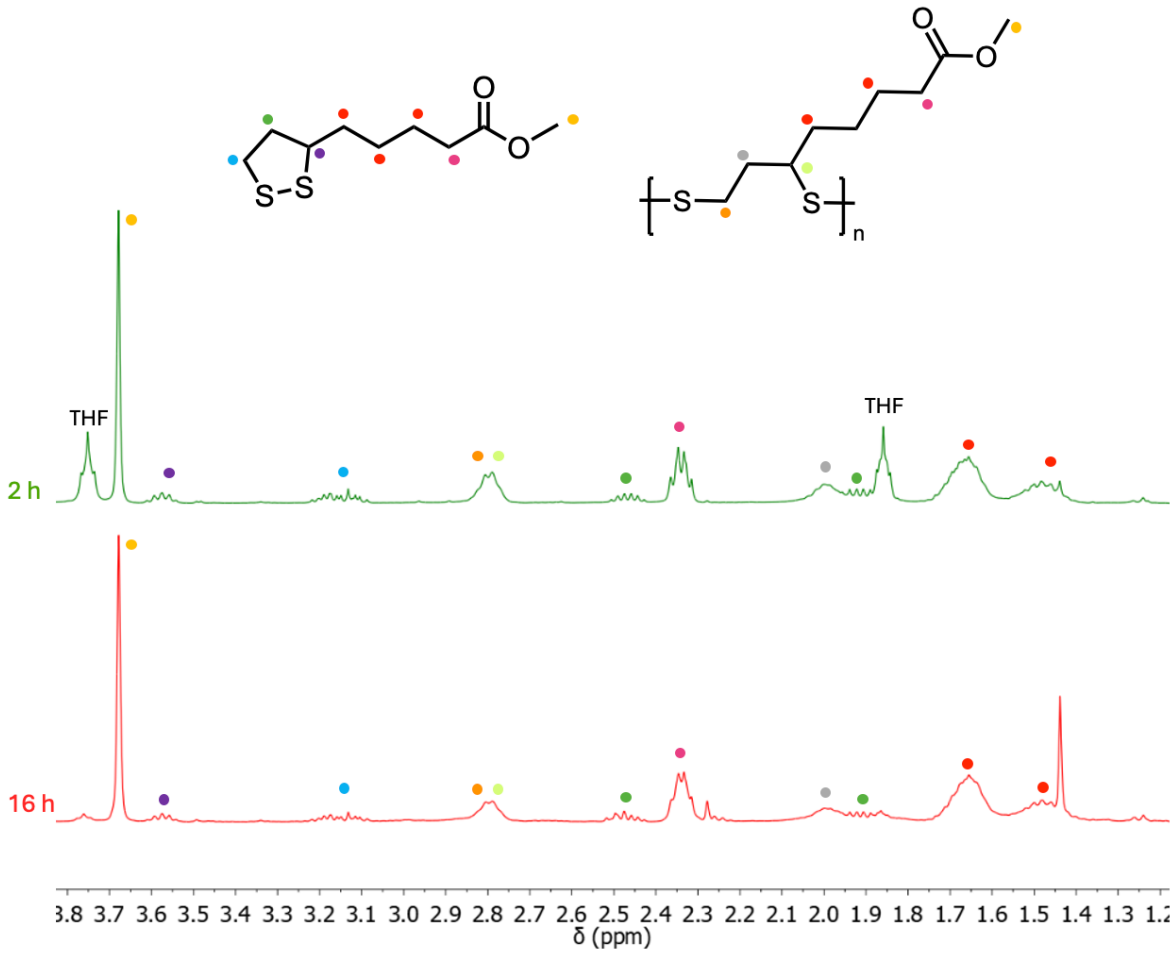

***Figure 56**: Comparison of the ^{1}H NMR spectra of PLpOMe degradation with 4CzIPN after 2 h (green) and 16 h (red) irradiation.*

Another hypothesis can be formulated by comparing the absorption spectra of the photocatalyst and LpOMe in THF. The absorption maximum of 4CzIPN in this solvent is reported at 438 nm, a wavelength close to that employed in the degradation experiments (λ =427 nm). Furthermore, in this spectral region, 4CzIPN exhibits a molar extinction coefficient (ε) of the order of 10^3-

10^4 M^{-1} cm^{-1} [74,75]. On the contrary, LpOMe, exhibits a relatively weak absorption at 427 nm, as evidenced in the UV-Vis spectrum reported in Figure 53 where the intensity of the absorption band is low. Consequently, at the irradiation wavelength, the incident light is expected to be preferentially absorbed by 4CzIPN rather than by LpOMe. This might significantly limit the direct excitation of the methyl lipoate, therefore limiting the formation of oligomers and resulting in a depolymerized product even after prolonged reaction times. In support of this hypothesis, the same experiment was conducted using $[Ir(ppy)_3]$ as photocatalyst and irradiating the system for 16 h. In this case, however, the irradiation wavelength was not 400 nm, as in the previous experiments performed with the metal-centred photocatalyst, but 427 nm. In fact, was selected the same wavelength used in the previous experiments with 4CzIPN, at which $[Ir(ppy)_3]$ presents a high absorption compared to the monomer. After the 16 hours irradiation of the homopolymer, the ^1H NMR spectrum of the product revealed the presence of LpOMe (Figure 57). This result, reinforced by the UV-Vis spectra of the photocatalysts (S24), supports the hypothesis that, due to the substantial difference between the molar extinction coefficients of the photocatalysts and the depolymerized monomer, light is predominantly absorbed by the photocatalysts, thereby inhibiting the oligomer formation process observed with the other photocatalysts. Accordingly, as shown in the UV-Vis spectra of TXO (Figure 53), this latter photocatalyst exhibits an absorbance comparable to that of the monomer at 427 nm, consequently, prolonged irradiation promotes oligomers formation.

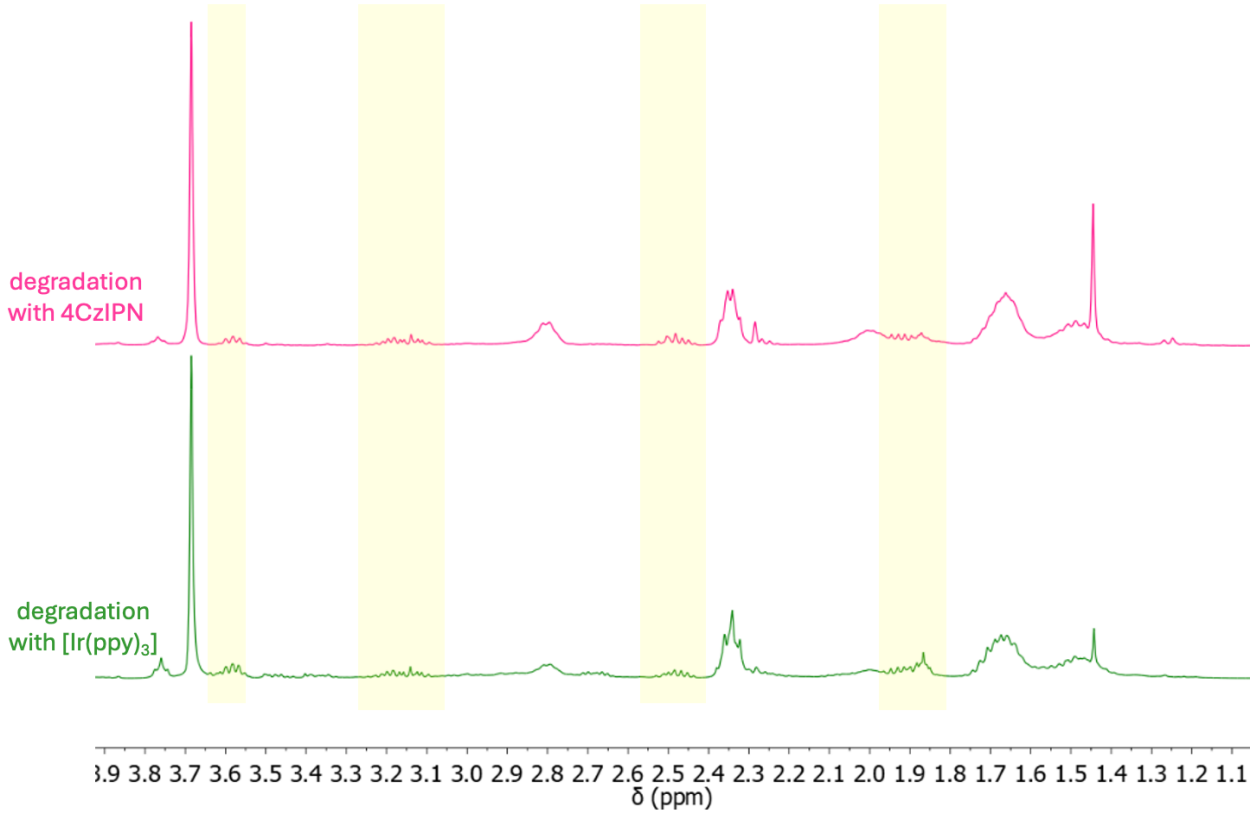

***Figure 57**: [1]H NMR spectra of the degradation products with 4CzIPN (fuchsia) and [Ir(ppy)3] (green). In yellow are highlighted the characteristic signals of the monomer.*

Photocatalyst	TEA	Solvent	Reaction time	Light wavelength	Oxygen	Depolymerization yield
PC-2 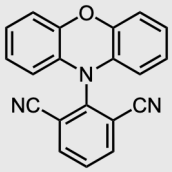	/	THF	2 h	400 nm	yes	42 %
PC-2	/	THF	16 h	400 nm	yes	degradation
PC-3 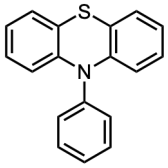	/	THF	2 h	365 nm	yes	41 %
PC-3	/	THF	16 h	365 nm	yes	degradation
PC-5	/	THF	2 h	365 nm	yes	54 %

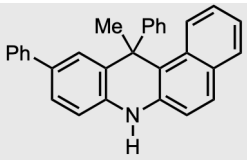						
PC-5	/	THF	16 h	365 nm	yes	degradation
4CzIPN 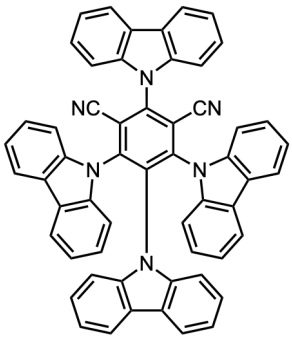	/	THF	2 h	427 nm	yes	50 %
4CzIPN	/	THF	16 h	427 nm	yes	42 %
$[Ir(ppy)_3]$	/	THF	2 h	400 nm	yes	29 %
$[Ir(ppy)_3]$	/	THF	16 h	400 nm	yes	degradation
$[Ir(ppy)_3]$	/	THF	16 h	427 nm	yes	40 %

***Table 2**: Reaction conditions and obtained results for the degradation experiments of PLpOMe with different photocatalysts.*

7.2.3 Homopolymer Degradation with Eosin Y

Due to the light absorption of the homopolymer in the 300-450 nm region, photocatalysts that can be excited at higher wavelengths were investigated. Eosin Y (EY) is an organic dye photocatalyst that can be excited with green light (λ_{max}= 525 nm), within visible light region. Upon photoexcitation, eosin Y undergoes a rapid intersystem crossing from its singlet excited state to the triplet excited state becoming both a more reducing and oxidizing agent[76].

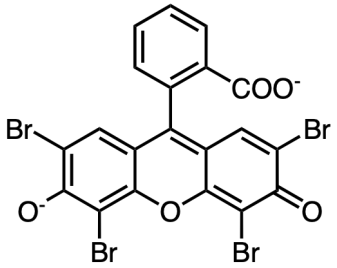

***Figure 58**: Molecular structure of eosin Y.*

This photocatalyst can exist in four different forms depending on the pH of the solution: spirocyclic form, monoanionic form, neutral form and di-anionic form. Furthermore, the presence of Br, a heavy atom, facilitates efficient intersystem crossing (ISC), leading to the formation of the triplet excited state that is enhancing also the reductive and oxidizing abilities. Bromine also enhances the redox properties of eosin Y, promoting both its oxidative and reductive capabilities[77].

mol% EY	TEA	Solvent	Reaction time	Light wavelength	Oxygen	Depolymerization yield
5	10 mM	THF	24 h	525 nm	no	84 %
5	10 mM	THF	2 h	525 nm	no	86%
5	10 mM	THF	2 h	525 nm	yes	66%
5	/	THF	2 h	525 nm	yes	58%
5	/	DCM	2 h	525 nm	yes	74%
5 + 5 mol% BHT	/	THF	2 h	525 nm	yes	33%
5	/	THF	2 h	525 nm	open air	37%

***Table 3**: Reaction conditions and obtained results for the degradation experiments of PLpOMe with eosin Y as photocatalyst.*

Also for those experiments the degradation reaction mixture comprised 0.09 M of homopolymer PLpOMe, 5 mol% of eosin Y, 10 mM of triethyl amine (TEA) as electron donor in 1 mL of tetrahydrofuran (THF) (Table 3).

After 24 hours of green light irradiation (λ_{max} =525 nm) under oxygen-free conditions and in the presence of eosin Y and TEA, the ^{1}H NMR spectrum revealed the presence of the regenerated monomer, consistent with the occurrence of depolymerization (Figure 60). An 84% depolymerization yield was obtained, and a decrease in M_n of 126 kDa was observed through SEC analysis (starting from a 127 kDa homopolymer) (Figure 59).

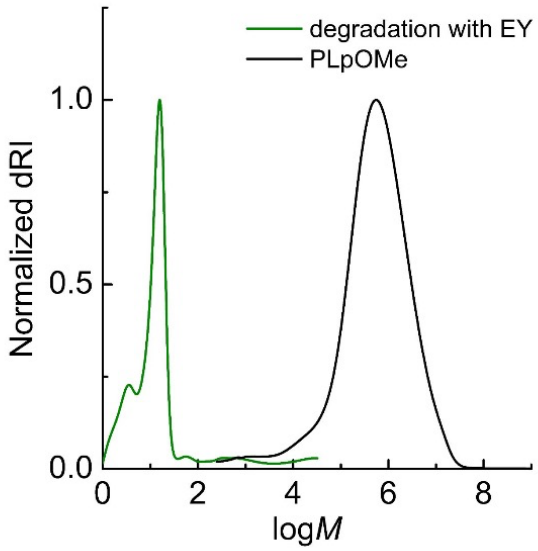

Figure 59*: GPC traces of the homopolymer before and after for 24 h irradiation at 525 nm with eosin Y, in the presence of TEA and following prior deoxygenation of the system.*

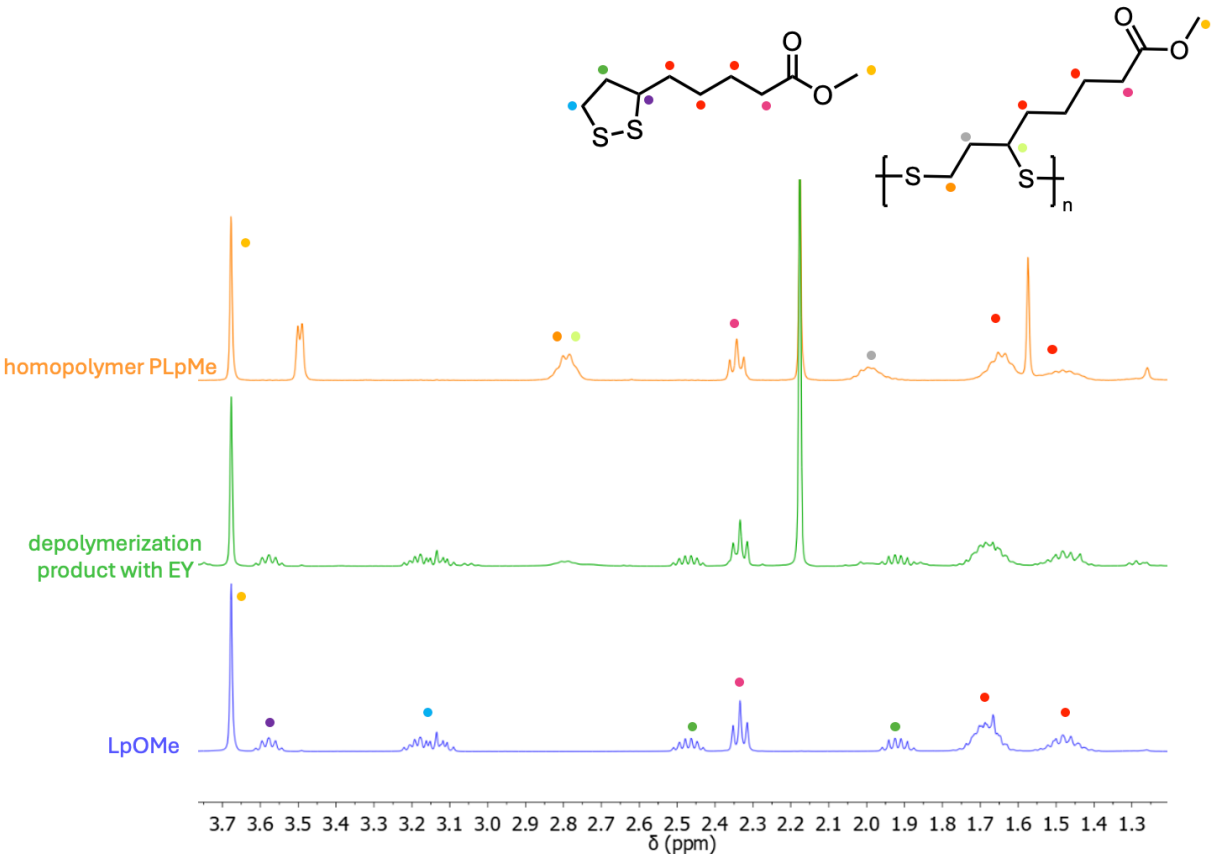

Figure 60: *^{1}H NMR spectrum of the homopolymer PLpOMe (orange), the depolymerized product after 24 h irradiation with eosin Y (green) and the monomer (blue).*

An analogous experiment was conducted using eosin Y and TEA under oxygen-free conditions, irradiating the system with green light for only 2 hours to investigate the kinetic of the depolymerization process. In this case, the ^{1}H NMR spectrum revealed a depolymerization yield of 86%, confirming that the reaction can proceed efficiently within a shorter irradiation time (Figure 62).

These results support the hypothesis previously proposed for TXO and XO, namely that the irradiation wavelength influences the outcome of the reaction. The results suggest that the photocatalysts enhance the depolymerization of PLpOMe, while light, depending on the wavelength employed, may also favour the oligomers formation from the resulting LpOMe. In the case of EY though, this second process does not appear to occur because, as shown in the UV-Vis spectra of the monomer (Figure 61), LpOMe exhibits no absorption at the longer irradiation wavelength.

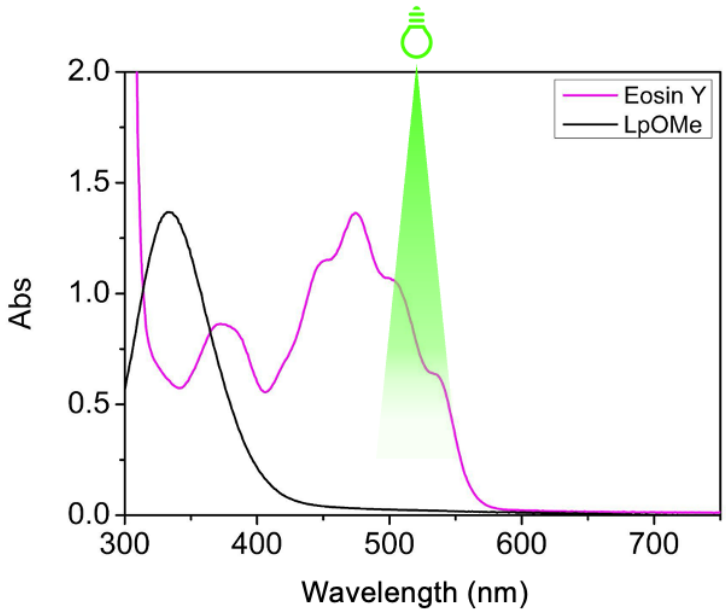

***Figure 61**: UV-Vis absorption spectra of eosin Y and LpOMe in THF.*

When the same experiment was conducted using only 2 hours of light irradiation and without prior deoxygenation, a depolymerization yield of 66% was achieved (Figure 62), while SEC analysis revealed a decrease in M_n from 693 kDa to 66 kDa (Figure 63a). Both these results evidenced that the depolymerization occurs in a shorter time than initially anticipated. Furthermore, the presence of oxygen appears to have an effect on the reaction under the investigated conditions, as molecular oxygen can act as a radical scavenger and thereby interfere with radical-mediated processes. These observations therefore suggest that the depolymerization mechanism may involve the formation of radical species.

The reaction was then repeated under identical conditions for 2 hours, but also in the absence of the electron donor, triethylamine, and without previous deoxygenation step. Under these conditions, the monomer was regenerated in 58% yield (Figure 62) and, starting from a homopolymer with a 693 kDa molecular weight, the final M_n measured through SEC analysis was about 36 kDa (Figure 63b). This latter experiment highlights that TEA is not required for this reaction mechanism involving eosin Y, suggesting that in this case the photocatalytic cycle might proceed through a different pathway compared to the one with thioxanthone and xanthone.

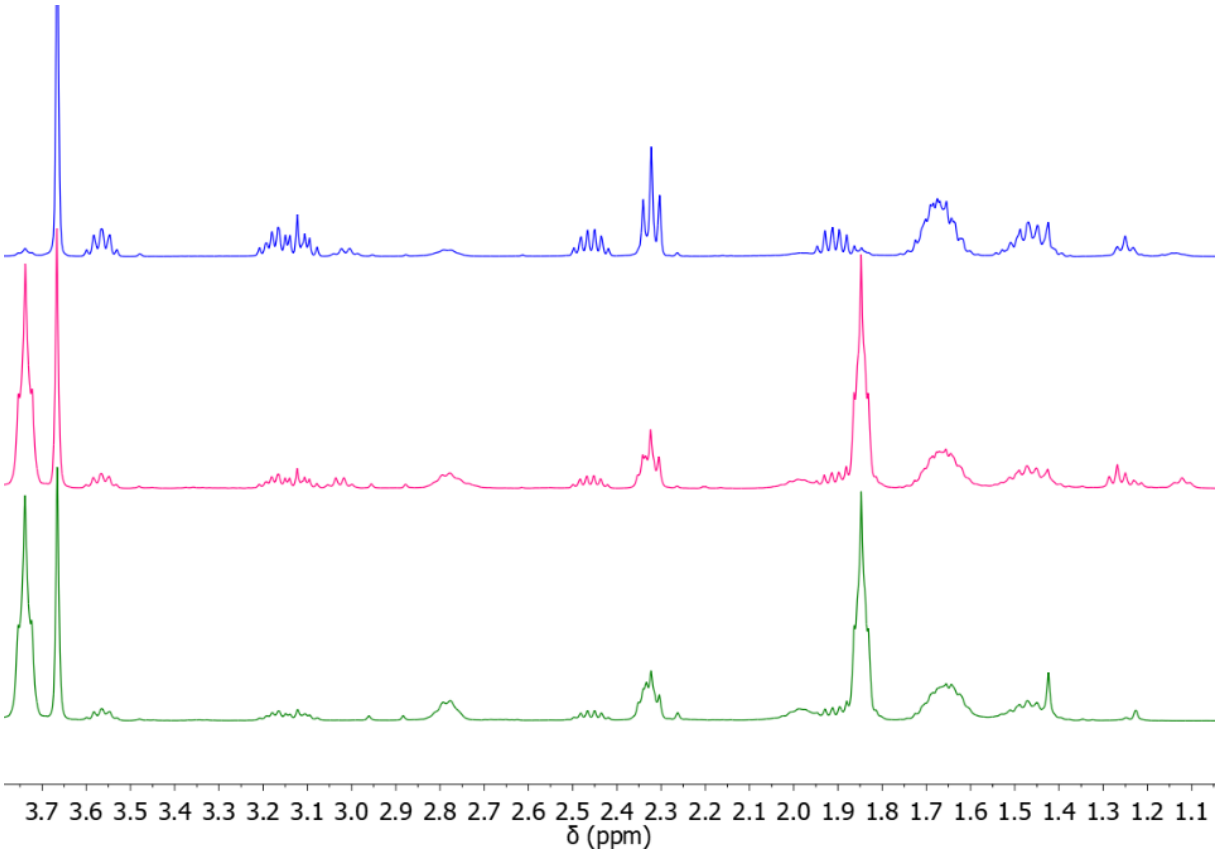

***Figure 62**: [1]H NMR spectrum of PLpOMe depolymerization products obtained with EY under 2 h irradiation of green light with: TEA and previous deoxygenation (blue), TEA and no previous deoxygenation (fuchsia) and no TEA and no previous deoxygenation (green).*

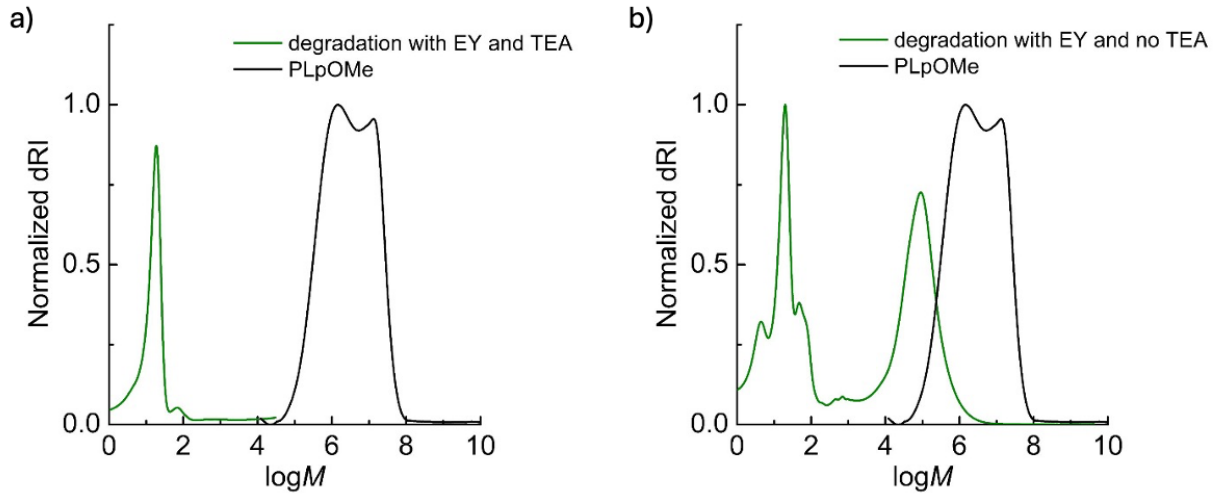

***Figure 63**: Evolution of the molecular weight distribution determined by SEC before and after 2h depolymerization with EY in the presence of TEA (a) and without TEA (b).*

Furthermore, the products obtained after different reaction times, 2 and 24 h of irradiation, exhibited comparable depolymerization yields and decreases in molecular weight, consistent with the rationale for employing a photocatalyst absorbing at higher wavelengths. Since LpOMe does not absorb green light, the regenerated monomer cannot be directly photoexcited after its formation by the excited eosin Y (Figure 61). Consequently, formation of radical species initiating a polymerization process is prevented, allowing the depolymerization process to proceed without regeneration of oligomeric species.

To elucidate the reaction mechanism, the depolymerization of PLpOMe was carried out in the presence of 5 mol% eosin Y and in the absence of TEA for 2 hours under green light irradiation in dichloromethane (DCM) (Table 3). A depolymerization yield of 74% was obtained, comparable to that achieved in THF, indicating that also with this photocatalyst the reaction pathway is likely independent of the solvent (S18).

When the reaction was conducted in the presence of 5 mol% butylated hydroxytoluene (BHT), an organic antioxidant and radical scavenger, after 2 hours irradiation depolymerization still occurred, although a lower monomer yield of 33% was obtained (S17). BHT is a synthetic phenolic antioxidant largely used as food additive. When added into a reaction mixture in which radical species are generated, BHT can efficiently scavenge them until it is completely consumed, thereby suppressing radical-mediated pathway[78]. The lower depolymerisation yield observed in the presence of BHT suggests that radical species may play a role in the depolymerization process. It is subsequently hypothesized that photoexcitation of eosin Y leads to the generation of radical species that, in the presence of the radical scavenger BHT, are efficiently quenched, thereby reducing the extent of depolymerization. Once all the radical scavenger is consumed, depolymerization might proceed regularly.

To further investigate this hypothesis, a 2 h depolymerization experiment was conducted under completely open-air conditions. Molecular oxygen can act as a radical scavenger by reacting with radical intermediates and forming peroxyl radicals. Therefore, continuous exposure of the reaction mixture to oxygen is expected to suppress radical-mediated pathways, comparable with a continuous addition of BHT. If the photocatalytic cycle proceeds exclusively through radical intermediates, no significant depolymerization would be expected under these conditions. In this case though, a 37% depolymerization yield was measured through ^{1}H NMR spectroscopy (S19), suggesting that the reaction might not proceed exclusively through radical intermediates. It is evident though how radicals play a key role in the reaction pathway since in both cases, with the addition of BHT and in open-air conditions, the reaction outcome is strongly inhibited.

Those results, combined with the lower yield obtained for the reactions performed in a confined system without prior degassing, support the hypothesis that radical species are involved in the depolymerization process.

Different photocatalysts absorbing in the 500–600 nm visible spectral range were subsequently evaluated. Rose Bengal was selected first because it exhibits photoredox properties comparable to those of eosin Y (since both are xanthene dyes), and both photocatalysts possess similar ground- and excited-state redox potentials. This supposition was confirmed as a 24 h reaction carried out in the presence of TEA after a degassing step yielded a depolymerized product with a depolymerization yield of 65%, comparable to that obtained with eosin Y (Table 3 and 4, Figure S20, S21). Thereafter methylene blue was also tested, a chromophore that has been largely used in biological and medical applications. Under the explicated conditions (Table 4), a depolymerization yield comparable to those obtained with eosin Y and Rose Bengal was observed, with regeneration of the monomer in 44% yield after 16 h of red-light irradiation (S22).

Photocatalyst	TEA	Solvent	Reaction time	Light wavelength	Oxygen	Depolymerization yield
Rose Bengal 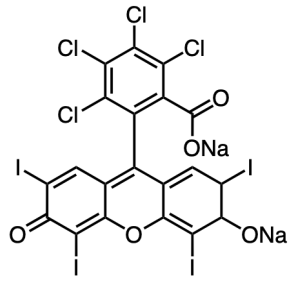	10 mM	THF	24 h	525 nm	no	65 %
Methylene blue 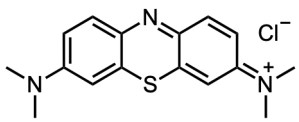	/	THF	16 h	625 nm	yes	46%

Table 4*: Reaction conditions and obtained results for the degradation experiments of PLpOMe with Rose Bengal and Methylene blue as photocatalysts.*

7.2.4 Hypothesised Reaction Mechanisms

To further rationalize the degradation and depolymerization of the homopolymer promoted by the investigated photocatalysts, cyclic voltammetry (CV) measurements were conducted, and the obtained results were confronted with the redox potentials of the photocatalysts reported in literature. Those measurements were in fact performed to evaluate the redox potentials of the disulfide groups in the homopolymer PLpOMe. Moreover, since it was hypothesized that the homopolymer undergoes depolymerization during the photocatalytic reactions, leading to the formation of the monomer LpOMe, the latter was also investigated by cyclic voltammetry.
The oxidation-reduction cycle obtained for the homopolymer PLpOMe represented in Figure 64, was obtained through a CV performed with a scan rate of 100 mV/s. The peak corresponding to the two-electron reduction of the disulfide bond to form a dianion is observed at −2.42 V vs SCE. After the reduction of the S-S group, through reversion of the potential scan, was possible to detect the oxidation peak at -0.92 V vs SCE. This peak is attributed to the re-oxidation of the reduced products.

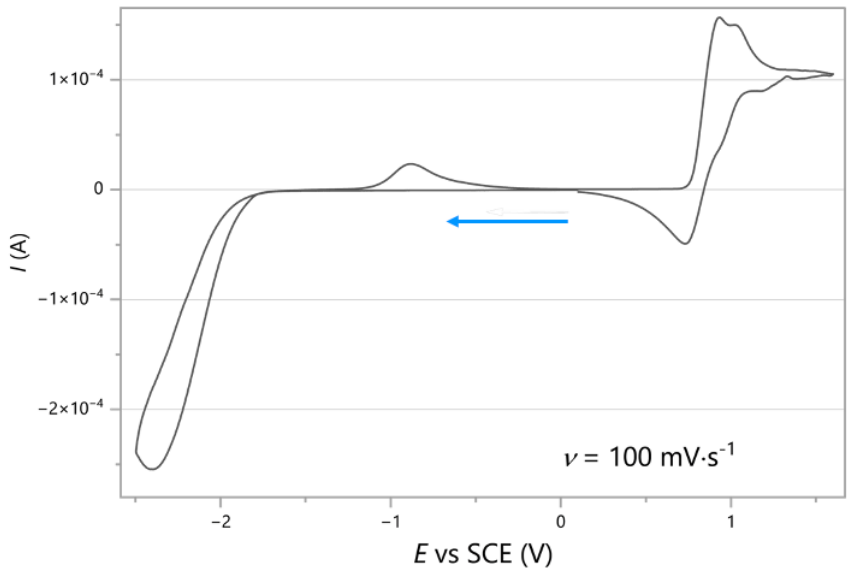

***Figure 64**: Cyclic voltammetry analysis of the homopolymer in MeCN.*

To determine the redox potential of methyl lipoate, the same analytical procedure was performed and the obtained results reported in Table 5.

	E_{pc} (V vs SCE)	E_{pSH} (V vs SCE)
LpOMe	-2.00	/
PLpOMe	-2.42	-0.92

***Table 5**: Redox potential determined by CV for the monomer LpOMe and the homopolymer PLpOMe.*

The obtained values were confronted with the redox potentials of the photocatalyst (Table 6) reported in literature to contextualise the photocatalytic reactions of degradation and depolymerization of the homopolymer[79].

Photocatalyst	$E_{1/2}^{red}$ (V vs SCE)	$E_{1/2}^{ox}$ (V vs SCE)	E_{red}^{S1} (V vs SCE)	E_{ox}^{S1} (V vs SCE)	E_{red}^{T1} (V vs SCE)	E_{ox}^{T1} (V vs SCE)
Thioxanthone	-1.62	+1.69	+1.52	-1.45	+1.18	-1.11
Xanthone	-1.65-	+1.8	+1.76	-1.61	+1.57	-1.42
Eosin Y	-1.08	+0.76	+1.23	-1.58	+0.83	-1.15

***Table 6**: Redox potential of the photocatalysts.*

For an electron-transfer (ET) photocatalytic cycle to occur, the redox potentials of the photocatalyst (PC) must be compatible with those of the substrate (in this case the homopolymer). This represents a key electrochemical requirement for achieving efficient electron transfer through either a reductive or oxidative quenching pathway[80]. When the oxidation or reduction potentials of the substrate are incompatible with that of the excited photocatalyst, an alternative photocatalytic pathway might be considered. For photocatalysts with a relatively high energy of the triplet state of the excited PC can occur an energy transfer (EnT) pathway. These processes indeed mainly depend on the triplet state energies of the organic substrates and the excited photocatalyst[81].

Considering the obtained redox potentials from cyclic voltammetry measurements and comparing them with those reported for the photocatalysts in literature, an electron transfer process appears to be rather unlikely for all the three photocatalysts mainly studied - xanthone, thioxanthone and eosin Y-. In contrast, all three photocatalysts possess a relative high energy triplet state, suggesting the EnT pathway as the most suitable one[68]. As described in Chapter

5, two different mechanisms have been proposed for energy-transfer processes: the Förster (Resonance) Energy Transfer (FRET), and the Dexter mechanism. Since the experiments conducted in this work are in solution, the Dexter mechanism is considered the most representative of the degradation/depolymerization process. In solution systems, indeed, the overall rate of EnT depends on both the diffusion rates of the interacting species, as the two molecules must encounter each other to transfer energy (is required a physical contact between energy acceptor and energy donor), and the intrinsic rate of the EnT event. In a collision complex the rate of the EnT is mainly governed by the spectral overlap integral, J, which quantifies the overlap between the donor T_1–S_0 emission and the acceptor S_0–T_1 absorption. In the context of a Jablonski diagram, J represents the number of transitions T_1–S_0 of the excited donor that can energetically induce a coupled S_0–T_1 transition in the ground-state acceptor. This quantity is directly related to the number of effective energy-transfer events and, consequently, to the rate of EnT. A significant spectral overlap is therefore required for efficient energy transfer, provided that the donor and acceptor are sufficiently close for the short-range Dexter interaction to occur. To determine the efficiency of an energy transfer process, that corresponds to the magnitude of J, it can be calculated a prediction based on the difference in the triplet excited state energies ΔE_T defined as the energy gap between the two T_1 states (Equation 5):

$$\Delta E_T = E_T(A) - E_T(D) \tag{5}$$

where D is the donor molecule, the photocatalyst, and A the acceptor molecule, the poly(methyl lipoate) in this case.

Energy transfer processes can promote the homolytic cleavage of σ bonds. It has been reported though how challenging can be the prediction of the bond dissociation based just on the triplet excited states energy values alone. Despite this, in combination with bond dissociation energy (BDE) values, the general likelihood of a dissociation event under EnT conditions can be predicted. In particular, when the BDE is approximately $\leq E_T$, the homolytic cleavage may become energetically accessible under EnT conditions[62]. Dexter-type energy transfer process in which the homolytic cleavage of disulfide bonds was promoted in the presence of an organic alloxazine photocatalyst and an Ir centred complex was reported by Teders *et al.*. They highlighted the possibility of this reaction based on the energetic compatibility between the excited triplet state energies of the PCs and the BDE of the disulfide bonds[82].

The BDE of lipoic acid was reported to be 60.52 kcal/mol (253.2 kJ/mol), based on the DFT calculations reported by Qui *et al.*[83] while in another work[82] the BDE of aliphatic disulfides is reported to be near 65 kcal/mol. Given the structural similarity between lipoic acid and the methyl lipoate units incorporated in the homopolymer, and the aliphatic disulfides and PLpOMe, these values can be considered a useful reference to evaluate the energetic feasibility of the S-S bond cleavage in the polymer.

Photocatalyst	**E_T (kcal/mol)**
Thioxanthone	63.4-65.4
Xanthone	74.1
Eosin Y	44.0
Rose Bengal	40.9
Methylene blue	32.0
4CzIPN	59.8
$[Ir(ppy)_3]$	57.8

***Table** 7: Triplet state energies of the photocatalysts reported in literature*[84]

Considering the triplet state energies of the commercial photocatalysts reported in Table 7, it is observable how, except for eosin Y, Rose Bengal and Methylene blue, the E_T values are approximately higher than the BDE of disulfides in the homopolymer. Based on these findings and previous literature reports, it can be hypothesised that the reaction pathways proceed via an energy-transfer mechanism. The photocatalysts are initially excited to their single excited states and subsequently undergo rapid ISC to populate their triplet excited states. The excited photocatalysts then transfer their excited state energies to the homopolymer, promoting the homolytic cleavage of disulfide bonds and the consequent formation of sulfur centred radicals. The generated $S^{\bullet}$ species subsequently promotes the unzipping of the PLpOMe, with the consequent generation of monomers or oligomers (Figure 65).

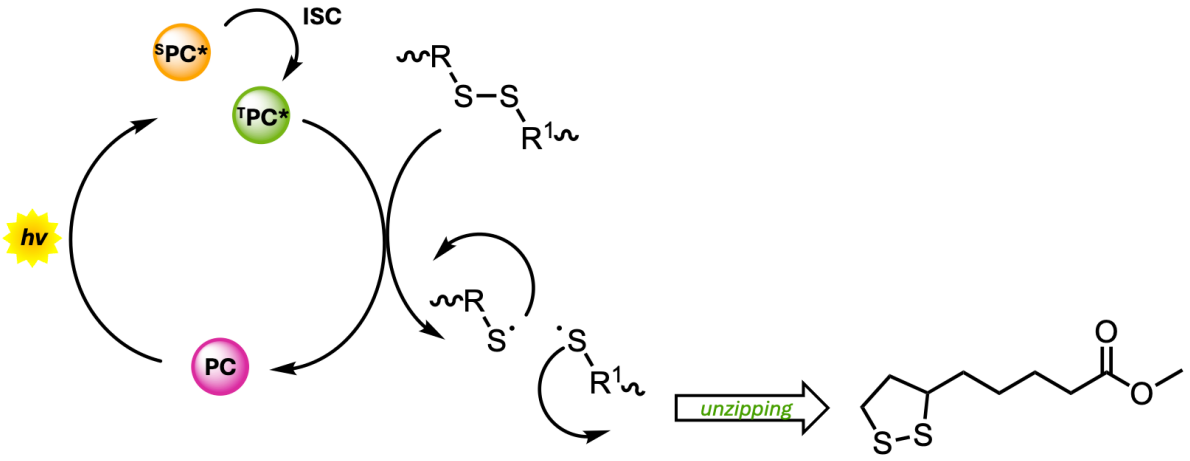

***Figure 65**: Proposed reaction pathway: the photocatalyst is excited to its singlet excited state and subsequently undergoes ISC to reach its triplet excited state. The latter transfer its energy to the homopolymer, promoting the homolytic cleavage of S-S. The resulting excited S• subsequently promotes the unzipping process, forming LpOMe.*

Despite this, the depolymerization pathways promoted by eosin Y – and Rose Bengal and Methylene blue– cannot be attributed to an energy transfer mechanism based solely on a comparison between the E_T of the photocatalysts and the BDE of the disulfide bonds in the homopolymer. Nevertheless, an EnT-mediated pathway cannot be completely excluded, as the comparison between the energies of the BDE of disulfides and the E_T of the PC provides only a general indication of the feasibility of the process. The E_T of the homopolymer might be of a comparable energy to the E_T of the photocatalysts, potentially promoting the triplet-triplet energy transfer and subsequent depolymerization. Despite these findings, further mechanistic investigations are necessary to elucidate the photocatalytic cycles.

7.2.5 Copolymer Degradation

The straightforward strategy to obtain polymers combining the desirable properties and broad applicability of conventional vinyl polymers with the degradability of lipoate-derived polymers, is to copolymerize acrylate monomers with lipoate monomers.

In this thesis, the optimized reaction conditions and the identified photocatalysts for the degradation and depolymerization of poly(methyl lipoate) were subsequently applied to the copolymer synthetized via RAFT polymerization of methyl lipoate and *n*-butyl acrylate (polymerization procedure reported in the Supporting Information).

The first experiment with the 70:30 *n*BA:LpOMe copolymer was performed maintaining the same reaction conditions of previous degradations with thioxanthone (Table 1); in the presence of triethyl amine (10 mM), was prepared a THF solution containing the copolymer and the photocatalyst (5 mol%) in a confined system. Following 24 hours of light irradiation (λ_{max}=427 nm), the obtained product was characterized through ^{1}H NMR spectroscopy and size exclusion chromatography (SEC).

The ^{1}H NMR spectrum revealed the characteristics thiols signals, identified around 1.3 ppm (Figure 66), confirming the occurrence of degradation. Furthermore, starting from a 14.9 kDa copolymer, the analysis of the chromatograph obtained for the resulting product revealed a final molecular weight M_n of 7.5 kDa (Figure 67b), indicating a substantial reduction in the polymer chain length.

When the photocatalytic reaction was performed under the same reaction conditions using eosin Y as photocatalyst, in the presence of TEA and under green light irradiation (λ_{max}=525 nm), after 24 hours the SEC analysis revealed a product with a 11.3 kDa final molecular weight M_n, starting from a 14.9 kDa copolymer (Figure 67a). However, the ^{1}H NMR spectrum showed neither the presence of the characteristic signals of thiols groups, nor those of the LpOMe monomer (Figure 66).

Repeating the reaction under the same conditions but with a shorter irradiation time, 16 hours, resulted in a product with a comparable decrease in molecular weight, final M_n=11.1 kDa. In the ^{1}H NMR spectrum, signals were observed in the characteristic chemical-shift region of thiol groups; however, their assignment to thiol functionalities could not be confirmed unambiguously and could not be quantified (S23).

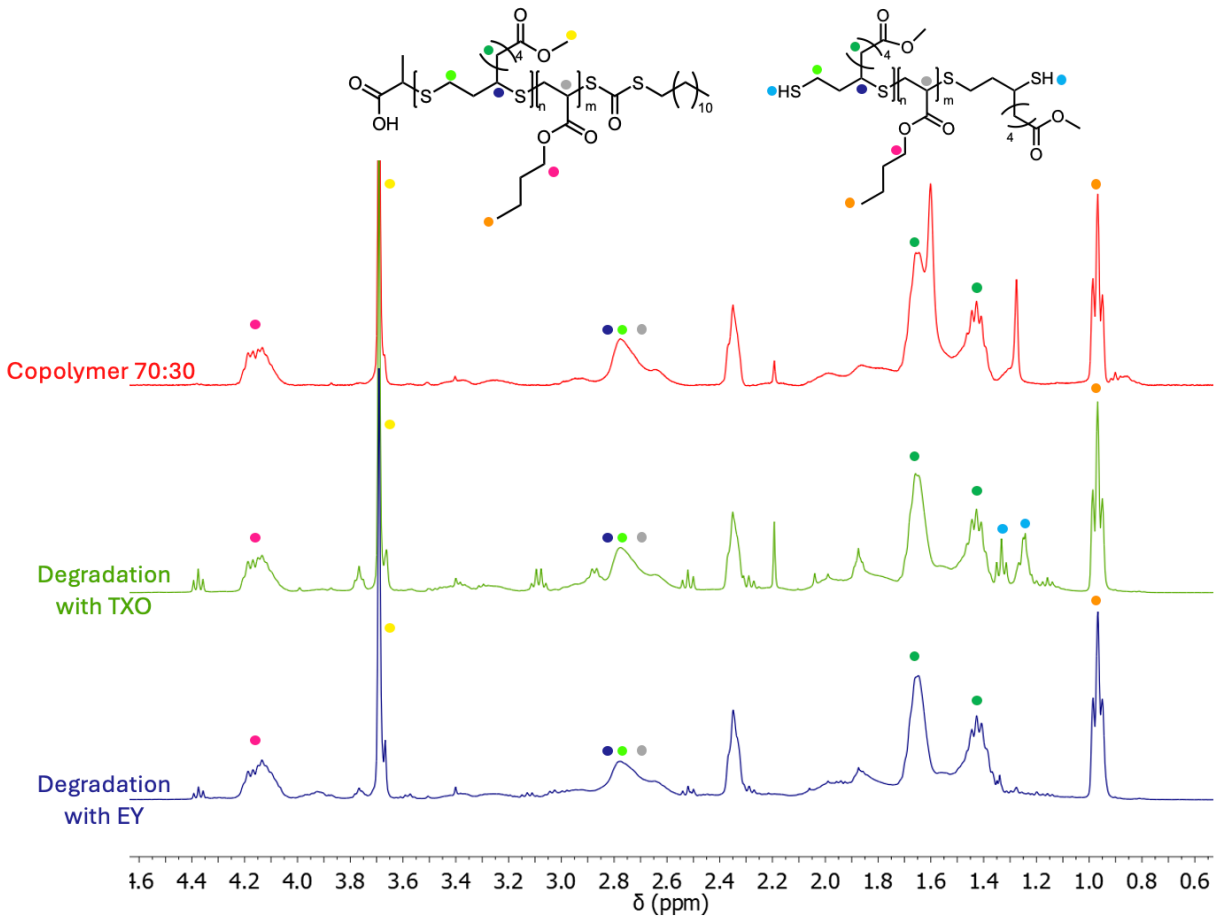

***Figure 66**: [1]H NMR spectra of the copolymer (red), and the degradation products obtained with thioxanthone (green) and eosin Y (blue) after 24 h of light irradiation.*

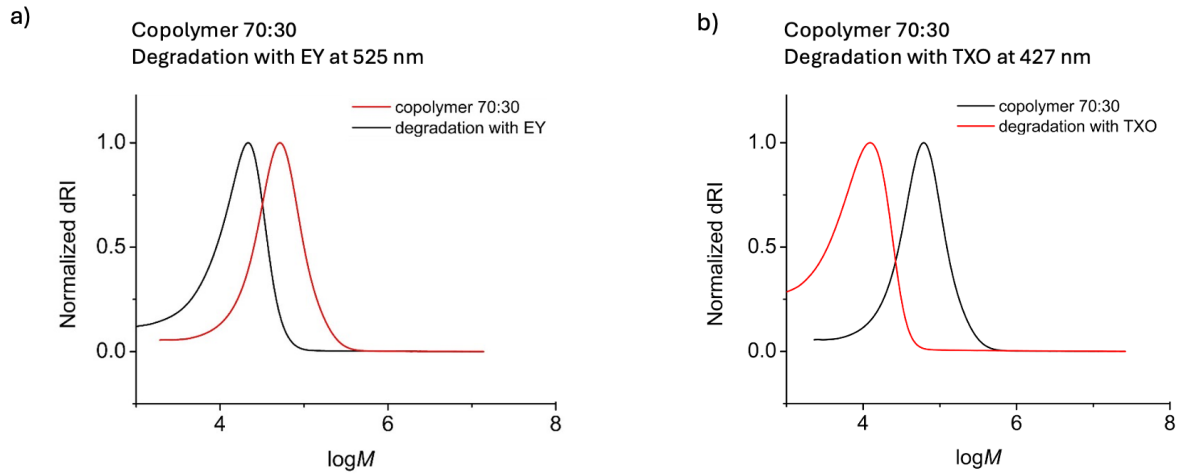

***Figure 67**: Evolution of the molecular weight distribution determined by SEC before and after depolymerization with EY (a) and TXO (b).*

Based on the previously results obtained for the depolymerization of PLpOMe with eosin Y, the presence of monomer signals was expected in the NMR spectrum of the degradation with this photocatalyst.

Hypothesis for the lack of depolymerization of the copolymer were formulated. Kinetic studies reported in literature by Albanese *et al.*[6] indicate a faster incorporation of lipoic acid compared to *n*BA during their RAFT copolymerization. In support to this, the previous study of Albanese *et al.*[85] where ethyl lipoate was copolymerized with *n*BA, reported the reactivity ratios for *n*BA−ELp copolymerization to be r_{ELp} = 18.5 and r_{nBA} = 0.36. Therefore, a similar reactivity trend can be expected for the RAFT copolymerization of LpOMe and *n*BA.

Because of the different reactivity ratios of the two comonomer, is promoted the LpOMe incorporation in the polymer backbone and this kinetic behaviour is favoured for the formation of disulfide diads along the polymer chain, that enable the degradation. Conversely, in order to have depolymerization, at least three subsequent LpOMe monomer units are needed in the polymer backbone.

Through analysis of the NMR spectra was possible to estimate the proportion of disulfide bonds in the copolymer at 13%. Given this relatively low concentration of disulfide-containing units, the probability of their occurring as consecutive LpOMe sequences forming triads is expected to be limited. Therefore, the effective concentration of LpOMe triads may be too low to enable significant formation of LpOMe units. This structural feature may thus provide a rationale for the observed reaction outcome. Although the disulfide-containing monomer is expected to be incorporated preferentially over the acrylate monomer, the higher concentration of *n*BA in the reaction mixture may reduce the probability of forming triads of LpOMe along the polymer backbone. Consequently, even if such sequences are present within the polymer chains, their concentration might be too low to promote significant depolymerization, resulting in a concentration of methyl lipoate below the detection limit of ^{1}H NMR spectroscopy.

To elucidate the reaction pathway, also in the case of the copolymer, cyclic voltammetry studies were performed to evaluate the redox potentials of the disulfide bonds. The peak corresponding to the reduction of the disulfide bonds was observed at -2.31 V vs SCE, whereas the thiol oxidation peak potential E_{pSH}, was found at -0.16 V vs SCE (Figure 68). As expected, also in this case, the redox potentials of the photocatalysts (Table 6) are not compatible with those of the copolymer, thereby making an electron transfer mechanism unlikely. Consequently, considering the energies of the triplet excited states of the photocatalysts and the BDE of disulfide bonds reported in literature, together with the previous considerations discussed for

the homopolymer, an energy transfer reaction pathway is likely to occur when thioxanthone is employed. Hence, similarly to what previously hypothesised, the excited photocatalyst undergoes ISC reaching its triplet excited state. From the triplet excited state the TXO transfers its energy to the disulfide bonds in the copolymer, promoting their homolytic cleavage. In this specific case though, owing to the alternation between LpOMe and *n*BA monomeric units, the unzipping process, proposed for PLpOMe, is promoted only when more than two consequent LpOMe units are present. Otherwise sulfur centred radicals are quenched either through recombination reactions with other sulfur centred radicals or by reaction with protons present in the solution mixture, presumably originating from the solvent. The latter pathway is supported by the observation of the corresponding thiol signals in the NMR spectra (Figure 66).

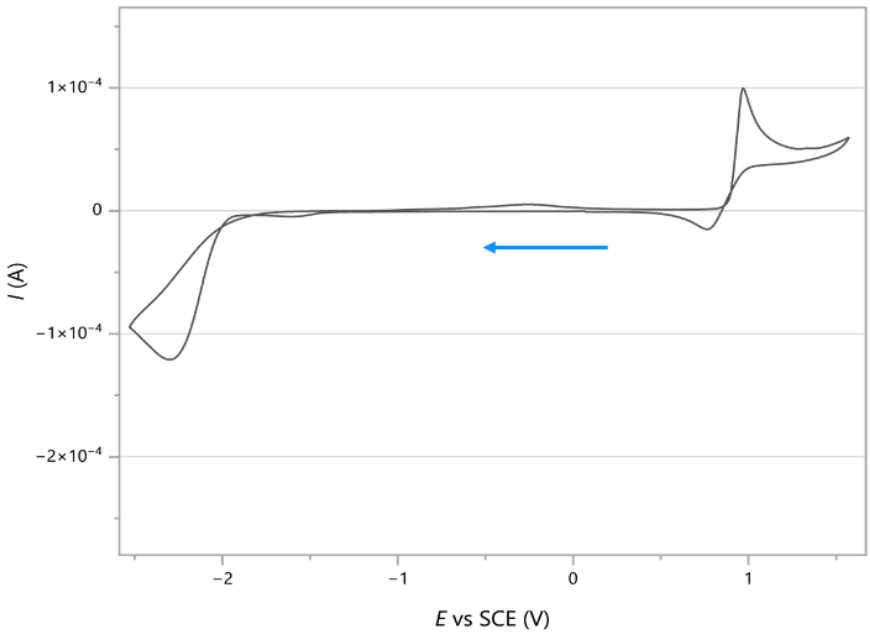

***Figure 68**: Cyclic voltammetry analysis of copolymer in MeCN.*

For eosin Y, however, also in the degradation of the copolymer, the reaction mechanism cannot be unambiguously assigned to an energy-transfer pathway.

7.2.6 Conclusions

It has been demonstrated that different photocatalysts, upon excitation, can promote the cleavage of disulfide bonds within polymer chains, thereby leading to a reduction in molecular weight.

Studies on the homopolymer revealed that, depending on the photocatalyst employed, the reaction resulted either in depolymerization or in degradation of the polymer. The final outcome did not depend directly on the photocatalyst employed, but rather on the wavelength used to excite the photocatalyst. In fact, as demonstrated by both studies on the monomer and kinetic analysis of the degradation/depolymerization processes, it has been hypothesised that the excited photocatalyst promotes the homolytic cleavage of the disulfide bonds within the homopolymer backbone. Consequently, the resulting sulfur-centred radicals, potentially involving a backbiting step, progressively lead to the formation of the monomer, the methyl lipoate. Depending on the wavelength used to irradiate the system, the latter may subsequently form oligomeric species due to its chromophoric nature. Indeed, upon irradiation at 365 nm and 427 nm, the resulting products after just 2 h irradiation showed the presence of monomer, whereas no monomer signals were detected in the NMR spectra at longer reaction times. This hypothesis was further confirmed by irradiation of the monomer at 365 nm and 427 nm for 16 h, after which no monomer signals were detected in the NMR spectra of the resulting products. On the other hand, reactions performed using eosin Y as the photocatalyst continued to show monomer signals even after prolonged irradiation, as eosin Y was excited at 525 nm.

Cyclic voltammetry studies enabled the determination of the redox potentials of disulfide bonds in PLpOMe, which were subsequently compared with those of the photocatalysts (TXO, XO, EY). The obtained values elucidate the improbability of an electron transfer pathway to occur, contrary to the initial assumption based on the photocatalytic cycle proposed by Zhou *et al*[66]. Alternatively, comparison of the energies of the triplet excited state of photocatalysts with the BDE of disulfide bonds suggests that an energy transfer mechanism may rationalize the homolytic cleavage of S-S bonds within the polymer backbone with TXO and XO. The energy-transfer pathway, however, cannot be considered a plausible mechanism in the case of eosin Y since the E_T is substantially lower than the BDE of the S–S bond.

Preliminary studies were also conducted for the degradation of the copolymer using TXO and eosin Y. in both cases, irradiation of the 70:30 *n*BA:LpOMe copolymer with both photocatalysts resulted in a decrease in the molecular weight of the resulting products, indicating the occurrence of degradation processes. When thioxanthone was employed, the

degradation process resulted in the reduction of S-S bonds to thiol groups, as highlighted in the NMR spectrum. On the contrary, thiols evaluation was not possible in the presence of eosin Y, although a decrease in molecular weight was still observed by SEC. Furthermore, no depolymerization products were detected, conversely on the results obtained for the homopolymer. This behaviour was hypothesised to be related to the quantity of triads of LpOMe units along the polymer backbone. A lower number of disulfide bonds within the polymer backbone is expected to reduce the probability of LpOMe triad formation. The relatively low estimated content of disulfide bonds in the copolymer (13%) raises the possibility that the quantity of triads is too low to promote significant depolymerization. Consequently, even if depolymerization occurred, the detection of LpOMe units may be impossible to be detected by ^{1}H NMR spectroscopy.

A possible direction for future investigations would be to further investigate the homopolymer degradation with the different photocatalysts in order to gain a more comprehensive understanding of the corresponding photocatalytic cycles, especially for the depolymerization with eosin Y. The photocatalytic pathways previously mentioned indeed are hypothesis and need to be supported by stronger investigations.

Additional studies should also be carried out on the copolymer. To obtain copolymers with a major incorporation of disulfide units along the polymer backbone, copolymers with a different nBA:LpOMe ratio (50:50 for example) can be synthetized, increasing the lipoate monomer quantity. An increased LpOMe content is expected to increase the probability of forming consecutive LpOMe sequences, including triads, thereby potentially enhancing the extent of the depolymerization process. In conclusion, to better understand the mechanism, a more detailed investigation of the copolymer degradation/depolymerization process is required to gain a more precise understanding of the photocatalytic pathways with the different photocatalysts investigated.

Supporting Information

8.1 Materials and Instruments

Commercial grade reagents and solvents were purchased from Sigma Aldrich, FluoroChem or BLDpharma and used as received, unless otherwise stated.

Commercial liquid monomers were purified by passing through a basic aluminum oxide column to remove the inhibitor before use. Also synthetized LpOMe was purified by passing through a basic aluminum oxide column to remove the BHT before use.

Ultrapure water was purified with a Millipore Direct-Q 5 ultrapure water system or a Milli-Q® IQ 7003 purification system.

Surface modifications were performed on manually cut silicon wafers (single polished) purchased from Si-Mat (Landsberg, Germany).

NMR spectra were recorded on Bruker AVANCE Neo 400 Nanobay equipped with a BBFOATM-z grad probehead. All NMR spectra were processed and analyzed using MestreNova software. The chemical shifts (δ) for ^{1}H and ^{13}C are given in ppm relative to residual signals of the solvents ($CHCl_3$ @ 7.26 ppm ^{1}H NMR, 77.16 ppm ^{13}C NMR). Coupling constants (J) are given in Hertz (Hz). The following abbreviations are used to indicate the multiplicity: s, singlet; d, doublet; t, triplet; q, quartet; m, multiplet; bs, broad signal.

Chromatographic purification of products was accomplished using flash chromatography on silica gel (SiO_2, 0.04-0.063 mm) purchased from Merck, with the indicated solvent system. Thin-layer chromatography (TLC) analysis was performed on pre-coated Merck TLC plates (silica gel 60 GF254). Visualization of the developed chromatography was performed by checking with aqueous potassium permanganate solutions. Organic solutions were concentrated under reduced pressure on a Büchi rotary evaporator.

Thickness measurements were performed with a variable-angle spectroscopic ellipsometer from Semilab ZRt (Semilab SE2000). Ellipsometric data (i.e., Ψ and Δ plotted towards beam wavelength) was recorded at an incident angle of 70° and wavelength range of 275–990 nm at

room temperature. For each substrate, a minimum of three points was taken for the measurements. The resulting spectra were fitted with the in-suite SEA software, using a four-layer Si/SiOx/polymer/air model.

Brush thickness was evaluated by AFM mechanically removing the films by plastic tweezers and subsequently measuring step-height in air. To this end, AFM height micrographs were acquired by standard tapping-mode method using a Dimension Icon AFM (Bruker, Santa Barbara, USA) equipped with RTESPA-300 (Bruker, Santa Barbara, USA) cantilevers having a spring constant of ~40 N m^{-1}.

Static water contact angles (CA) were determined using a manual goniometer (model 100, Ramé Hart Inc., USA) at room temperature and using ultrapure water (5 μL). A 5 μL droplet of ultrapure water was deposited onto the substrate. The contact angle was measured immediately after droplet deposition.

UV–Vis spectra were recorded on an Agilent Cary 60 spectrophotometer equipped with an 18-cell holder coupled to a Huber thermostat, using Suprasil quartz cuvettes (114- QS) 10 mm path length.

The irradiated power of the LEDs source was measured using a Thorlabs PM100D power meter equipped with a Thorlabs S142C sensor (responsive in the range 350–1100 nm). Photochemical reactions performed with Kessil lamps were irradiated using a Kessil PR160L LED PhotoReaction Lighting system (Kessil, USA), equipped with a 400 nm, 427 nm and 525 nm, LED module.

Electrochemical measurements for cyclic voltammetry were performed using a VIONIC potentiostat controlled by NOVA software (Metrohm Autolab). All experiments were carried out in a conventional three-electrode cell configuration. A platinum wire electrode (99.9%, ST 0.6/40 mm) was used as the counter electrode, while a glassy carbon electrode (70 mm length, 2 mm diameter, body diameter 6 mm) served as the working electrode. A non-aqueous Ag/Ag+ refillable electrode (6 mm diameter) was employed as the reference electrode.

Purification of the polymers was carried out by dialysis using Spectra/Por® dialysis membranes with molecular weight cut-offs (MWCO) of 1, 3.5, 8, 10 kDa.

Gel permeation chromatography (GPC). For the resulting copolymers and their corresponding degradation SEC was performed using a Shimadzu NEXERA system equipped with two PSS Agilent columns and one Phenogel column (SDV, 300 × 8 mm, pore sizes of 500, 1000, and 105 Å), and a refractive index detector. Stabilized tetrahydrofuran (THF) was used as the mobile phase at a flow rate of 1 mL min^{-1} and a temperature of 40 °C. Each sample was prepared by dissolving the polymer at a defined concentration of 1 mg mL^{-1} in THF. Instrument's calibration was performed using poly(methyl methacrylate) (PMMA) standards of known molecular weight (2680–400000 Da) supplied by Polymer Laboratories Ltd.

8.2 Photochemical Reaction Setup for Polymer Brushes Experiments

For the photochemical reactions, UV light-emitting diodes (LEDS) were employed: Philips TL-D 15W ACTINIC BL (8K) with λ_{max}= 365 nm. The tubes were placed at a distance of 9 cm from the light source, where the measured power density corresponded to 7.0 (± 0.7) mW/cm^2. A fan was used to maintain a constant temperature (25°C) (Figure S1).

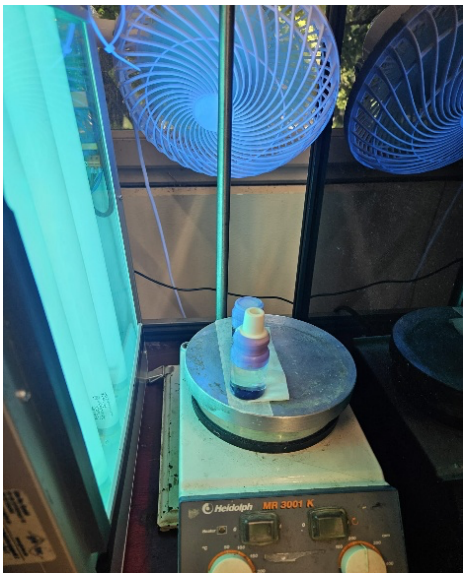

Figure S1*: Photo of the polymerization set up. At the side, a fan is present to control the temperature.*

8.3 Photochemical Reaction Setup for Degradation Experiments

For the degradation and depolymerization reactions, UV light-emitting diodes (LEDS) provided by Philips TL-D 15W ACTINIC BL (8K) with λ_{max}= 365 nm were used for the

experiments at 365 nm. Kessil lamps operated at 25% intensity were employed for the experiments performed at 427, 525 and 400 nm while, for experiments with red light, LEDS with λ_{max}= 625 nm were used, with a measured power density of 50 mW/cm^2.

When the system was irradiated with LEDS (λ_{max}= 365 nm), vials containing the reaction mixture were placed at a distance of 9 cm from the light source. When Kessil lamps and red light LEDS were employed to irradiate the system, vials were placed at a distance of 5 cm from the lamps. To maintain a constant temperature (25°C), a fan was used (Figure S2).

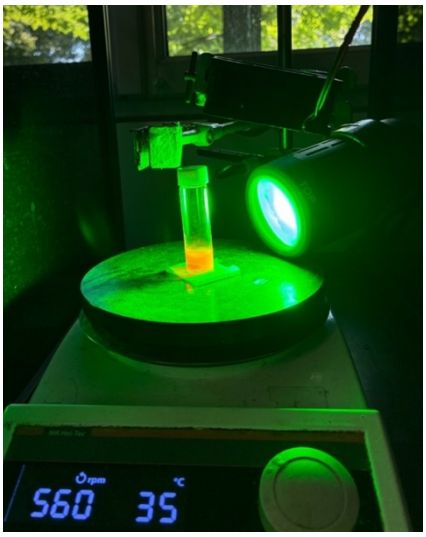

Figure S2*: Photo of the polymerization set up with Kessil lamp. At the side, a fan is present to control the temperature*

8.4 Synthetic procedures

8.4.1 Synthesis of methyl α-bromoacrylate (BrMA).

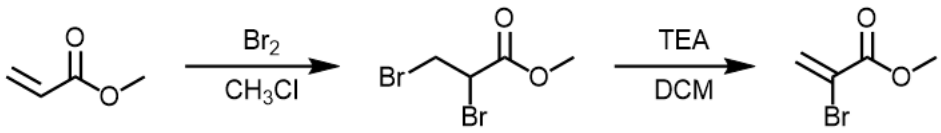

Figure S3: *Synthesis of BrMA.*

A 250 mL round-bottom flask equipped with a magnetic stir bar was charged with methyl acrylate (5.0 g, 52 mmol, 1 eq.) and dissolved in methylene chloride (105 mL). The flask was sealed with a septum, and bromine (9.65 g, 60 mmol, 1.16 eq.) was added via syringe. The

progress of the reaction was monitored by the gradual disappearance of the characteristic dark bromine colour, yielding an orange-yellow solution. The reaction mixture was stirred for 4 h. Upon completion, excess bromine was quenched by addition of sodium sulfite (20.0 g, 158 mmol), and the mixture was stirred until the colour changed from orange to pale yellow. The resulting suspension was filtered, and the solids were washed with methylene chloride. Methyl 2,3-dibromopropionate was obtained in quantitative yield and used in the subsequent step without further purification. To a stirred solution of methyl 2,3-dibromopropionate (12.8 g, 52 mmol, 1 eq.) in DCM (100 mL), Et_3N (6.30 g, 62.4 mmol, 1.2 eq.) was added dropwise at 0 °C. The mixture was slowly raised to room temperature and stirred at the same temperature for 24 h. The generated salts were then dissolved by water and the mixture was extracted with Et_2O. The combined organic layers were dried over Na_2SO_4, filtered, and concentrated. After purification by flash column chromatography on silica gel (n-hexane/EtOAc = 9/1 as eluent), BrMA (6.35 g, 38.5 mmol) was obtained in 74% yield as a colourless liquid.

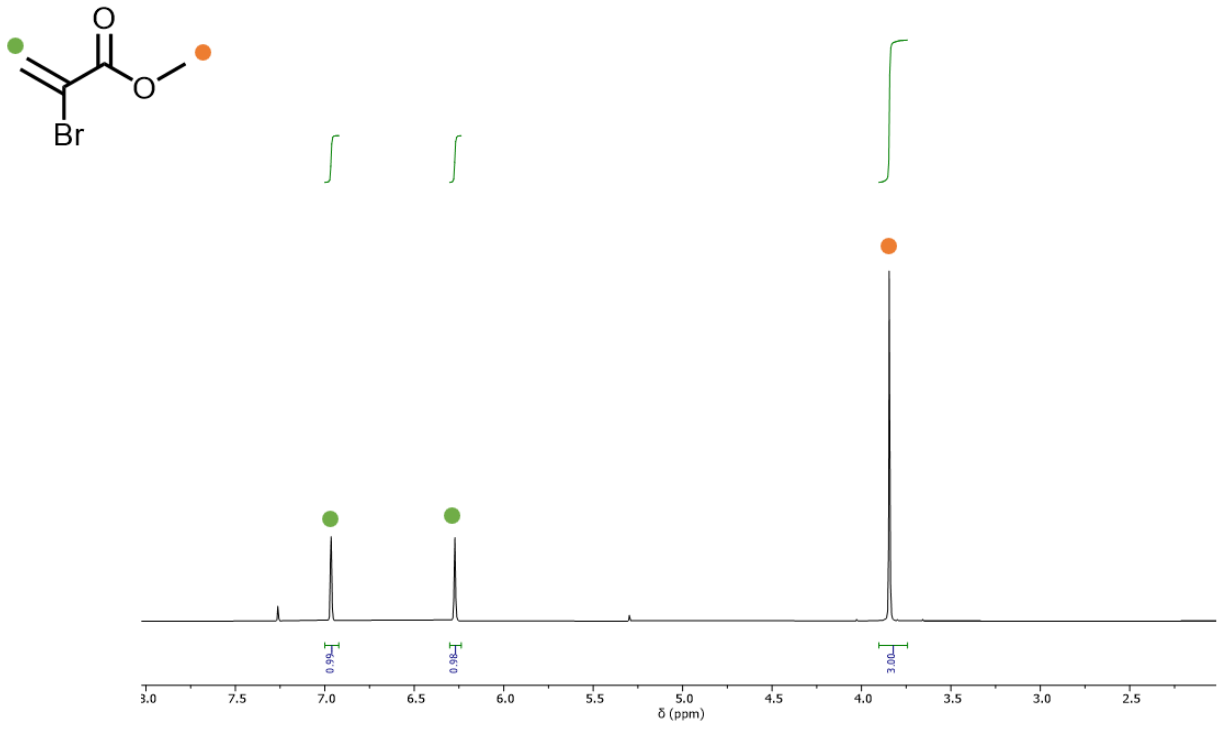

***Figure S4**: ^1H NMR spectrum of the synthetized inibramer.*

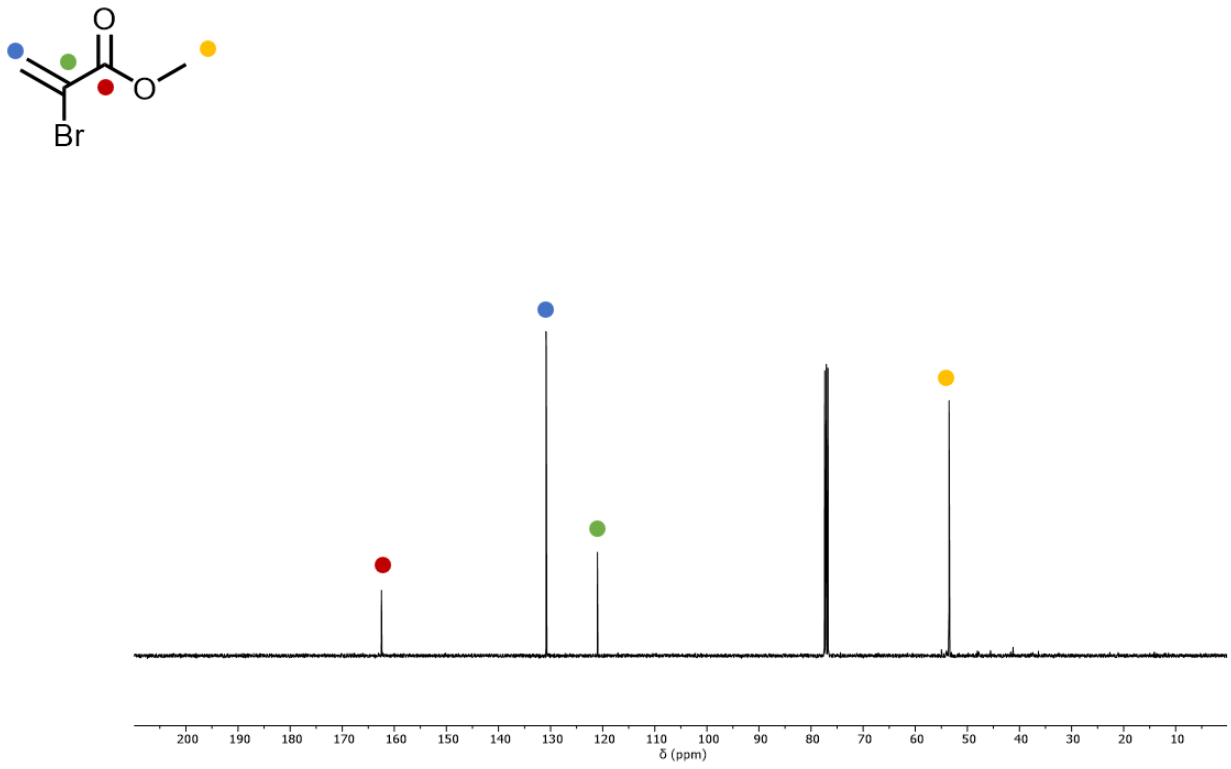

***Figure S5**: ^{13}C NMR (125 MHz, CDCl3) spectrum of the synthetized inibramer.*

8.4.2 Procedure for the Preparation of ATRP Initiator Layer on SiOx Substrate

Silicon substrates of size 15x20 mm were first cleaned in piranha solution (3:1 mixture (v/v) of H_2SO_4 and H_2O_2) for 1 h and then washed with ultrapure milliQ water (Millipore Milli-Q grade) and absolute ethanol before being dried under a stream of N_2. Subsequently, SiOx surfaces were functionalized with (3-Aminopropyl)triethoxysilane (APTES) by vapor deposition in a desiccator maintained under vacuum for 3 h, then rinsed sequentially with ultrapure water, ethanol and toluene before being dried with N_2. Following this, the APTES-bearing substrates were soaked in a dry DCM solution containing α-bromoisobutyryl bromide (BiB) (0.12 M) and TEA (0.12 M). The reaction was performed overnight at room temperature. The following day, substrates were washed with DCM, followed by ethanol and dried under nitrogen. The functionalized substrates were then stored in a Petri dish to avoid contamination.

8.4.3 General Procedure for SI-photoATRP

All polymerization mixtures were prepared in the same way. For all the polymerization mixture the final volume was set to 6 ml. The final concentration of *t*BA and *n*BA monomer was 1.35 M whereas for OEGA480 (M_n ~ 480 Da) the concentration was 0.71 M. The concentration of BrMA was varied accordingly to the experiment and inserted from different stock solution at different concentration. The solution containing monomers and DMSO was degassed for 20 min with argon. The catalytic system, comprising $CuBr_2$ as catalyst and Me_6TREN as ligand in a ratio [CuBr2]:[L] of 1:6, and at concentration 16:96 mM was degassed separately for 20 min and then 50 ul of solution were added to the solution of monomers and DMSO and put under UV light (λ_{max}= 365 nm) and irradiated for the desired time. After that the substrate was removed from the vial and cleaned with ethanol, DCM and ethanol. Finally, the substrates were dried under a stream of N_2.

8.4.4 Synthesis of the Monomer Methyl Lipoate (LpOMe) [86]

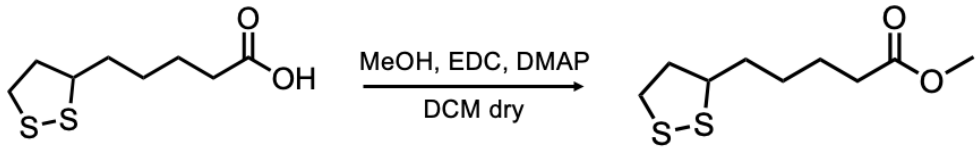

Figure S6: *Synthesis of LpOMe.*

In a round-bottom flask equipped with a magnetic stir bar, lipoic acid (6.67 g, 32.3 mmol), 4-(N,N-dimethylamino)piridine (DMAP, 1.97 g, 16.17 mmol) and N-(3-dimethylamino-propyl)-N' -ethylearbodimide hydrochloride (EDCI, 7.43 g, 38.67 mmol) and a spatula tip of BHT were dissolved in anhydrous dichloromethane (100 mL). Subsequently the resulting solution was cooled in an ice bath, and methanol (10.3 g, 323.3 mmol) was added dropwise under magnetic stirring while maintaining the reaction flask in the ice bath. The reaction mixture was then covered from light with aluminium foil, stirred and warmed to room temperature overnight. The following day, the organic solution was concentrated under reduced pressure on a rotary evaporator. Afterwards the crude product was purified by column chromatography on silica gel using a n-hexane/DCM = 3/7 eluent. The collected LpOMe fractions were concentrated under reduced pressure on a rotatory evaporator after the addition of a small amount of BHT. The resulting yellow oil was stored in a freezer after the ^1H NMR analysis (Figure S7).

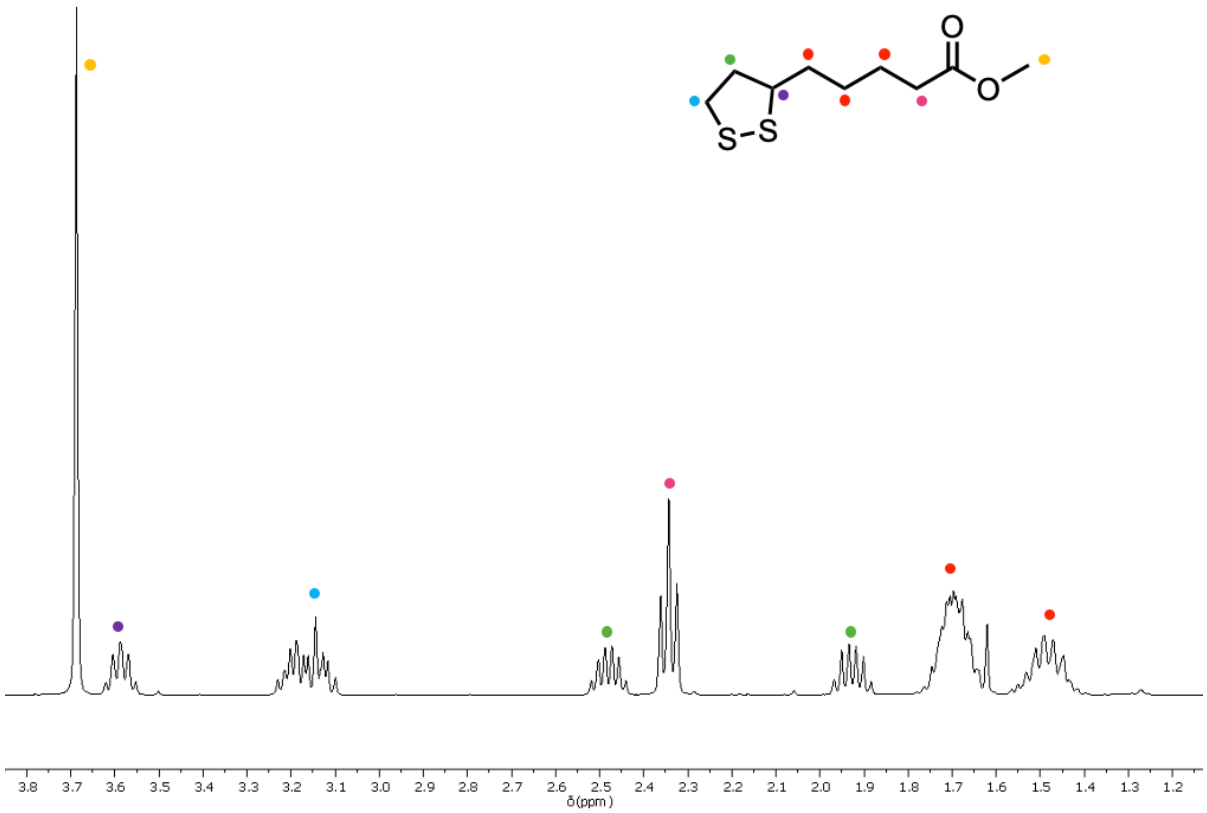

***Figure S7**: [1]H NMR spectrum of the resulting product LpOMe.*

8.4.5 Synthesis of the Homopolymer PLpOMe [87]

For the synthesis of the homopolymer, a modified procedure of Endo *et.al* was followed. Specifically, 2 g of LpOMe were added to a two neck schlenk flask after the inhibitor, BHT, removal. The monomer was then subjected to three vacuum-argon cycles before immersing the flask in an oil bath at 90 °C. The reaction was performed overnight. The obtained polymer was then purified using a 10 kDa molecular weight cut-off (MWCO) dialysis membrane in acetone for 2 days, replacing the acetone every 8 h.

The homopolymer was then dried removing the solvent under reduced pressure using a rotatory evaporator and subsequently analysed by ^{1}H NMR spectroscopy (Figure S8) and size exclusion chromatography (SEC).

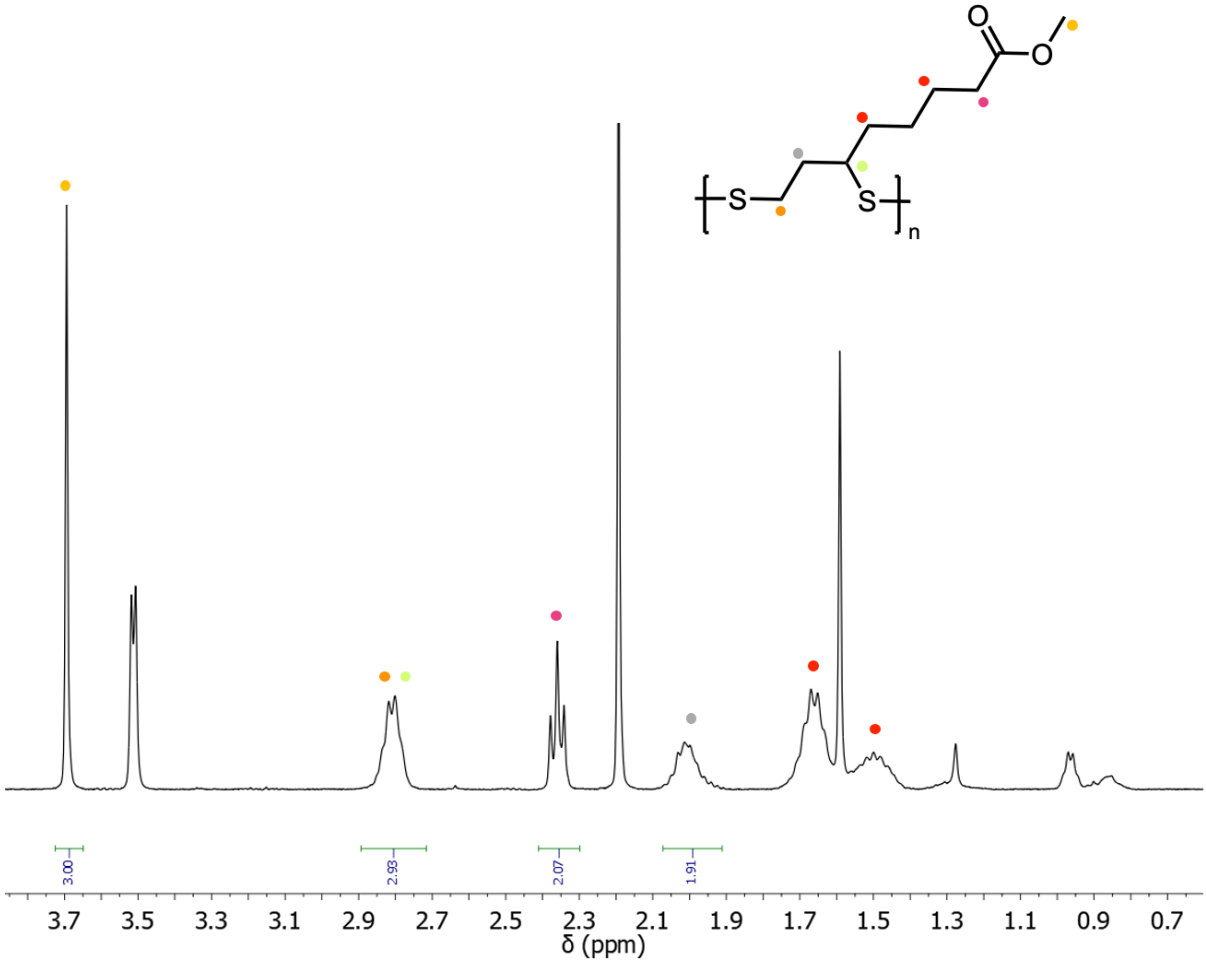

***Figure S8**: [1]H NMR spectrum of the resulting homopolymer after purification with dialysis.*

8.4.6 Synthesis of the Copolymer through RAFT Polymerization

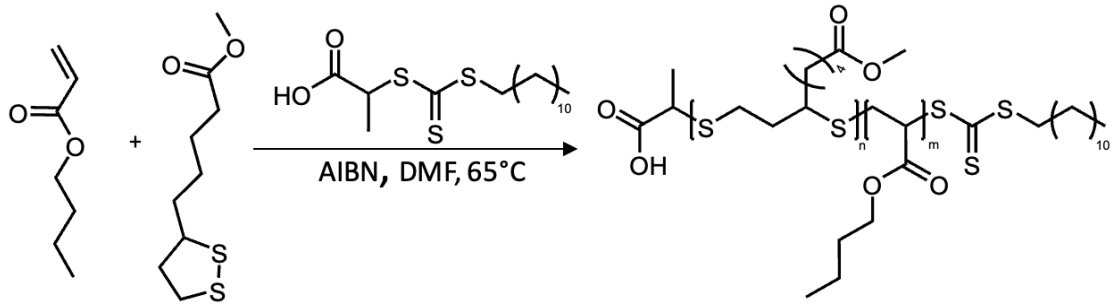

***Figure S9**: Schematic representation of the RAFT polymerization of the copolymer.*

For the synthesis of the copolymer, were employed methyl lipoate (LpOMe) and *n*-butyl acrylate (*n*BA), with a ratio of 30:70 LpOMe:*n*BA, targeting a degree of polymerization (DP) of 500, and the expected molecular weights (M_n) was approximatively 78 kDa.

The copolymer was synthetised through RAFT polymerization, following a procedure adapted from that reported by C.J. Hawker *et al.*[6].

In a vial immersed in an ice bath, were added the two monomers, the LpOMe (2.7 mmol) and *n*BA (6.4 mmol), and 18 umol of 2-(dodecylthiocarbonothioylthio)propionic acid, the CTA. Subsequently was added azobisisobutyronitrile (AIBN) (1.8 umol) as radical initiator through a stock solution, previously prepared. Ultimately, DMF was added and everything was mixed through magnetic stir. The final reaction volume was set to 1 mL. The solution was degassed for 20 minutes with argon. Subsequently, the vial was immersed in an oil bath maintained at 70°C. Lastly, the copolymer was purified by dialysis against acetone for two days.

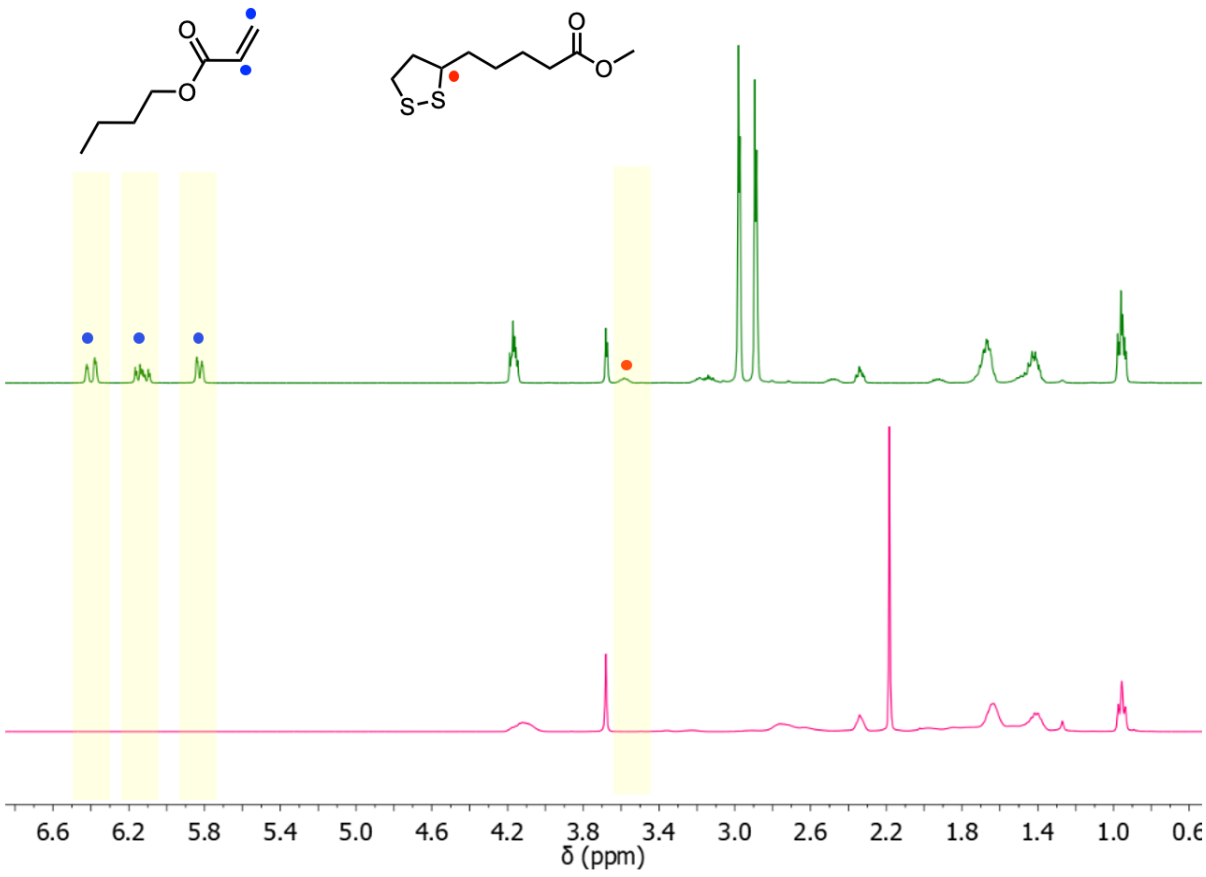

Figure S10: *^{1}H NMR spectra of the copolymer before polymerization (green) and after polymerization and purification (fuchsia). The characteristic monomer signals of nBA and LpOMe, highlighted in yellow, disappear upon polymerization.*

8.5 General Procedure for Degradation/Depolymerization Reactions

All degradation mixtures were prepared following the same general procedure. For all the depolymerization reactions the final volume was set to 1 mL. The photocatalyst concentration was fixed at 5 mol%, whereas the concentration of the electron donor, triethylamine (TEA), was varied depending on the specific experimental conditions and the photocatalyst employed. For the experiment conducted under oxygen-free conditions, the vial containing the solution was degassed for 20 minutes with argon prior to irradiation. For experiments performed in the presence of oxygen, the reaction vial was sealed to provide a confined atmosphere, whereas for the reaction carried out under open-air conditions, the vial was left open. After the solution was prepared and the polymer dissolved in the solvent, the vial was irradiated with light at the desired wavelength (depending on the photocatalyst employed) for the specified reaction time under magnetic stirring. Upon completion of the irradiation, the solvent was removed under reduced pressure using a rotatory evaporator. The resulting product was first characterized by ^{1}H NMR spectroscopy, followed by size exclusion chromatography (SEC) to determine its molecular weight.

8.6 Cyclic Voltammetry in Acetonitrile

Cyclic voltammetry (CV) measurements were performed in acetonitrile (MeCN) using a standard three-electrode cell configuration with a total solution volume of 10 mL. The electrolyte solution consisted of 0.1 M of tetraethylammonium tetrafluoroborate $TEABF_4$ as the supporting electrolyte. A glassy carbon electrode (70 mm length, 6 mm body diameter) was employed as the working electrode, while a platinum wire (99.9%, ST 0.6/40 mm) served as the counter electrode. An Ag/Ag^{+} non-aqueous refillable electrode (6 mm diameter) was utilized as the reference electrode. Prior to each measurement, the solution was thoroughly degassed with argon for 2 minutes through the dedicated ports in the Teflon cap to ensure an oxygen-free environment. The CVs were recorded at a stable scan rate of 0.1 Vs^{-1} ($100mVs^{-1}$).

8.7 NMR Spectra and GPC Traces

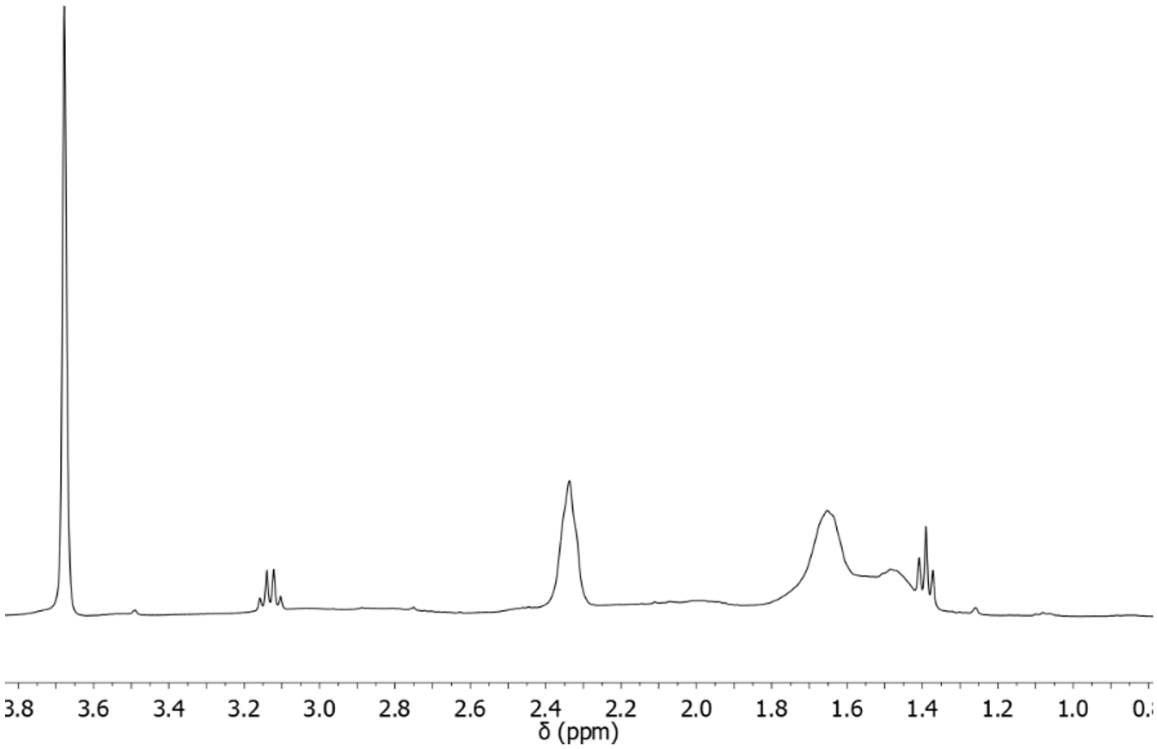

Figure S11: *^{1}H NMR spectra of the PLpOMe degradation with xanthone in DCM.*

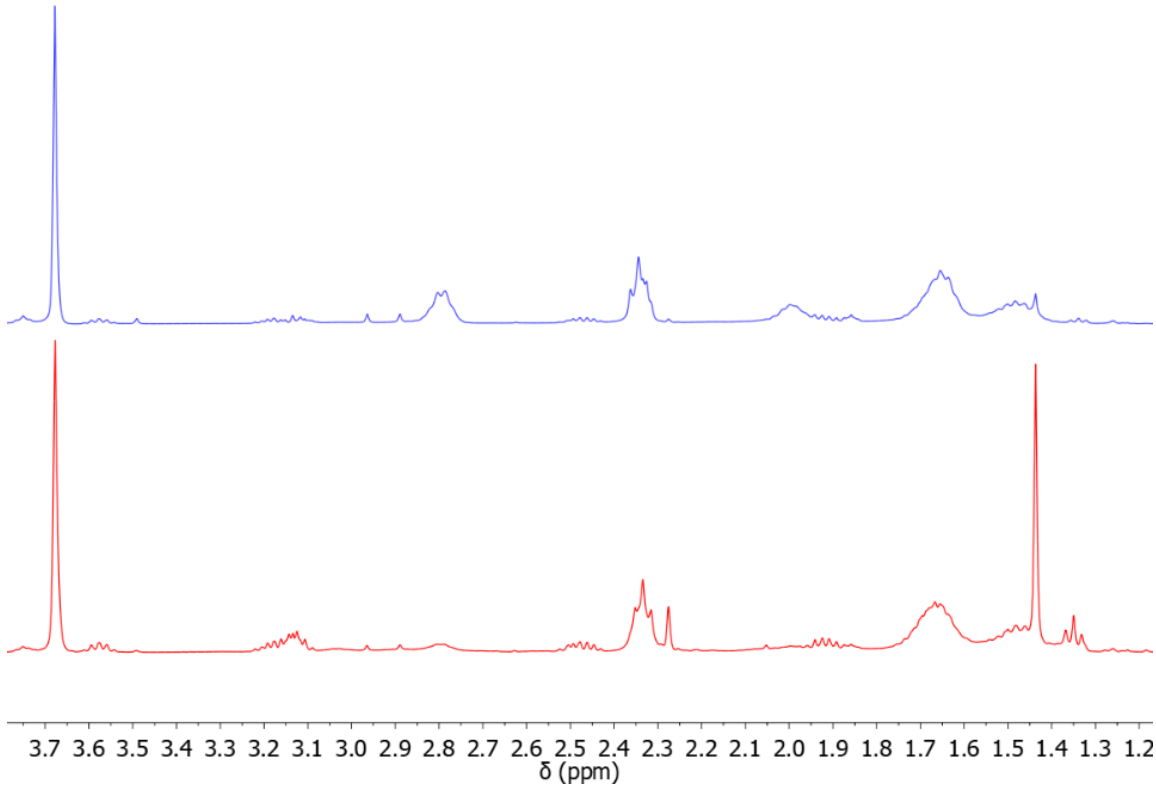

Figure S12: *^{1}H NMR spectra of the PLpOMe degradation with xanthone at 365 nm (blue) and thioxanthone at 427 nm (red) for 2 h irradiation time. In the two spectra are detectable the monomer signals.*

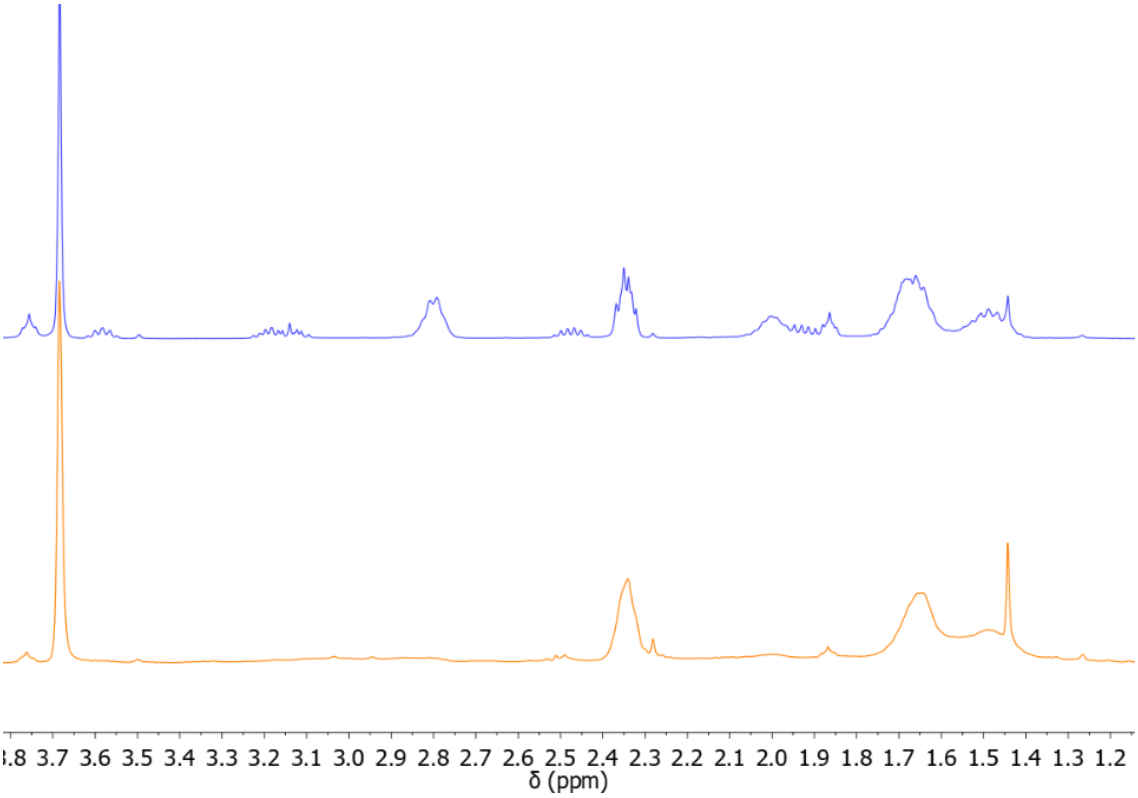

***Figure S13**: Comparison of the ^{1}H NMR spectra of PLpOMe degradation with PC-2 after 2 h (blue) and 16 h (orange) irradiation.*

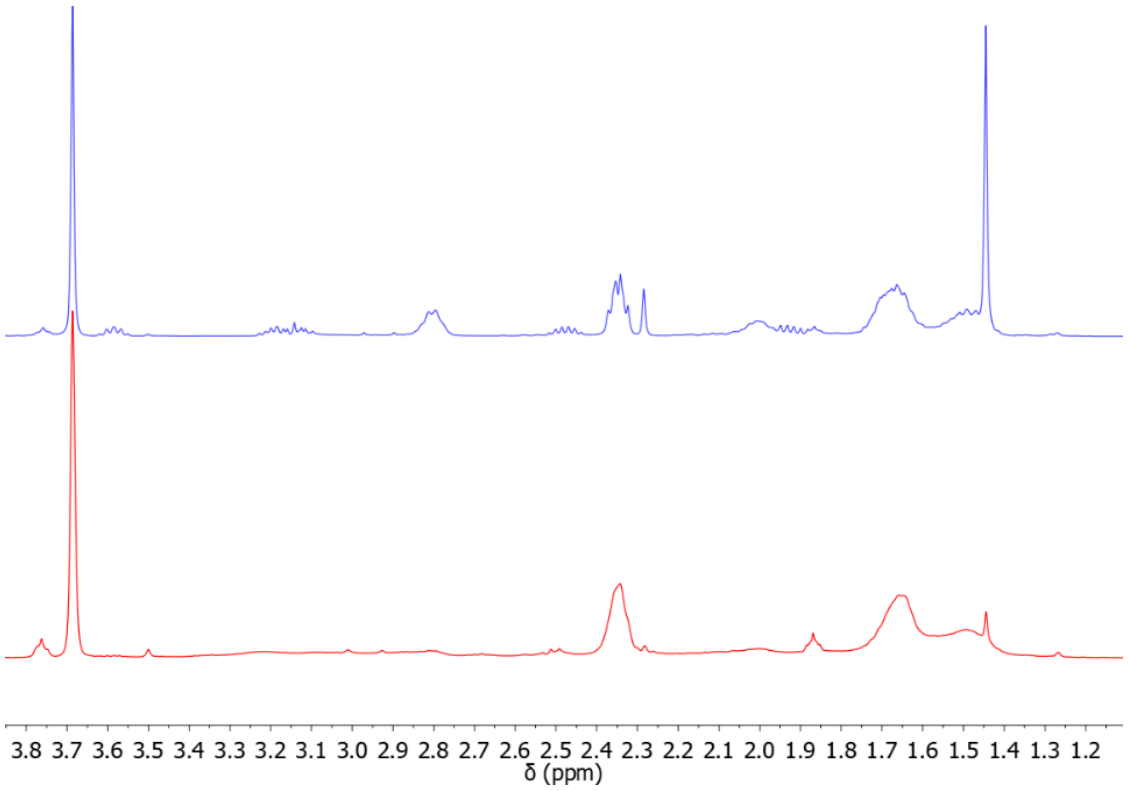

***Figure S14**: Comparison of the ^{1}H NMR spectra of PLpOMe degradation with PC-3 after 2 h (blue) and 16 h (red) irradiation.*

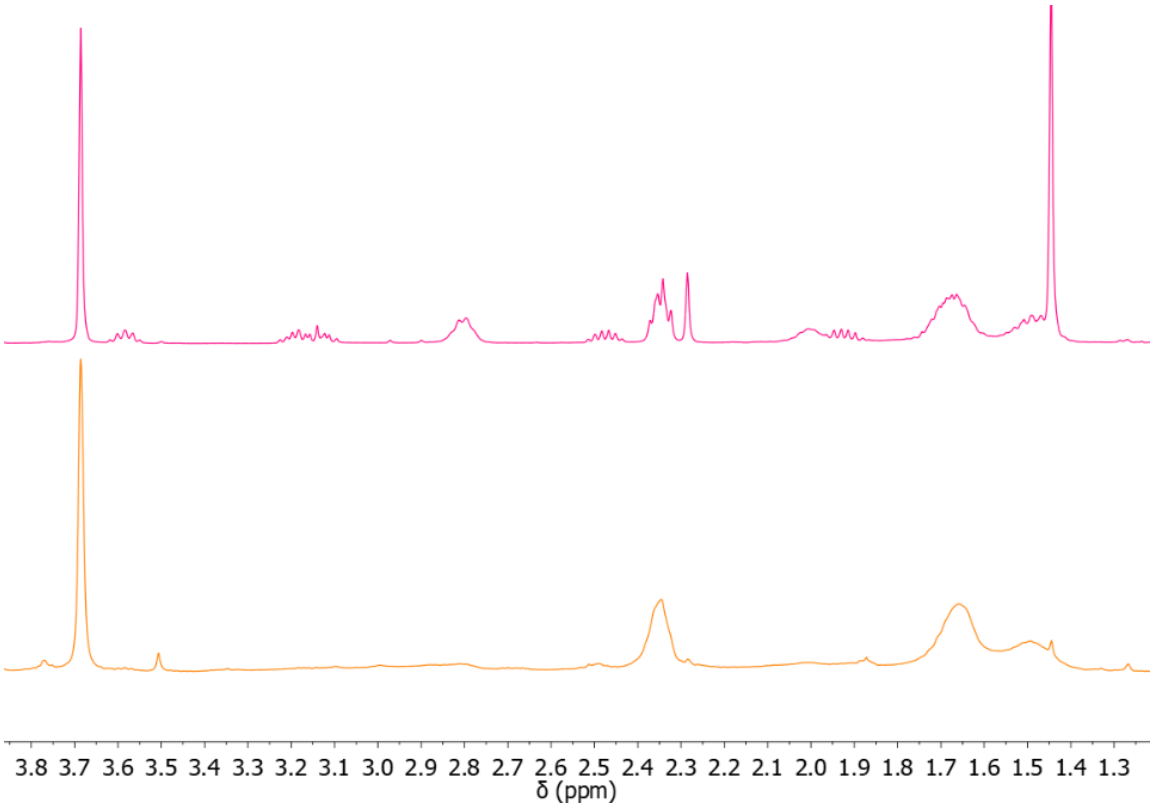

***Figure S15**: Comparison of the ^{1}H NMR spectra of PLpOMe degradation with PC-5 after 2 h (fuchsia) and 16 h (orange) irradiation.*

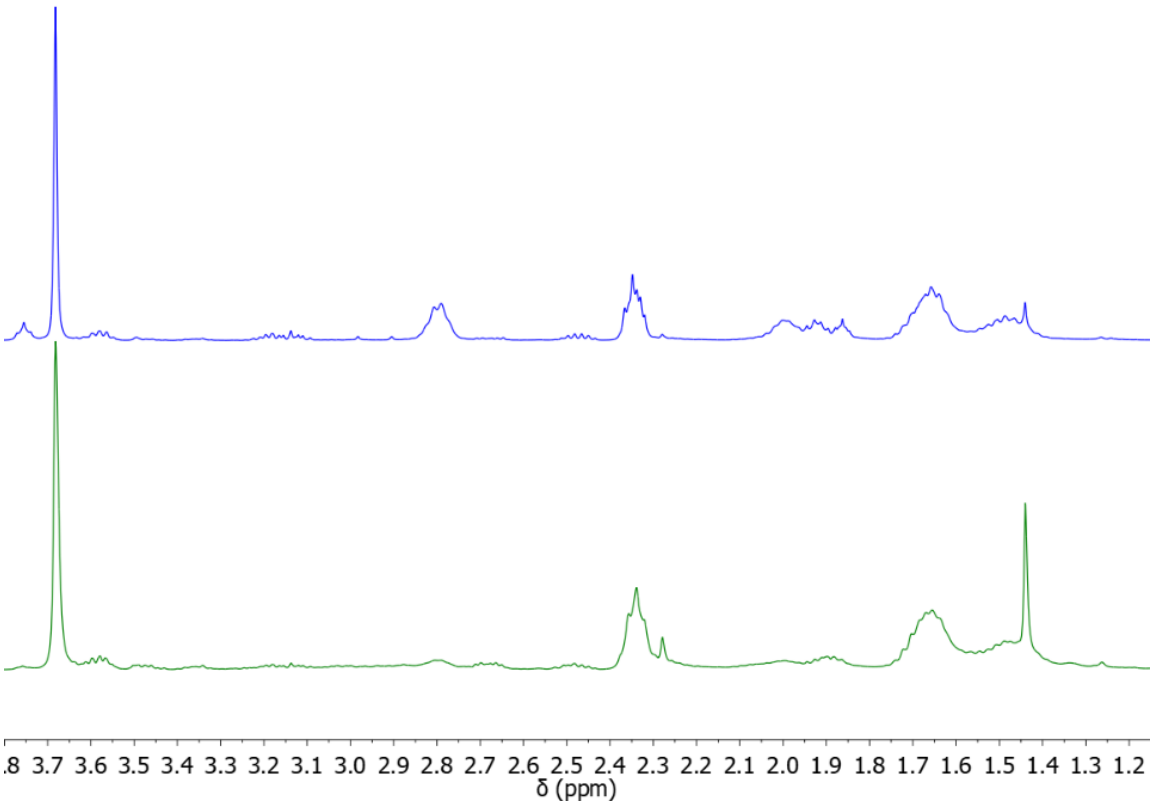

***Figure S16**: Comparison of the ^{1}H NMR spectra of PLpOMe degradation with [Ir(ppy)$_3$] after 2 h (blue) and 16 h (green) irradiation.*

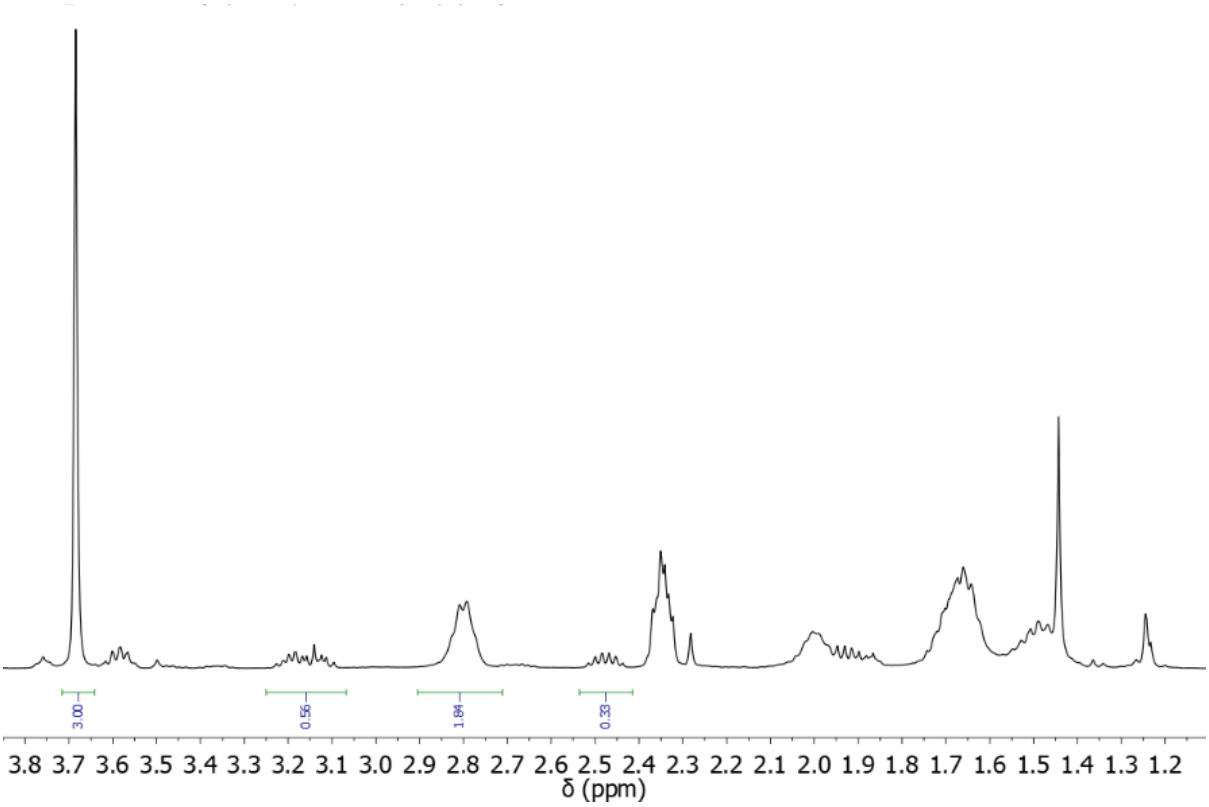

***Figure S17**: [1]H NMR spectra of the PLpOMe degradation with eosin Y in the presence of BHT.*

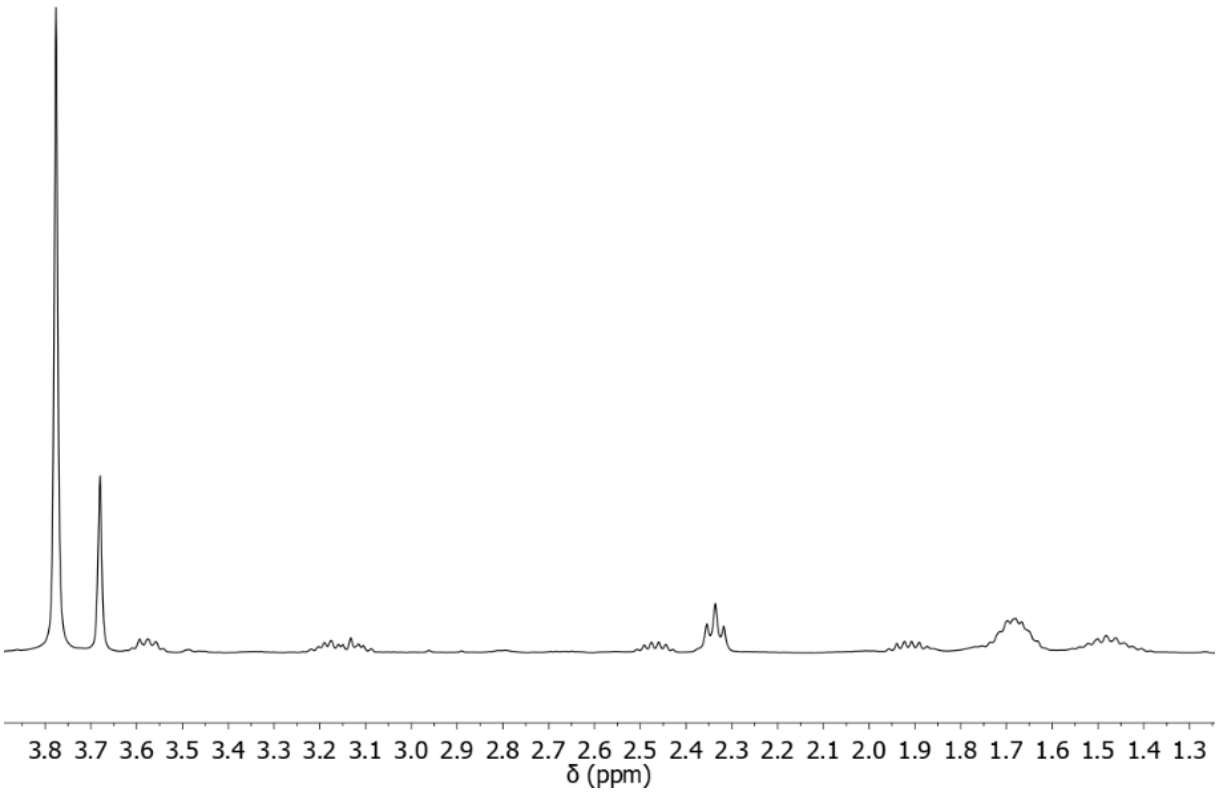

***Figure S18**: [1]H NMR spectra of the PLpOMe degradation with eosin Y DCM.*

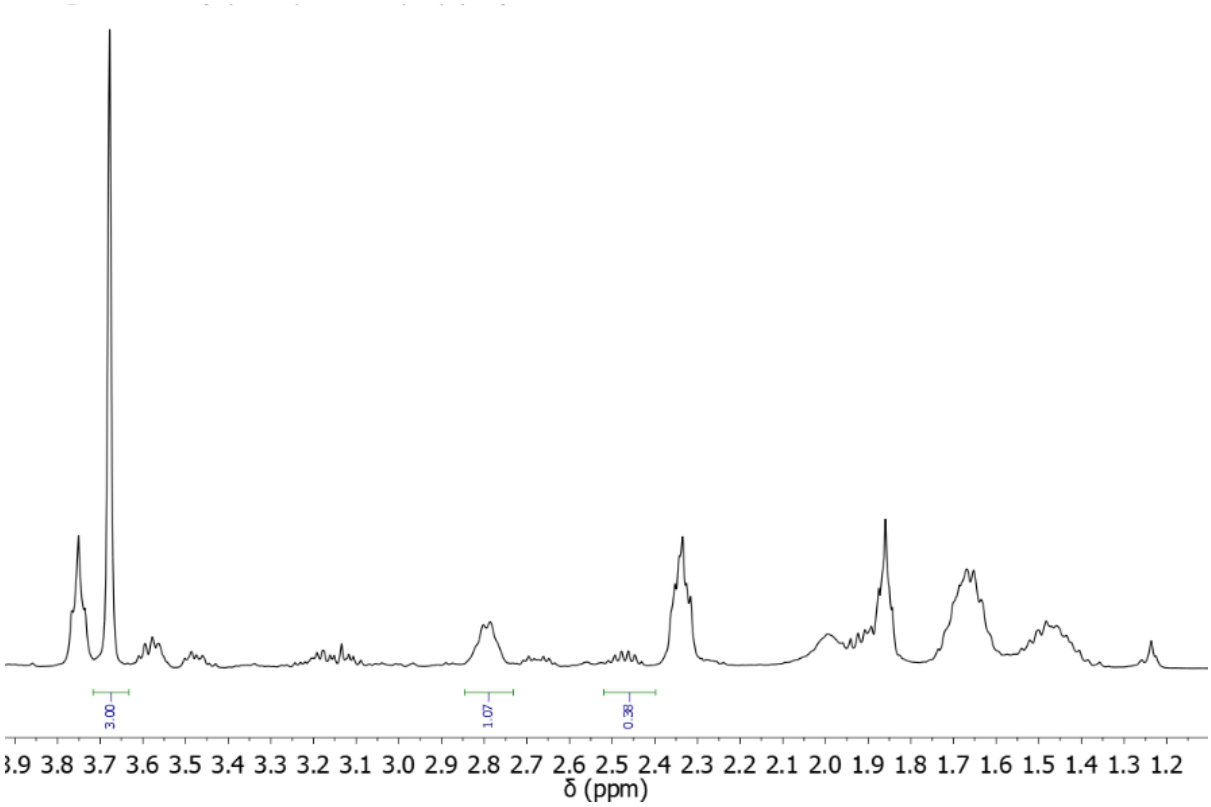

***Figure S19**: [1]H NMR spectra of the PLpOMe degradation with eosin Y in open-air conditions.*

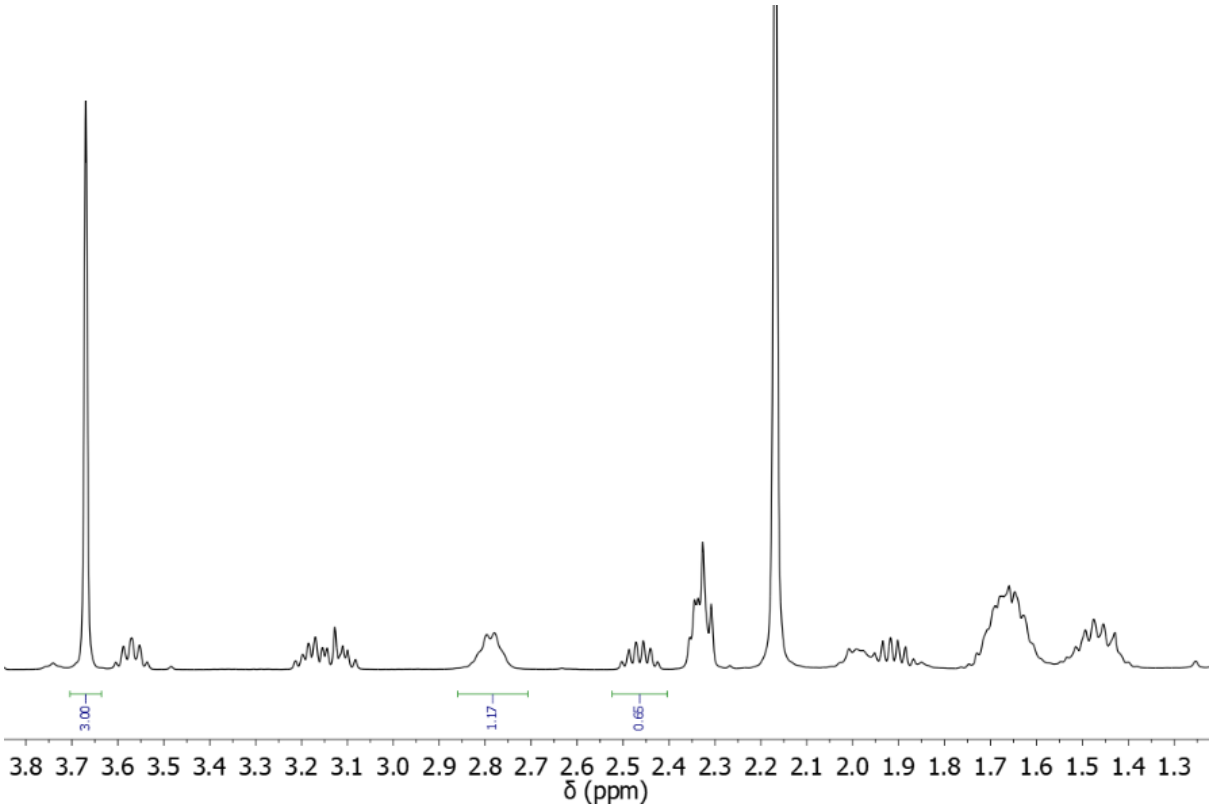

***Figure S20**: [1]H NMR spectra of the PLpOMe degradation with Rose Bengal.*

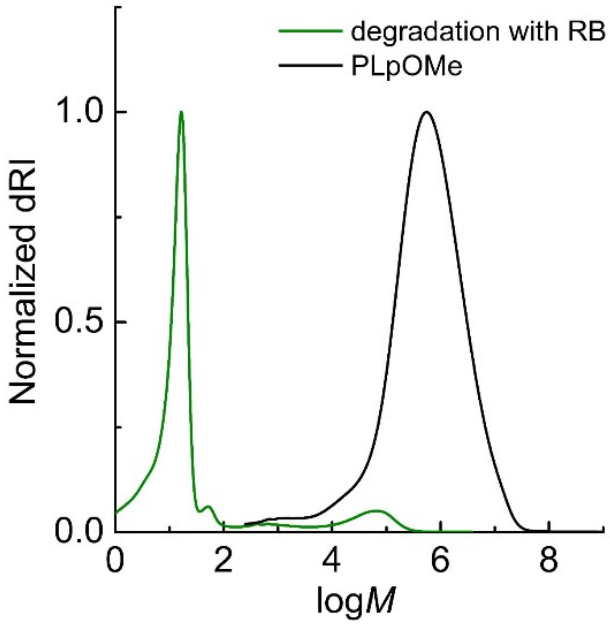

***Figure S21**: GPC traces of the homopolymer PLpOMe and the degradation product with Rose Bengal.*

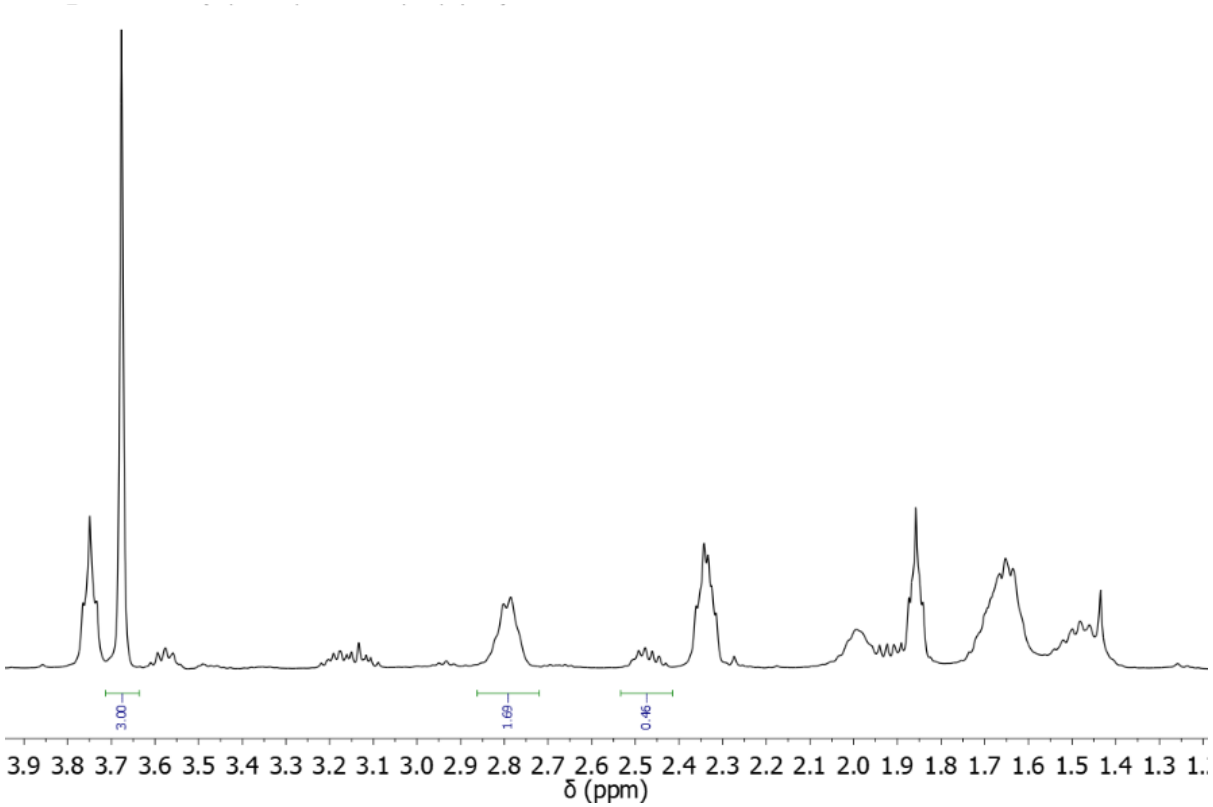

***Figure S22**: ^{1}H NMR spectra of the PLpOMe degradation with Methylene blue.*

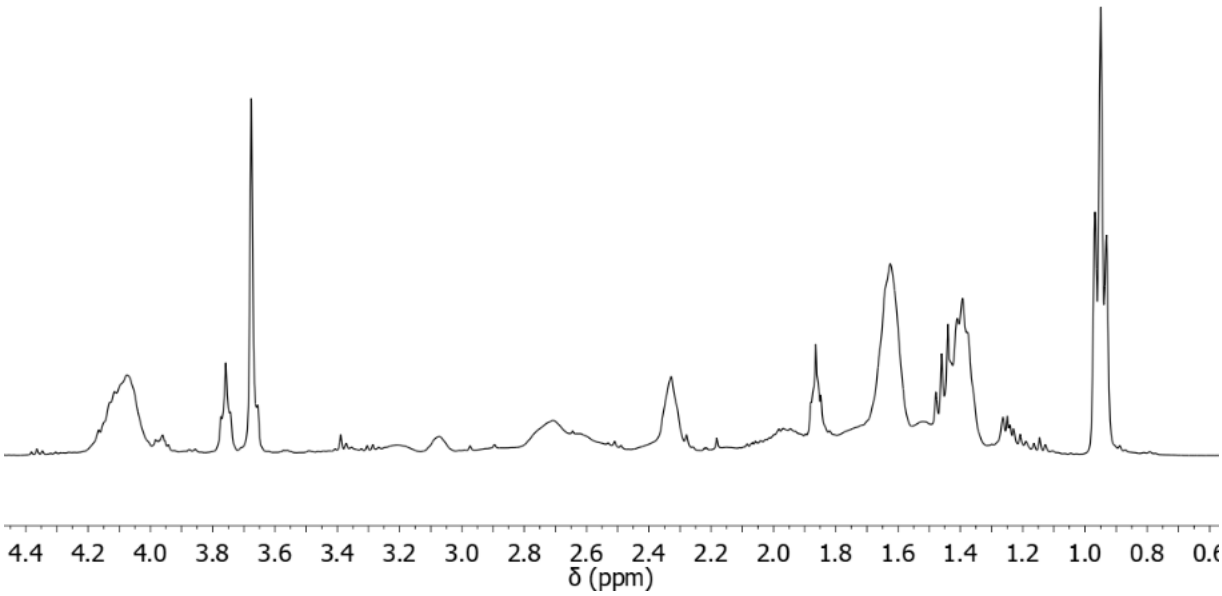

***Figure S23**: [1]H NMR spectra of the copolymer degradation with EY after 16 h irradiation time.*

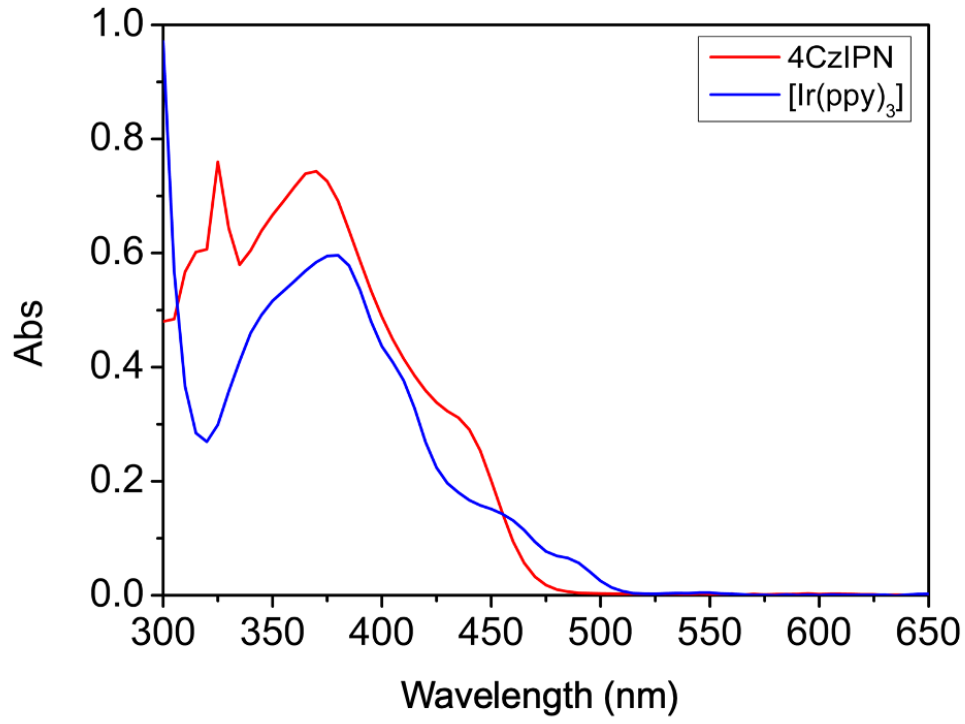

***Figure S24**: UV-Vis spectra of 4CzIPN and [Ir(ppy$_3$)] in THF.*

Bibliography

[1] J.-B. Kim, W. Huang, M. D. Miller, G. L. Baker, M. L. Bruening, *J. Polym. Sci. Part Polym. Chem.* **2003**, *41*, 386.

[2] D. Xiao, M. J. Wirth, *Macromolecules* **2002**, *35*, 2919.

[3] F. J. Arraez, P. H. M. Van Steenberge, D. R. D'hooge, *Macromolecules* **2020**, *53*, 4630.

[4] F. J. Arraez, P. H. M. Van Steenberge, J. Sobieski, K. Matyjaszewski, D. R. D'hooge, *Macromolecules* **2021**, *54*, 8270.

[5] M. Cao, M. Zhong, *Polym. Int.* **2022**, *71*, 501.

[6] K. R. Albanese, P. T. Morris, J. Read de Alaniz, C. M. Bates, C. J. Hawker, *J. Am. Chem. Soc.* **2023**, *145*, 22728.

[7] Y. Okayama, P. Morris, K. Albanese, S. Olsen, A. Mori, J. R. de Alaniz, C. M. Bates, C. J. Hawker, *J. Polym. Sci.* **2025**, *63*, 1345.

[8] N. Corrigan, K. Jung, G. Moad, C. J. Hawker, K. Matyjaszewski, C. Boyer, *Prog. Polym. Sci.* **2020**, *111*, 101311.

[9] K. Matyjaszewski, *Curr. Opin. Solid State Mater. Sci.* **1996**, *1*, 769.

[10] W. A. Braunecker, K. Matyjaszewski, *Prog. Polym. Sci.* **2007**, *32*, 93.

[11] J. Nicolas, Y. Guillaneuf, C. Lefay, D. Bertin, D. Gigmes, B. Charleux, *Prog. Polym. Sci.* **2013**, *38*, 63.

[12] M. Hartlieb, *Macromol. Rapid Commun.* **2022**, *43*, e2100514.

[13] D. J. Keddie, G. Moad, E. Rizzardo, S. H. Thang, *Macromolecules* **2012**, *45*, 5321.

[14] S. Perrier, *Macromolecules* **2017**, *50*, 7433.

[15] J. Chiefari, Y. K. (Bill) Chong, F. Ercole, J. Krstina, J. Jeffery, T. P. T. Le, R. T. A. Mayadunne, G. F. Meijs, C. L. Moad, G. Moad, E. Rizzardo, S. H. Thang, *Macromolecules* **1998**, *31*, 5559.

[16] G. Moad, E. Rizzardo, S. H. Thang, *Aust. J. Chem.* **2012**, *65*, 985.

[17] J.-S. Wang, K. Matyjaszewski, *J. Am. Chem. Soc.* **1995**, *117*, 5614.

[18] M. Kato, M. Kamigaito, M. Sawamoto, T. Higashimura, *Macromolecules* **1995**, *28*, 1721.

[19] P. Krys, K. Matyjaszewski, *Eur. Polym. J.* **2017**, *89*, 482.

[20] K. Matyjaszewski, J. Xia, *Chem. Rev.* **2001**, *101*, 2921.

[21] K. Matyjaszewski, *Macromolecules* **2012**, *45*, 4015.

[22] W. Tang, K. Matyjaszewski, *Macromolecules* **2006**, *39*, 4953.

[23] Externally controlled atom transfer radical polymerization | Chemical Society Reviews | The Royal Society of Chemistry, .

[24] Y. Kwak, K. Matyjaszewski, *Polym. Int.* **2009**, *58*, 242.

[25] W. Jakubowski, K. Min, K. Matyjaszewski, *Macromolecules* **2005**, *39*, 39.

[26] W. Yan, S. Dadashi-Silab, K. Matyjaszewski, N. D. Spencer, E. M. Benetti, *Macromolecules* **2020**, *53*, 2801.

[27] C. M. University, *Photoinitiated ATRP - Matyjaszewski Polymer Group - Carnegie Mellon University*.

[28] G. Gazzola, I. Filipucci, A. Rossa, K. Matyjaszewski, F. Lorandi, E. M. Benetti, *ACS Macro Lett.* **2023**, *12*, 1166.

[29] S. T. Milner, *Science* **1991**, *251*, 905.

[30] E. S. Dehghani, N. D. Spencer, S. N. Ramakrishna, E. M. Benetti, *Langmuir ACS J. Surf. Colloids* **2016**, *32*, 10317.

[31] E. M. Benetti, X. Sui, S. Zapotoczny, G. J. Vancso, *Adv. Funct. Mater.* **2010**, *20*, 939.

[32] B. Zdyrko, I. Luzinov, *Macromol. Rapid Commun.* **2011**, *32*, 859.

[33] J. O. Zoppe, N. C. Ataman, P. Mocny, J. Wang, J. Moraes, H.-A. Klok, *Chem. Rev.* **2017**, *117*, 1105.

[34] R. M. BIELECKI, E. M. BENETTI, N. D. Spencer, *Lubrication with oil-compatible polymer brushes*, **2012**.

[35] L. Michalek, L. Barner, C. Barner-Kowollik, *Adv. Mater.* **2018**, *30*, 1706321.

[36] C. W. Pester, E. M. Benetti, *Adv. Mater. Interfaces* **2022**, *9*, 2201439.

[37] J. C. Conrad, M. L. Robertson, *JACS Au* **2023**, *3*, 333.

[38] C. W. Pester, H.-A. Klok, E. M. Benetti, *Macromolecules* **2023**, *56*, 9915.

[39] Y. Zhang, A. Lo Bocchiaro, X. Hu, C. Pavon, C. Pezzato, K. Matyjaszewski, F. Lorandi, E. M. Benetti, *ACS Appl. Mater. Interfaces* **2025**, *17*, 38773.

[40] Y. Zhang, M. Li, B. Li, W. Sheng, *Langmuir* **2024**, *40*, 5571.

[41] A. L. Bocchiaro, E. Avanzini, F. Lorandi, E. M. Benetti, *Eur. Polym. J.* **2025**, *232*, 113927.

[42] D. Zhou, X. Gao, W. Wang, S. Zhu, *Macromolecules* **2012**, *45*, 1198.

[43] S.-Y. Hsu, Y. Kayama, K. Ohno, K. Sakakibara, T. Fukuda, Y. Tsujii, *Macromolecules* **2019**, *53*, 132.

[44] Y. Zeng, L. Xie, F. Chi, D. Liu, H. Wu, N. Pan, G. Sun, *Macromol. Rapid Commun.* **2019**, *40*, 1900078.

[45] J. Iruthayaraj, S. Chernyy, M. Lillethorup, M. Ceccato, T. Røn, M. Hinge, P. Kingshott, F. Besenbacher, S. U. Pedersen, K. Daasbjerg, *Langmuir* **2010**, *27*, 1070.

[46] K. Kapil, A. M. Jazani, J. Sobieski, L. P. Madureira, G. Szczepaniak, M. R. Martinez, A. Gorczyński, H. Murata, T. Kowalewski, K. Matyjaszewski, *Macromolecules* **2024**, *57*, 5368.

[47] K. Kapil, G. Szczepaniak, M. R. Martinez, H. Murata, A. M. Jazani, J. Jeong, S. R. Das, K. Matyjaszewski, *Angew. Chem. Int. Ed.* **2023**, *62*, e202217658.

[48] F. Li, M. Cao, Y. Feng, R. Liang, X. Fu, M. Zhong, *J. Am. Chem. Soc.* **2018**, *141*, 794.

[49] M. Cao, Y. Liu, X. Zhang, F. Li, M. Zhong, *Chem* **2022**, *8*, 1460.

[50] S. Biswas, Y. Liu, V. V. Yashin, T.-C. Lin, K. Kapil, T. Kowalewski, K. Matyjaszewski, A. C. Balazs, *Polymer* **2024**, *312*, 127620.

[51] N. V. Tsarevsky, K. Matyjaszewski, *Macromolecules* **2005**, *38*, 3087.

[52] S. Han, K. Lee, P. T. Morris, M. Michelas, G. Moad, C. M. Bates, C. J. Hawker, C. Boyer, *Macromolecules* **2025**, *58*, 13288.

[53] I. O. Levkovsky, L. Trachsel, H. Murata, K. Matyjaszewski, *Angew. Chem. Int. Ed.* **2025**, *64*, e202516164.

[54] M. Raeisi, N. V. Tsarevsky, *J. Polym. Sci.* **2021**, *59*, 675.

[55] G. Ciamician, *Science* **1912**, *36*, 385.

[56] A. Albini, V. Dichiarante, *Photochem. Photobiol. Sci.* **2009**, *8*, 248.

[57] C. K. Prier, D. A. Rankic, D. W. C. MacMillan, *Chem. Rev.* **2013**, *113*, 5322.

[58] H. Huang, X. Li, C. Yu, Y. Zhang, P. S. Mariano, W. Wang, *Angew. Chem.* **2017**, *129*, 1522.

[59] A. Vega-Peñaloza, J. Mateos, X. Companyó, M. Escudero-Casao, L. Dell'Amico, *Angew. Chem. Int. Ed.* **2021**, *60*, 1082.

[60] L. Capaldo, D. Ravelli, *Eur. J. Org. Chem.* **2017**, *2017*, 2056.

[61] F. Juliá, T. Constantin, D. Leonori, *Chem. Rev.* **2021**, *122*, 2292.

[62] F. Strieth-Kalthoff, M. J. James, M. Teders, L. Pitzer, F. Glorius, *Chem. Soc. Rev.* **2018**, *47*, 7190.

[63] Y. Zhang, T. S. Lee, J. L. Petersen, C. Milsmann, *J. Am. Chem. Soc.* **2018**, *140*, 5934.

[64] T. Bortolato, G. Simionato, M. Vayer, C. Rosso, L. Paoloni, E. M. Benetti, A. Sartorel, D. Lebœuf, L. Dell'Amico, *J. Am. Chem. Soc.* **2023**, *145*, 1835.

[65] P. Franceschi, E. Rossin, G. Goti, A. Scopano, A. Vega-Peñaloza, M. Natali, D. Singh, A. Sartorel, L. Dell'Amico, *J. Org. Chem.* **2023**, *88*, 6454.

[66] K. Zhou, X. Yang, H. Ren, Y. Xia, *J. Phys. Chem. A* **2025**, *129*, 7421.

[67] N. F. Nikitas, P. L. Gkizis, C. G. Kokotos, *Org. Biomol. Chem.* **2021**, *19*, 5237.

[68] V. P. Demertzidou, E. Skolia, C. G. Kokotos, *ChemCatChem* **2025**, *17*, e00760.

[69] E. Studer, S. Mandal, T. Stünkel, R. Gilmour, *Angew. Chem.* **2025**, *137*, e202513320.

[70] A. Chemtob, N. Feillée, C. Vaulot, C. Ley, D. Le Nouen, *ACS Omega* **2019**, *4*, 5722.

[71] T. I. U. of P. and A. Chemistry (IUPAC), *IUPAC - depolymerization (D01600)*.

[72] G. Morselli, C. Bellatreccia, M. Mazzanti, V. Cristino, A. Ianniello, S. Caramori, R. Mazzaro, P. Ceroni, *Adv. Opt. Mater.* **2024**, *12*, 2400259.

[73] C. Choi, J. L. Self, Y. Okayama, A. E. Levi, M. Gerst, J. C. Speros, C. J. Hawker, J. Read de Alaniz, C. M. Bates, *J. Am. Chem. Soc.* **2021**, *143*, 9866.

[74] M. A. Bryden, E. Zysman-Colman, *Chem. Soc. Rev.* **2021**, *50*, 7587.

[75] M. A. Bryden, F. Millward, T. Matulaitis, D. Chen, M. Villa, A. Fermi, S. Cetin, P. Ceroni, E. Zysman-Colman, *J. Org. Chem.* **2023**, *88*, 6364.

[76] Synthetic applications of eosin Y in photoredox catalysis | Chemical Communications | The Royal Society of Chemistry, .

[77] D. Singla, V. Luxami, K. Paul, *Org. Chem. Front.* **2023**, *10*, 237.

[78] S. Fujisawa, Y. Kadoma, I. Yokoe, *Chem. Phys. Lipids* **2004**, *130*, 189.

[79] N. A. Romero, D. A. Nicewicz, *Chem. Rev.* **2016**, *116*, 10075.

[80] L. Marzo, S. K. Pagire, O. Reiser, B. König, *Angew. Chem. Int. Ed.* **2018**, *57*, 10034.

[81] Q.-Q. Zhou, Y.-Q. Zou, L.-Q. Lu, W.-J. Xiao, *Angew. Chem.* **2019**, *58*, 1586.

[82] M. Teders, C. Henkel, L. Anhäuser, F. Strieth-Kalthoff, A. Gómez-Suárez, R. Kleinmans, A. Kahnt, A. Rentmeister, D. Guldi, F. Glorius, *Nat. Chem.* **2018**, *10*, 981.

[83] X. Qiu, J. Liu, X. Li, Y. Wang, X. Zhang, *Nat. Commun.* **2024**, *15*, 9759.

[84] V. P. Demertzidou, E. Skolia, C. G. Kokotos, *ChemCatChem* **2025**, *17*, e00760.

[85] K. R. Albanese, Y. Okayama, P. T. Morris, M. Gerst, R. Gupta, J. C. Speros, C. J. Hawker, C. Choi, J. R. de Alaniz, C. M. Bates, *ACS Macro Lett.* **2023**, *12*, 787.

[86] Y. Liu, Y. Jia, Q. Wu, J. S. Moore, *J. Am. Chem. Soc.* **2019**, *141*, 17075.

[87] A. Kisanuki, Y. Kimpara, Y. Oikado, N. Kado, M. Matsumoto, K. Endo, *J. Polym. Sci. Part Polym. Chem.* **2010**, *48*, 5247.